CHEMICAL REVIEWS

Review

Cite This: *Chem. Rev.* XXXX, XXX, XXX−XXX

pubs.acs.org/CR

Simulation Studies of Amyloidogenic Polypeptides and Their Aggregates

Ioana M. Ilie* and Amedeo Caflisch*

Department of Biochemistry, University of Zürich, Zürich CH-8057, Switzerland

ABSTRACT: Amyloids, fibrillar assembly of (poly)peptide chains, are associated with neurodegenerative illnesses such as Alzheimer's and Parkinson's diseases, for which there are no cures. The molecular mechanisms of the formation of toxic species are still elusive. Some peptides and proteins can form functional amyloid-like aggregates mainly in bacteria and fungi but also in humans. Little is known on the differences in self-assembly mechanisms of functional and pathogenic (poly)peptides. We review atomistic and coarse-grained simulation studies of amyloid peptides in their monomeric, oligomeric, and fibrillar states. Particular emphasis is given to the challenges one faces to characterize at atomic level of detail the conformational space of disordered (poly)peptides and their aggregation. We discuss the difficulties in comparing simulation results and experimental data, and we propose new simulation studies to shed light on the aggregation processes associated with amyloid diseases.

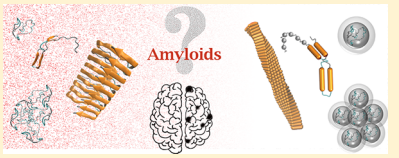

CONTENTS

1. INTRODUCTION

Soluble peptides and proteins can undergo conformational changes and aggregate into threadlike, elongated insoluble intra- and extra-cellular accumulations known as amyloid fibrils.[1−8] Their presence is frequently linked to the pathology of neurodegenerative diseases, including Parkinson's disease (PD) and Alzheimer's disease (AD).[1,3,7−9] The sequences, structures, and physiological functions (if any) of amyloidogenic (poly)peptides are very diverse, yet they all share the common feature that under given conditions they can aggregate into amyloids.[1,9,10] Whether mature amyloid fibrils or oligomeric species are responsible for triggering neurodegeneration is not clear. A large variety of experimental and computational tools are used to shed light into the aggregation mechanisms of amyloidogenic structures and their toxicity, and to find strategies to block their advancement.

At first, amyloids were associated with disease and tissue damage,[6,8,9] but over the past years a growing body of evidence suggests that the self-assembly of certain (poly)peptides can have a functional role in healthy human cells and micro-organisms.[8,10−13] Examples include the involvement in melanin synthesis,[14] storage of peptide hormones,[15] long-term memory consolidation,[16] biofilm formation,[11,17,18] and mediation of tumor necrosis.[19]

Received: November 30, 2018

DOI: 10.1021/acs.chemrev.8b00731
Chem. Rev. XXXX, XXX, XXX−XXX

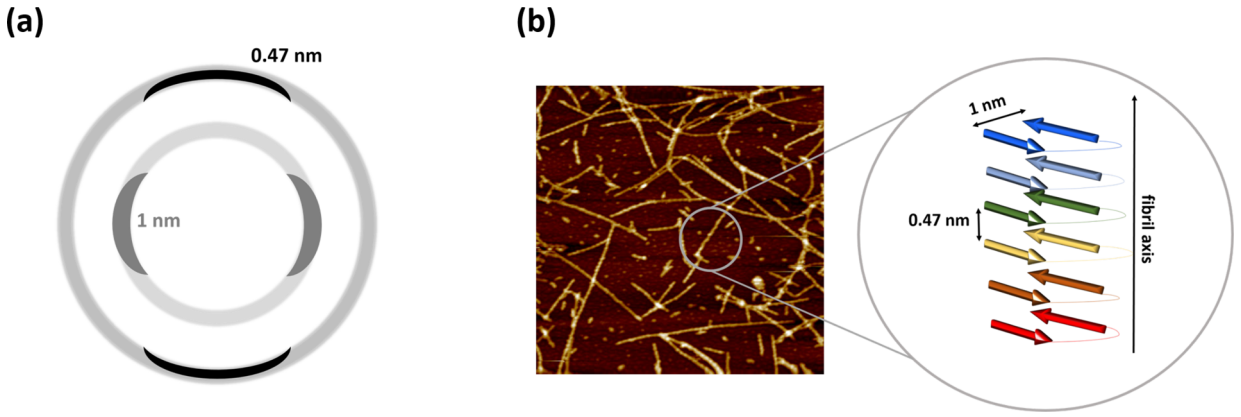

Figure 1. (a) Cartoon of the amyloid cross-β diffraction pattern. (b) Atomic force microscopy image of an amyloid fibril (left, courtesy of Dr. Slav Semerdzhiev) and schematic representation of the distances within an amyloid fibril (right).

Amyloid formation is commonly described as a nucleation−elongation mechanism.[20−22] The nucleus is the unstable species that has the same probability to dissociate and to form a fibril. It acts as the initial template of aggregation for the free monomers in solution. The nucleation of pathological amyloids can be a one-step process in which monomers simultaneously adopt the fibrillar structure and aggregate, or it can involve a disordered aggregated state (two-step process).[7,23] In contrast, functional amyloids have been (so far) identified to nucleate in a single step.[12] While the nucleation is a rare stochastic event, the elongation is much faster and occurs through monomer binding at fibrillar ends.

Amyloid aggregation can be modulated by varying the solution pH[24,25] and temperature,[26,27] by adding cosolvents or osmolytes,[28] or by the presence of membranes. For example, the nucleation rate of α-synuclein can be increased in the presence of lipid membranes,[29] DOPC lipid vesicles accelerate the Aβ_{42} growth rate or can augment monomer-dependent secondary nucleation.[30] Furthermore, bilayers consisting of lipids commonly found in membranes of synaptic vesicles (DOPE, DOPC, DOPS, POPS, and cholesterol) do not enhance α-synuclein aggregation substantially, whereas DMPS and DLPS model membranes significantly increase its aggregation rate.[31] On the other hand, upon interaction with membranes amyloidogenic aggregates can have modulating or disruptive effect, resulting in cell dysfunction.[32,33] Amyloid fibrils attached to membranes have been observed to extract lipids,[33−36] and oligomeric aggregates were shown to perturb the membrane and disrupt the cellular function by insertion into lipid bilayers, which ultimately leads to leakage.[32] We refer the reader to a series of reviews addressing the interaction of amyloidogenic peptides with membranes in refs 37−39.

The molecular mechanisms underlying the formation of early stage aggregates, oligomers, and amyloid fibril are still elusive and pose a series of difficulties to classical simulation approaches, *e.g.,* molecular dynamics. One of the most challenging aspects is recovering relevant experimental time- and length-scales. In classical molecular dynamics the computational demand depends on the simulated time and the number of atoms. The dependence on number of atoms is linear thanks to nonbonding cutoffs and neighboring lists. The size of a simulation system spans usually from a few nanometers and 10^3 to 10^4 atoms for single peptides to micrometers and 10^4 to 10^5 atoms for fibrils. The length of the longest simulations even on the fastest (dedicated) hardware is less than 1 ms. As a consequence the time scales of minutes to hours required for amyloid aggregation *in vitro*[40−42] are several orders of magnitude longer than those acessible by atomistic simulations. While experimental methods enable the monitoring over relevant time and length scales, simulations require special techniques to circumvent this problem. These include coarse-grained descriptions of (poly)peptides, simplified treatment of the aqueous solvent (implicit solvent) and/or membranes, and protocols for accelerating rare events (enhanced sampling).[43−45]

This review describes the challenges inherent to the simulations of amyloid forming (poly)peptides and their aggregates, as well as the difficulties in comparing to experimental data. In particular, this review will address the generic amyloid growth mechanisms and the associated kinetics from interdisciplinary, multiscale simulation, and experimental perspectives, with an emphasis on the complementarity between them. Next, it will provide a perspective on the future problems that can be tackled using computational methods, the predictive role of simulations, and their limitations. It lies outside the scope of this paper to review the force-fields or water models used when dealing with amyloid forming proteins or any experimental techniques, as these have been reviewed elsewhere.[46−49] It is unavoidable that this review does not include all simulation studies of (poly)peptide self-assembly. We made a selection of amyloidogenic (poly)peptides and tried to exhaustively mention the simulation studies that were carried out with them. Lists of human (poly)peptides that can form pathogenic and functional amyloids are provided in Tables 1 and 3, respectively, of ref 8.

2. EXPERIMENTAL BACKGROUND

Under specific conditions, (poly)peptides can aggregate into amyloids both *in vitro* and *in vivo*.[9,23,50] *In vitro* experiments try to reproduce cellular conditions to shed light on the mechanisms of amyloid formation and the structure of the fibrils.[51] We refer the interested reader to a review addressing the various experimental techniques used to study the formation of amyloids *in vitro* in ref 51 and proceed with discussing the fibrillar structures and mechanisms of amyloid aggregation.

2.1. Cross-β Structure

An amyloid fibril can consist of a single filament or of several protofilaments wrapped around each other in an ordered fashion. Structurally, amyloids follow the same X-ray diffraction fingerprint,[52] in which two major reflections are observed at 0.47 nm and about 1 nm on perpendicular axes (Figure 1(a)).[53]

DOI: 10.1021/acs.chemrev.8b00731
Chem. Rev. XXXX, XXX, XXX−XXX

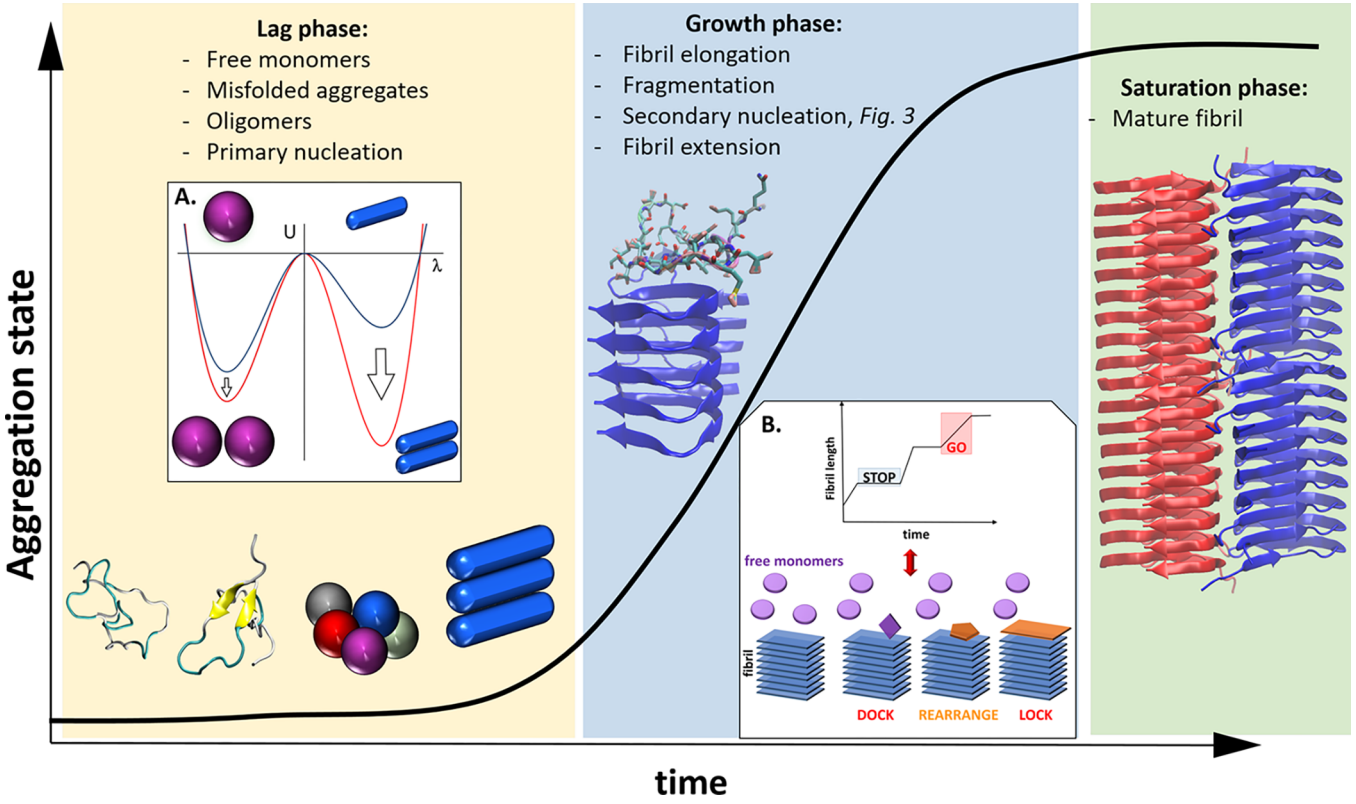

Figure 2. Schematic representation of the three phases of amyloid aggregation. The sigmoidal curve (solid line) is a simplified representation of the temporal evolution of a fluorescent signal. Inset A shows the change in internal free energy of a peptide (U) in the free state (blue profile) as compared to the bound state (red profile). The spheres represent peptides in the disordered conformation, and the spherocylinders symbolize ordered β-rich peptides. Note that the change in internal free energy for cross-β association (arrow on the right) is more favorable than the one for disordered aggregation (arrow on the left). Moreover, the cross-β association more than compensates for the increase in the internal free energy associated to the conformational change of the monomer. Inset B shows the equivalence between the experimental "stop-and-go" mechanism and the computational "dock–lock" mechanism.

These reflections correspond to distances between β-strands stabilized by backbone hydrogen bonds and packing of β-sheets stabilized by side chain contacts, respectively (Figure 1(b)). In this arrangement the β-sheets and backbone hydrogen bonds are parallel to the fibrillar axis with β-strands perpendicular to the axis (cross-β).[5,8,9,54−57] The common features of amyloids are

(i) the diffraction fingerprint corresponding to the cross-β architecture,[58,59]

(ii) binding affinities to specific dyes, i.e., thioflavin-T, Congo red, etc.,[60,61] and

(iii) structural and mechanical stability of the fibrils.[62,63]

It has been proposed that some functional amyloids form β-helical structures, rather than the conventional cross-β arrangement observed for the pathological aggregates, but with diffraction patterns matching the amyloid fingerprint[64] (Figure 1(a)). The relationship between the two types of amyloids is still unknown, as well as the ability of the cell to discern between toxic and useful fibrillar aggregates.

2.2. Kinetics

Amyloid self-assembly is a complex multiphase process governed by noncovalent interactions with a delicate balance of enthalpic and entropic contributions.[65] Generally, amyloid aggregation is considered a nucleation-dependent polymerization mechanism, in which the formation of nuclei is obligate for fibril formation.[23,50,66,67]

Experimentally fibril growth is described by a sigmoidal curve (Figure 2), which results from the temporal monitoring of the binding of a dye to the cross-β aggregates.[9,68,69] This enables the identification of three main regions along the aggregation process:

- the *lag phase*, during which soluble monomers undergo structural rearrangements and self-assembly into dimers, trimers, and/or oligomers;
- the *growth or elongation phase* which starts from an oligomeric nucleus that acts as template for the monomers in solution and proceeds by fibril elongation, aided by fragmentation, secondary nucleation, and fibril conjoining;
- the *saturation phase* in which the system reaches an equilibrium consisting of mature fibrils and a reduced concentration of the monomeric species.

2.2.1. Nucleation. Nucleation is a thermodynamically disfavored process, as peptides are required to overcome a free energy barrier that originates from the loss of conformational entropy (see inset A, Figure 2). In principle, *nucleation* can occur in *one step* (1SN), during which two peptides in the "binding-prone" conformation spontaneously meet and aggregate. It is more likely that monomers aggregate to form intermediate metastable species consisting of peptides in various conformations. The constituents of the aggregate simultaneously undergo structural rearrangements to give rise to β-rich nuclei, a process referred to as *two-step nucleation* (2SN) (Figure 3). Both nucleation mechanisms can occur simultaneously, but only the dominating one can be observed experimentally.[70] Among the

DOI: 10.1021/acs.chemrev.8b00731
Chem. Rev. XXXX, XXX, XXX−XXX

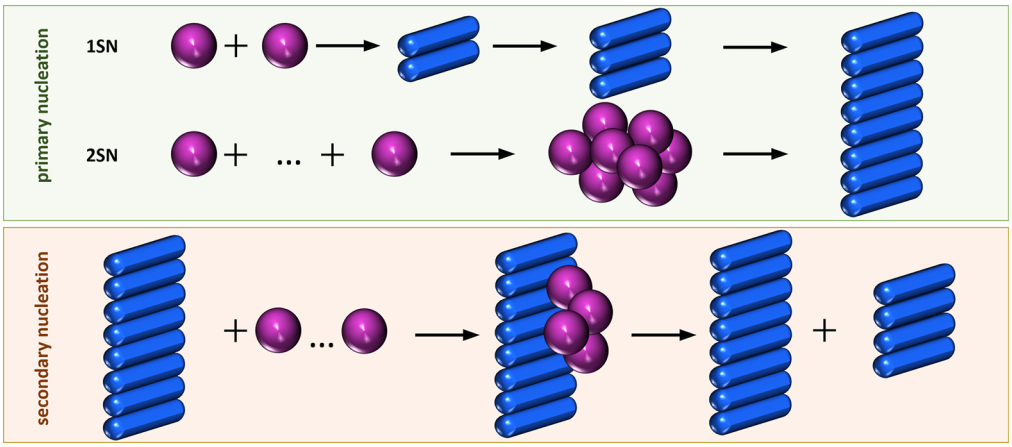

Figure 3. Schematic representation of the main nucleation mechanisms investigated by atomistic and coarse-grained simulations. Purple spheres depict monomers in the disordered state, and blue spherocylinders illustrate monomers in the cross-β conformation. Agglomerations of spheres form an oligomer while spherocylinders aggregate into fibrils. Abbreviations: 1SN, one-step-nucleation; 2SN, two-step-nucleation.

intermediate species there are dimers, the smallest toxic aggregate for some peptides, which can later evolve into oligomers by further monomer addition.[23,71] Oligomers are nonfibrillar aggregates, which consist of partially (mis)folded peptides and have been identified to fulfill several roles. They can be intermediate structures toward attaining the final fibrillar aggregate ("on-pathway"),[23,72−74] or they can grow into disordered aggregates without converting into fibril ("off-pathway").[75,76] Furthermore, disordered aggregates can interact with the fibril surface to be involved in secondary nucleation[25,77−80] (discussed in Section 2.2.2) or bind to membranes.[37,39,81,82] Conflicting hypotheses have risen regarding which type of aggregate is the most toxic for the cell. On the one hand, fibrils have been shown to be the toxic species,[83,84] while on the other hand, evidence suggests that off-pathway oligomers may be the more toxic species responsible for neuronal loss.[79,85] Oligomeric species are difficult to detect because of their transient existence. Differentiating between on- and off-pathway oligomers is very challenging but crucial in understanding the fibrillization kinetics[86,87] and for possible stabilization of the nontoxic structures.

2.2.2. Growth and Saturation. The exponential part of the curve in Figure 2 is associated with all the mechanisms involved in fibril elongation. During the growth phase the fibrils elongate while the concentration of free monomers decreases steadily. Soluble monomers diffuse and attach to the end of the fibrils, followed by structural rearrangements to adopt the cross-β conformation, and act as a template for incoming monomers. Kinetic studies have shown that fibril elongation can be described by a two-phase process.[42,88−91] An active growing phase, in which the fibril elongation occurs by monomer addition (referred to as "go"), is interrupted by long pauses in which no elongation is observed (referred to as "stop"), inset B in Figure 2. During the "stop" phase growth can be limited by the structural rearrangements of the attaching monomer, which needs to overcome a high free energy barrier to adopt the fibrillar template. Furthermore, a monomer can attach and detach to and from the fibril several times until it binds "correctly" to its ends.

A number of secondary processes contribute to the kinetics of the growth phase. These include secondary nucleation (Figure 3), fibril breaking, and merging. With increasing number of fibrils, the probability of new nuclei to form and transform into fibrils decreases. In contrast, the *secondary nucleation* mechanism[22,80,92] becomes more likely as more fibrils can act as catalyst for free monomers to form a new aggregate, which can shrink or grow until the critical nucleus has been formed. The new fibril can preserve the structural characteristics of the parent fibril, but whether this is a generic feature or not remains elusive. Secondary nucleation is a structurally and energetically different process from primary nucleation; that is, a foreign surface is involved,[80,93] and it can be several orders of magnitude faster.[94] The theoretical framework behind nucleation in general has been derived and reviewed by several research groups,[38,40,80,95,96] and we will therefore not discuss it here.

Fibril breakage or *fragmentation* is another mechanism that has been proposed to generate new nuclei during the growth phase. Amyloid fibrils are stabilized by optimal van der Waals packing within and between β-sheet structures and the backbone hydrogen bonds of the cross-β arrangement. Thus, they have high values of Young's modulus.[97] As a consequence fragmentation can be usually achieved by using external stimuli such as variations in temperature[26,27] or mechanical stress.[41] It has been experimentally proposed that fibril fragmentation is length dependent and that breakage can occur through three different mechanisms depending on the environment.[98] In particular, one can experience breakage at the ends (erosion) at high temperatures[26] or fragmentation around the center of the fibril (central) or with equal probability at any location within the fibril (random) at low temperatures[27] and under mechanical stress.[41]

In the *saturation* phase, a low concentration of monomers is in equilibrium with the fibrillar aggregates, and the growth curve reaches a plateau. It is important to note that monomers continuously detach and reassociate noncovalently at the tips of the fibrils in the final equilibrium. Thus, fibrils are aggregates that dynamically recycle their (poly)peptide chains.[99]

3. SIMULATION STUDIES

In this section we first focus on the simulations dealing with monomeric systems followed by the computational studies (Table 1) of nucleation and growth.

3.1. Monomeric State

3.1.1. Amyloid-β(42) and Its Variants. Amyloid-β (Aβ) is an intrinsically disordered peptide (IDP) up to 43 residues long cleaved from the Alzheimer polypeptide precursor (APP). It can aggregate into oligomers, fibrils, or amyloid plaques, the

DOI: 10.1021/acs.chemrev.8b00731
Chem. Rev. XXXX, XXX, XXX−XXX

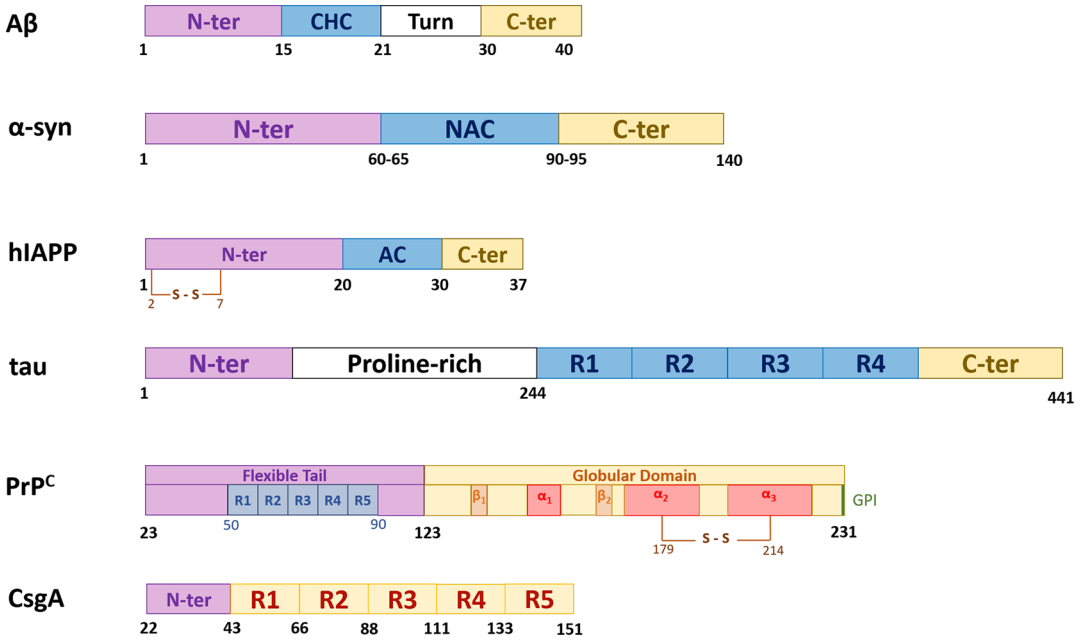

Figure 4. Schematic representation of the sequences of the amyloidogenic (poly)peptides discussed in this review. The relative residue boundaries are marked by the numbers. The sequence lengths are not up to scale. Notation. Aβ, amyloid-β peptide; α-syn, α-synuclein; hIAPP, human islet amyloid polypeptide; tau, tau protein; PrP^C cellular prion protein; CsgA, major curli subunit, N-ter, N-terminus; CHC, central hydrophobic cluster; C-ter, C-terminus; NAC, nonamyloid component; AC, amyloid core; R1−R5, repeat regions.

presence of the latter being considered the hallmark of Alzheimer's disease. The Aβ peptide exists in two dominant forms consisting of 40 (Aβ_{40}) or 42 residues (Aβ_{42}), respectively. The latter variant was shown to aggregate faster,[127] be more toxic,[128] and be the main species present in amyloid plaques.[129] The Aβ peptide consists of a highly unstructured N-terminus (first 15 residues) followed by a central hydrophobic cluster (CHC), and a hydrophobic C-terminus (last 10−12 residues); see Figure 4. Whether 40 or 42 residues long, the Aβ variants and the effect of mutations have been widely investigated by means of computer simulations; both atomistic and coarse grained, in explicit or implicit solvent.

Garcia and co-workers[100−103] investigated the accessible conformations of both Aβ alloforms and various mutations by using Replica Exchange Molecular Dynamics (REMD) simulations in explicit solvent. They showed that Aβ_{42} samples more conformations than its two residue shorter variant and that its C-terminus is also more structured. A study using a similar simulation protocol and carried out later by Velez-Vega and Escobedo confirmed their results and extended the analysis to investigate the structural differences between wildtype (wt) Aβ_{42}, the soluble GM6 (F19S and L34P) mutant, and the highly insoluble Dutch mutant (E22Q).[104] They identified that the main structural differences between the peptides arise in the diversity of the structures sampled in the N-terminus. They correlated the relative N-terminus rigidity of the monomers with their relative aggregation tendency; that is, only the soluble mutant showed a stable well-conserved β-hairpin in this region. The mutants showed transient ordered structures in their central hydrophobic components, yet no clear differences arise in the CHC and the C-termini to distinguish between the three peptides. On the other hand, Ball et al. found that the CHC of Aβ_{42} forms an antiparallel β-hairpin, while the CHC of Aβ_{40} interacts with the N-terminus forming a less populated antiparallel β-hairpin.[130] Furthermore, the two C-terminal residues of Aβ_{42} appear to control the differences in β-strand propensity.

The unstructured nature of the N-termini was observed in a molecular dynamics (MD) study carried out by Olubiyi and Strodel.[105] They identified an increased disorder in the 40 residue long variant as compared to its more toxic partner, which can transiently adopt helical or β-conformations. Furthermore, they showed that the protonation of the histidine residues in Aβ_{42} stimulates the interactions between the N- and C-terminus, leading to an increased β-sheet content, which may be the cause of fast aggregation kinetics in an acidic environment.

Vitalis and Caflisch made use of Monte Carlo simulations (temperature replica exchange) with the ABSINTH implicit solvation model[131] to analyze the free-energy surface of the monomeric Aβ_{42} and Aβ_{40} peptides.[106] They observed that the N-termini are disordered with a more pronounced flexibility for Aβ_{42}. The simulations showed a micelle-like architecture of the monomer, in which the hydrophobic residues are buried in a fluid-like core and shielded from solvent exposure by the charged and polar side chains, which form the micellar surface. Importantly, the charged side chains and in particular the dyad of acidic sidechains E22-D23 protrudes toward solvent in both Aβ variants. Recent solution state nuclear magnetic resonance (ssNMR) structures have confirmed the exposure of the acidic dyad[132] as predicted in the simulations.[106]

In a recent paper Roeder and Wales explored the conformational energy landscape of the truncated Aβ_{17-42} monomer in the attempt of finding structures that may be precursors of the fibril bound monomer.[133] They used the generalized Born implicit solvation model[134] to perform simulations and found a rugged energy landscape. The monomer is highly dynamic with the lowest energies recorded by conformations with helical segments, mainly in the ^{20}FAED^{23} and 29−33 ^{29}GAIIG^{33} regions, and β-structures, with contacts formed between residues ^{17}LVFFA^{21} and ^{30}AIIGL^{34}.

DOI: 10.1021/acs.chemrev.8b00731
Chem. Rev. XXXX, XXX, XXX−XXX

Table 1. Computational Studies of the Monomeric State[a]

Reference	Peptide	Model	Solvent	Method	Sampling[b]
Sgourakiset al.[100]	$A\beta_{42}$	AMBER94	TIP3P	REMD	0.78 μs
		AMBER96			0.78 μs
		AMBER MOD-PARM			0.78 μs
		OPLS			2.08 μs
		GROMOS	SPC		0.78 μs
	$A\beta_{40}$	OPLS	TIP3P		2.08 μs
Sgourakis et al.[101]	$A\beta_{42}$	AMBER99SB	TIP4P-Ew	REMD	11.7 μs
Rosenman et al.[102]	$A\beta_{42}$	OPLS-AA/L	TIP3P	REMD	52 μs
	$A\beta_{40}$				52 μs
Rosenman et al.[103]	$A\beta_{42}$	OPLS-AA/L	TIP3P-Ew	REMD	52 μs
		AMBER99SB-ILDM	TIP4P		52 μs
		CHARMM22*	TIP3P		52 μs
	$A\beta_{40}$	CHARMM22*	TIP3P		52 μs
Velez-Vega and Escobedo[104]	$A\beta_{42}$	OPLS-AA	TIP3P	REMD/APE	1.76 μs
	$A\beta_{42}$ (E22Q)				2.72 μs
	$A\beta_{42}$ (F19S&L34P)				1.44 μs
Ball et al.[103]	$A\beta_{42}$	AMBER99SB	TIP4P-Ew	MREE	0.2 μs
	$A\beta_{40}$				0.2 μs
Olubiyi and Strodel et al.[105]	$A\beta_{42}$	GROMOS43a2 + 53a6	SPC	MD	2 × 3.5 μs
	$A\beta_{40}$				2 × 3.5 μs
Vitalis and Caflisch[106]	$A\beta_{42}$	ABSINTH	ABSINTH	REMC	48 × 10^8 steps
	$A\beta_{40}$				48 × 10^8 steps
Mudlela et al.[107]	$A\beta_{42}$	AMBER99SB	TIP3P	US+DFT	370 ns
Meng et al.[108]	$A\beta_{42}$	AMBER99SB	TIP4P/2005	REMD	740 ns
	$A\beta_{40}$				743 ns
	$A\beta_{42}$	AMBER03ws			750 ns
	$A\beta_{40}$				750 ns
Ilie et al.[109]	α-syn_{35-55}	CHARMM27/CMAP	TIP3P	MetaD	300 ns
	α-syn_{56-67}				500 ns
	α-syn_{68-78}				500 ns
	α-syn_{79-87}				500 ns
	α-syn_{88-97}				500 ns
Allison et al. [110]	α-syn	CHARMM19	EEF1	MD	720 ns
			SASA		580 ns
			EEF1	PRE-MD	488 μs
Jonsson et al. [111]	α-syn	atomistic	implicit	MC	76.8 × 10^{10} steps
Yu et al.[112]	α-syn	PACE	MARTINI	MD	32 μs
	α-syn_{36-55}				60 μs
	α-syn_{36-55}(A30P)				32 μs
	α-syn_{36-55}(A53T)				32 μs
Nath et al.[113]	α-syn	Rosetta	implicit	ECMC	10^6 steps
		AMBER99SB	TIP4P-Ew	MD	474 ns
Zerze et al.[114]	hIAPP	AMBER03w	TIP4P/2005	REMD	8 μs
				BEMD	4.5 μs
Reddy et al.[115]	hIAPP	GROMOS96 53a6	SPC	REMD	740 ns
Chiu et al.[116]	hIAPP	GROMOS96 53a6	SPC	BEMD	400 ns
	hIAPP(A25P)				400 ns
	hIAPP(S28P-S29P)				400 ns
	hIAPP(A25P-S28P-S29P)				400 ns
Singh et al.[117]	hIAPP	GROMOS96 53a6	SPC	BEMD	300 ns
Larini et al.[118]	$\tau_{273-284}$	OPLS-AA	TIP3P	REMD	15.5 μs
	$\tau_{273-284}\Delta$K280				15.5 μs
Nath et al.[113]	τ	Rosetta	implicit	ECMC	5 × 10^6 steps
Luo et al.[119]	$\tau_{244-372}$	CHARMM27/CMAP	TIP3P	REMD	3.36 μs
	$\tau_{244-372}\Delta$R2				3.36 μs
De Simone et al.[120]	$PrPC_{125-230}$	GROMOS96	SPCE	REMD	1.2 μs
Chebaro and Derremaux[121]	$PrPC_{125-228}$	OPEP	implicit	MD	350 ns
	$PrPC_{125-228}$(T183A)				600 ns
Camilloni et al.[122]	$PrPC_{143-157}$	OPLS	TIP3P	PT-MetaD	2.4 μs
Huang and Caflisch[123]	$PrPC_{125-226}$	CHARMM36	TIP3P	MD+US	6.5 + 1.15 μs
	$PrPC_{125-226}$(Y169G)				1.3 + 1.15 μs

DOI: 10.1021/acs.chemrev.8b00731
Chem. Rev. XXXX, XXX, XXX−XXX

Table 1. continued

Reference	Peptide	Model	Solvent	Method	Sampling[b]
	$PrPC_{125-226}$(Y169A)				1 + 1.15 μs
	$PrPC_{125-226}$(Y169F)			US	1.15 μs
	$PrPC_{125-226}$(R164A)				1.15 μs
	$PrPC_{125-226}$(F175A)				1.15 μs
	$PrPC_{125-226}$(D178A)				1.15 μs
Caldarulo et al.[124]	$PrPC_{121-231}$	AMBER99SB*-ILDM+CHARMM22*	TIP3P	PT-WTE+MW MetaD	1.84 + 4.25 μs
	$PrPC_{121-231}$(Y169A)				1.84 + 4.25 μs
Tian et al.[125]	CsgA	ProFASi	implicit	MC	10^8 steps
DeBenedictis et al.[126]	CsgA	CHARMM36	TIP3P	MD	150 ns
	CsgB				150 ns

[a]Abbreviations. MD, molecular dynamics; REM/APE, replica exchange molecular dynamics all pairs exchange; MREE, multi reservoir replica exchange; MhREX, multiplexed Hamiltonian replica exchange; REMD, replica-exchange molecular dynamics; US, umbrella sampling; MetaD, Metadynamics; PRE-MD, paramagnetic relaxation enhancement distances used as ensemble-averaged restraints in molecular dynamics simulations; ECMC, experimentally constrained Monte Carlo; BEMD, Bias exchange metadynamics; PT-MetaD, Parallel tempering metadynamics. PT-WTE, biased ensemble sampled by well-tempered metadynamics when the energy is used as collective variable; MW MetaD, multiple walkers metadynamics. [b]Cumulative sampling over all replicas.

Mudedla et al. used umbrella sampling and density functional theory calculations to investigate the conformational free energy landscape of the ^{33}GLMVGGVVIA^{42} sequence in solution and near molybdenum disulfide nanosurfaces.[107] They found that the solvated monomer prefers to adopt helical structures, while the surface stabilizes random coil conformations, preventing the sequence from forming β-rich aggregates and therefore reducing the fibrillization process.

Meng et al. used both conventional and replica exchange molecular dynamics simulations to complement their experimental studies and explore the conformations of Aβ_{42} and Aβ_{40} in explicit solvent.[108] They found that both peptides populate mainly random coil conformations with Aβ_{42} being slightly more compact than Aβ_{40}. Additionally, they identified small populations of short-lived collapsed and structured states, which differ from one peptide to the other in the contacts that are being formed. For Aβ_{40} contacts are formed between D23 and K28, while for Aβ_{42} the interaction hotspots are between Y10 and F4. Furthermore, only the longer polymorph forms long-range terminal contacts, which give rise to a hairpin arrangement.

To sum up, the two alloforms of Aβ visit transient β-hairpin conformations, with the Aβ_{40} variant experiencing more pronounced and well defined states than Aβ_{42}. The collapse of the peptides into semiordered structures is driven by the hydrophobic residues. For detailed reviews of the simulation studies of the Aβ polymorphs and their aggregates, we refer the reader to refs 135−138.

3.1.2. α-Synuclein. α-Synuclein is a 140 residue intrinsically disordered protein found mainly in the neuronal tissue. It has little or no secondary structure, low overall hydrophobicity, and a high net charge. Based on its amino acid sequence (Figure 4) three main regions can be defined: an amphipathic N-terminus (first 60 residues), a hydrophobic nonamyloid-β component (following 30 amino acids referred to as NAC), and a highly negatively charged C-terminus (last 50 residues). Depending on the surrounding environment α-synuclein can adapt its secondary structure; that is, it is mainly disordered in an aqueous solvent, or it curls into an α-helix near membranes[139] or stretches into β-sheets in fibrils or amyloids.[140] Due to the versatility of α-synuclein, its relatively large size, and its high net charge, it is difficult to characterize by computational means. Therefore, most studies either focus on fragments or use enhanced sampling methods, implicit solvent simulations, and/or coarse-grained representations.

Ilie et al. used metadynamics to dissect the conformational landscape of the hydrohpobic core of α-synuclein in explicit solvent.[109] Starting from the solid state NMR structure of the orthogonal Greek key topology of an α-synuclein filament (PDB ID: 2N0A[141]) they isolated the fragments building up the fibrillar core, i.e., segments 35−55, 56−67, 68−78, 79−87, and 88−97. They found that each fragment independently has a preference of attaining non-β conformations, and they showed that the fibrillar structure is stabilized by interactions with neighboring strands. By combining the information from individual fragments they demonstrated that the core of α-synuclein (residues 35−97) has to overcome a high conformational free energy barrier in order to attain the fibrillar β-rich structure, which is stabilized predominantly by hydrophobic contacts and hydrogen bonds.

Allison et al. used distances derived from spin label NMR measurements as restraints to their molecular dynamics simulations to obtain the free energy landscape of α-synuclein in implicit solvent.[110] They showed that the N-terminus has a slightly higher propensity to adopt helical conformations than the C-terminus. Furthermore, monomeric α-synuclein collapses into conformations with a radius of gyration larger than that of compact globular states, indicating that the protein becomes more expanded. Using implicit solvent atomistic Monte-Carlo simulations, Jonsson et al. add to the results of Allison et al.[110] the presence of two distinct phases for α-synuclein in solution:[111] a highly disordered one and one rich in β-content that shows a fold comparable to the one found in amyloid fibrils.

A variety of coarse-grained models have been employed to simulate α-synuclein . Some of them lump together the atoms within a residue while others are even coarser and consider one bead for several residues. Yu et al. used a united atom model (PACE—proteins with atomic details in coarse-grained environment[142]) and the MARTINI solvent model[143] to investigate the role of β-hairpin formation in α-synuclein aggregation.[112] In their model the essential structural features of the protein are preserved; i.e., packing of the side chains and directionality of hydrogen bonding. They showed that the β-hairpin conformation includes two antiparallel β-strands comprising residues 38−44 and 47−53, for systems consisting of either wild type α-synuclein or A30P and A53T single-point mutations. The mutations are shown to accelerate the formation

DOI: 10.1021/acs.chemrev.8b00731
Chem. Rev. XXXX, XXX, XXX−XXX

of β-hairpin conformations, suggesting that they may initiate the aggregation of α-synuclein. This finding is consistent with experimental results.[42]

Another approach introduced by Nath et al. used distances extracted from single-molecule fluorescence measurements as constraints in excluded volume Monte Carlo simulations.[113] The peptide backbone is represented by an all atom model while a single bead is used for each side chain, as modeled in Rosetta.[144] They investigated the polymeric properties of the protein and showed that at low pH α-synuclein becomes more compact.

Overall it is difficult to extract common observations from the simulation studies of full-length monomeric α-synuclein. Its broad conformational space, limited amount of regular secondary structure, and the influence of the environment are major hurdles for reaching convergence of sampling by atomistic models.

3.1.3. Islet Amyloid Polypeptide (IAPP). Islet amyloid polypeptide (IAPP or amylin) is a 37-residue hormone implicated in type II diabetes. Human amylin (hIAPP) is prone to form amyloids yet is largely disordered in aqueous solution.[145] For the full biological activity of amylin the formation of a disulfide bridge between residues C2 and C7 is required (Figure 4).[146] We refer the reader to the reviews in refs 147−149 for a detailed overview of models, methods, and force fields, physicochemical properties, functionality, etc. Below we will focus solely on the more recent advances. Briefly, the conformations hIAPP can be grouped in two main categories: an aggregation-prone one in which β-rich states are present and a physiological one consisting mainly of helix−coil conformations.[147]

Zerze et al. used enhanced sampling techniques to explore the free energy landscape of the amylin monomer.[114] Their results, obtained from both temperature replica exchange molecular dynamics and bias-exchange metadynamics in explicit solvent, are complementary along a range of collective variables. They found a rugged free energy landscape populated largely by unstructured conformations, moderately by helical structures (20%), and very little by β-rich motifs (6%), consistent with previous studies[147] and across various force fields.[150] These results are however in contrast to earlier findings based on all-atom replica exchange molecular dynamics which showed that hIAPP adopts 40% β-hairpin conformations, which are highly stable.[115] In the context of experimental findings, the β-hairpin has been proposed to be an on-pathway conformation toward attaining the fibrillar structure.[151]

The formation of β-hairpins has been identified also by Chiu et al. in their bias-exchange metadynamics simulations.[116] They explored the conformational free energy landscapes of hIAPP, the A25P, S28P-S29P, and A25P-S28P-S29P (pramlintide) mutations. They sampled mainly α-helices in the N-terminus, unstructred coils, and β-hairpins. They showed that the formation of β-hairpins is favored over the helical structures for wildtype hIAPP. With increasing number of proline mutations the free energy difference between the two states decreases until the β-conformations are no longer favored; that is, for pramilintide the α-helix is favored thermodynamically. This study was extended by Singh et al. to examine the transition pathways from helical to β-hairpin and unstructured coil conformations.[117] They identified two mechanisms of interconversion which exhibit comparable free energy barriers: direct transition from α-helical to β-hairpin conformations (barrier of 18.5 kJ/mol) or transformation via random coil structures (26.4 kJ/mol). In the first, a zipping mechanism has been identified, in which residues ^{16}AL^{17} and ^{23}TPIES^{27} initiate the formation of the β-turn. In the second, residue V15 triggers the loss of helical character followed by sampling of β-hairpin conformations.

A number of observations arise from the aforementioned studies. First, similar to Aβ, the amylin monomer shows formation of β-hairpins which are suggested to be on-pathway toward attaining fibrillar structures. Second, hairpin-like conformations form via structural transitions from helical arrangements. Third, prolines act as structure breakers reducing the stability of the β-hairpins.

3.1.4. Tau Protein. Tau is a 441 residue, highly soluble microtubule associated protein found in the neuronal tissue. In its aggregated form it has been connected to a number of tauopathies. Tau can hyperphosphorylate, aggregate, and form paired and straight helical filaments which present the cross-β motif characteristic of amyloids. These structures have been reported to be the second form of insoluble aggregates associated with Alzheimer's disease. Tau consists of four imperfect repeats (labeled R1 to R4) flanked by a proline-rich projection domain and the C-terminal segment (Figure 4). Under physiological conditions the repeats bind to axonal microtubules, stabilizing their structure. The projection domain gives rise to a long-range entropic repulsive force providing spacing between adjacent microtubules (MTs).[152] Under abnormal conditions the repeats have been identified as the primary region involved in forming the β-rich structure in the paired helical segments.[153] The size and flexibility makes it difficult to investigate the monomeric properties and accessible states of full length tau. Therefore, the focus is mainly on a reduced number of residues and various mutations.

Ciasca et al. performed short (6 ns) molecular dynamics simulations of the reconstructed tau monomer in explicit water at 333 K to complement their small-angle X-ray scattering (SAXS) experiments.[152] They observed a reduction of the radius of gyration (R_g) to 4.6 nm at 333 K as compared to earlier studies reporting 6.0 nm at 300 K.[154] Given the present computational power the length of these simulations could be extended to obtain statistically more relevant results. As a matter of fact, they later used both MD and metadynamics of 1000 conformers over a length of 10 ns and obtained slightly different values, *i.e.*, ∼6.5 nm at 293 K and ⩽5.7 nm at 333 K.[155]

Larini et al. used REMD in explicit water to investigate the ^{273}GKVQIINKKLDL^{284} wildtype and the ΔK280 mutant sequences.[118] The fragments contain the ^{275}VQIINK^{280} sequence which had been previously proposed to increase the aggregation propensity of tau.[156] In their study, also complemented by experimental findings, Larini et al. show that both monomers have a preference toward attaining compact conformations, with a slightly higher tendency of the mutant to adopt extended conformations.

Nath et al. used distance constraints extracted from single-molecule fluorescence experiments for their Monte Carlo simulations to calculate the polymeric properties of tau.[113] They measured a mean radius of gyration of 5.1 ± 0.5 nm at 293 K, which is slightly smaller than the one measured by Ciasca and collaborators[155] Furthermore, they investigated the effect of polyanion heparin, an aggregation enhancer of tau and determined an increased radius of gyration of 6.0 ± 0.6 nm. Heparin eliminates the long-range contacts between the N- and C-termini resulting in the increase of R_g.

Luo et al. explored the conformational ensembles of the microtubule binding region, *i.e.*, those sequences R1-R4(wt) and

DOI: 10.1021/acs.chemrev.8b00731
Chem. Rev. XXXX, XXX, XXX−XXX

R1-R4(ΔR2), by REMD simulations.[119] They characterized the conformational landscape as "a mixture of disordered and ordered structures" with the ordered states being highly unstable in solution. They identified the critical ordered states, the ones prone to adopt β-conformations and possibly act as aggregation centers for paired helical filaments, to be ^{275}VQIINK^{280} in R2 and ^{306}VQIVYK^{311} in R3 of wt, and ^{306}VQIVYK^{311} in R3 of the truncated mutant.

3.1.5. Prion Protein. Prions (proteinaceous infectious particle) are associated with mad cow disease and scrapie in cattle and Creutzfeldt-Jakob disease in humans.[157,158] These diseases, also called transmissible spongiform encephalopathies (TSEs), are linked to the conformational conversion of the cell-surface glycoprotein PrP^{c} into the toxic isoform PrP^{Sc}.[158] In its mature form, monomeric PrP^{c} consists of residues 23−231, as the first 22 residues are cleaved during trafficking and amino acids 231−253 are replaced by a glycosyl-phosphatidylinositol-anchor.[159] The remaining residues form an unstructured flexible tail (residues 23−123) and a globular domain (residues 124−230). The latter contains three α-helices, comprising residues 143−155 (α_1), 171−190 (α_2), and 199−226 (α_3), and an antiparallel β-sheet formed by residues 128−131 (β_1) and 160−162 (β_2)[158−160] (Figure 4).

De Simone et al. explored the free energy profile of the globular domain of the prion of the sheep by replica exchange molecular dynamics simulations in explicit solvent.[120] Their results showed that the three α-helices are structurally stable, yet interesting aspects arise in the global arrangement of the protein. In particular, the disulfide bond formed between residues C179 and C214 contributes to the structural stability of the α_2-α_3 cluster. The α_1 helix, however, shows a high degree of flexibility with respect to α_2−α_3. The main difference arises in the packing of α_1 to the rest of the globular domain; that is, it can be closely attached to the globular domain as well as completely detached from it. Thus, the mobility of α_1 may form a possible pocket for the binding of small molecules that could stabilize the globular structure to prevent aggregation.

Chebaro and Derreumaux investigated the structural and dynamical dimerization properties of the globular domain $PrP^{C}_{125-228}$ and the effect of the T183A Creutzfeldt-Jakob disease variant by performing coarse grained molecular dynamics simulations in implicit solvent at physiological and at high temperatures.[121] Their results showed structural stability for both variants, with a slight increase in flexibility recorded for α_3 and the two β-strands in the case of the mutant. They found that with increasing temperature the wt-protein maintains its tertiary structure, while the mutant undergoes structural changes with partial disorder in the α_2-α_3 segment. This disorder is compensated by the formation of transient helices in the β_1−α_1-β_2 region, in the β_2−α_2, and in the α_2−α_3 loops. Additionally, they found that in all cases α_1 maintains its helical structure despite being detached from the rest of the construct, consistent with the findings of De Simone et al.[120]

Camilloni et al. investigated the conformational free energy landscape of the α_1 containing sequence ^{143}ADYEDRYYR-ENMHRY^{157} of the prion of human by using metadynamics combined with NMR measurements.[122] Their results show that the peptide samples largely two conformations, populating mainly α-helical structures in equilibrium with random coils. The conformational free energy difference between these states ranges from 7.1 to 15.6 kJ/mol, depending on the α-helical conformation, with the coil state being more favorable.

Huang and Caflisch performed molecular dynamics and umbrella sampling simulations of the globular domains of PrP^{c} (residues 125−226) to investigate the conformational plasticity of the β2-α2 loop (^{165}PVDQYSNQNNF^{175}) and six point mutants (Y169G, Y169A, Y169F, R164A, F175A, and D178A).[123] They found that wild type PrP^{c} has a higher free energy barrier to convert a segment of the β2-α2 loop from a 3_{10}-helical to a β-turn conformation than any of the mutants. They showed that this transition is hampered by residue Y169, which stabilizes the 3_{10}-helical turn. Furthermore, their results indicate that the solvent exposure of Y169 is mediated by interactions with V166, F175, Y218, E221, and Y225 in the β-turn conformation.

Caldarulo et al. used parallel tempering in the well-tempered ensemble version and metadynamics to explore the conformational heterogeneity of the β2-α2 loop of the mouse and the mutated Y169A conformer.[124] They identified four main conformational preferred states, two of which have a helical character and two sampling mainly β-turns. In particular, they showed that the differences between the two helical basins arise from the different orientation of the carbonyl group of residue Y169 and that for both mutants the highest free-energy barrier corresponds to the transition from helical to β-states. Consistent with the results of Huang and Caflisch,[123] Caldarulo et al. provided further evidence that the side chain of Y169 contributes to the stabilization of the helical turn in the wild type protein.

3.1.6. Curli. Curli are amyloid fibrils of biological importance that contribute to autoimmunity activation,[161] biofilm formation, or cell adhesion.[11] The principal building block of curli is CsgA, a 151 residue long protein found in *E. coli*. CsgA is secreted through the outer membrane by protein CsgG and nucleated by CsgB to aggregate into amyloid fibrils following a β-helix-like structure.[12,162] The CsgA protein consists of a 22-residue N-terminus (N-ter) required for outermembrane secretion, and a C-terminal amyloid core domain (Figure 4). The first 21 amino acids are cleaved as CsgA transverses the inner membrane.[163] The amyloid core of CsgA comprises five quasi-identical repeats of 19−23 residues each (R1 - residues 43−65, R2 - residues 66−87, R3 - residues 88−110, R4 - residues 111−132, and R5 - residues 133−151), and minor sequence variations influence largely the aggregation capabilities of the protein.[12,164]

Tian et al. used implicit solvent Monte Carlo simulations to explore the thermodynamics of the individual CsgA sub-repeats.[125] Their results showed that the five repeats are mainly unstructured in the monomeris state, with transient β-hairpins being sporadically sampled. They extend the study toward the investigation of the dimerization process which we discuss in Section 3.2.1.1.

DeBenedictis et al. built four models of both CsgA and CsgB using various web servers (Robetta,[165] FALCON@home,[166] Quark,[167] RaptorX[168]) and then applied molecular dynamics simulations in explicit solvent to refine the proposed structures.[126] They found that the structures using Robetta and RaptorX correspond to β-helical arrangements. Furthermore, the predicted model structures are kinetically stable on a time scale of 150 ns.

3.2. Amyloid Aggregation

In the following subsections we will review simulation studies of the key phases of amyloid aggregation, *i.e.*, nucleation, growth, and saturation. The theoretical background of the kinetics of

DOI: 10.1021/acs.chemrev.8b00731
Chem. Rev. XXXX, XXX, XXX−XXX

amyloid growth has been widely explored and will not be reviewed here.[169−171]

3.2.1. Lag Phase and Primary Nucleation. In the lag phase soluble monomers undergo conformational changes, adopt folded and unfolded structures as described in Section 3.1, and/or bind to each other. This phase is generally the longest one ranging from milliseconds to days *in vitro*, and up to decades *in vivo*. Its length depends on the concentration of the amyloidogenic (poly)peptide, and buffer conditions, i.e., pH, temperature, salt concentrations, *etc*. Given the long time scales, in the attempt of finding the mechanisms behind nucleation, primarily coarse grained models have been developed and used. At high levels of coarse graining (multiple residues per particle) the generic nature of the process is captured, meaning the models describe, though crudely, a wide range of proteins and peptides. With this in mind we proceed with detailing the coarse-grained models in order of their granularity level from coarser to finer.

The model proposed by the Frenkel group describes the Aβ monomers as single spherocylinders with attractive patches able to switch between two states: a soluble conformation and a β-prone state similar to the one found in amyloid fibrils (Figure 5(a)).[172−175] They used a free energy difference of +15 kT for a particle to transform from a soluble state to a β-prone state and dynamic Monte Carlo simulations to propagate the dynamics of the system. To differentiate between the two states, they varied the interaction energies between the patches. In their study they showed that dimers and trimers are very dynamic, as they can interconvert between different aggrgation states or dissociate into monomers.[173] On the other hand, they found that tetramers always evolve into fibrils and that the critical nucleus consists of about four aggregated monomers. In a more recent study, using a slightly modified version of the same model, they investigated the effect of monomer concentration on the aggregation pathway.[174] They found that at high concentration monomers can spontaneously transform and aggregate into a fibril, a process referred to as one-step-nucleation, and at low concentrations fibrillar nucleation is preceded by the formation of oligomeric intermediates, two-step-nucleation. Additionally, they studied the temperature dependence of the nucleation and found a nonmonotonic dependence of the nucleation rate on the temperature.[175] First, at low temperatures the nucleation rate decreases with temperature and occurs mainly via 2SN. With increasing temperature the nucleation rate starts to increase and 1SN becomes predominant.

The Briels group developed a polymorph particle model inspired by the amyloidogenic core of α-synuclein[176] (Figure 5(b)). They created a particle that can alternate between a disordered state and a β-prone state by introducing a parameter to describe the internal state of the protein. More specifically, the disordered state is modeled as a single soft sphere with weak isotropic interactions, while the ordered β-prone conformation is represented as a single spherocylinder with strong directional interactions. Brownian dynamics was used to simulate the dynamics and the internal states of the particles.[177] They showed that the polymorph particles spontaneously form both oligomers of particles in the disordered state and fibrils of particles in the folded state. Furthermore, by regulating the internal parameter, *i.e.*, changing the internal free energy barrier of the particles, they found that amyloid aggregation can occur in one step, driven by the simultaneous transformation and binding of two particles in the β-prone state, or in two steps, in which aggregates can transform from one type into another. Additionally, they proposed that the conversion of oligomers into new fibrils is enhanced in the presence of mature fibrils, a process that may explain the rapid generation of nuclei and implicitly lead to an increased growth rate of fibrils. We will discuss the extension of the model and the relevant details in Section 3.2.2.

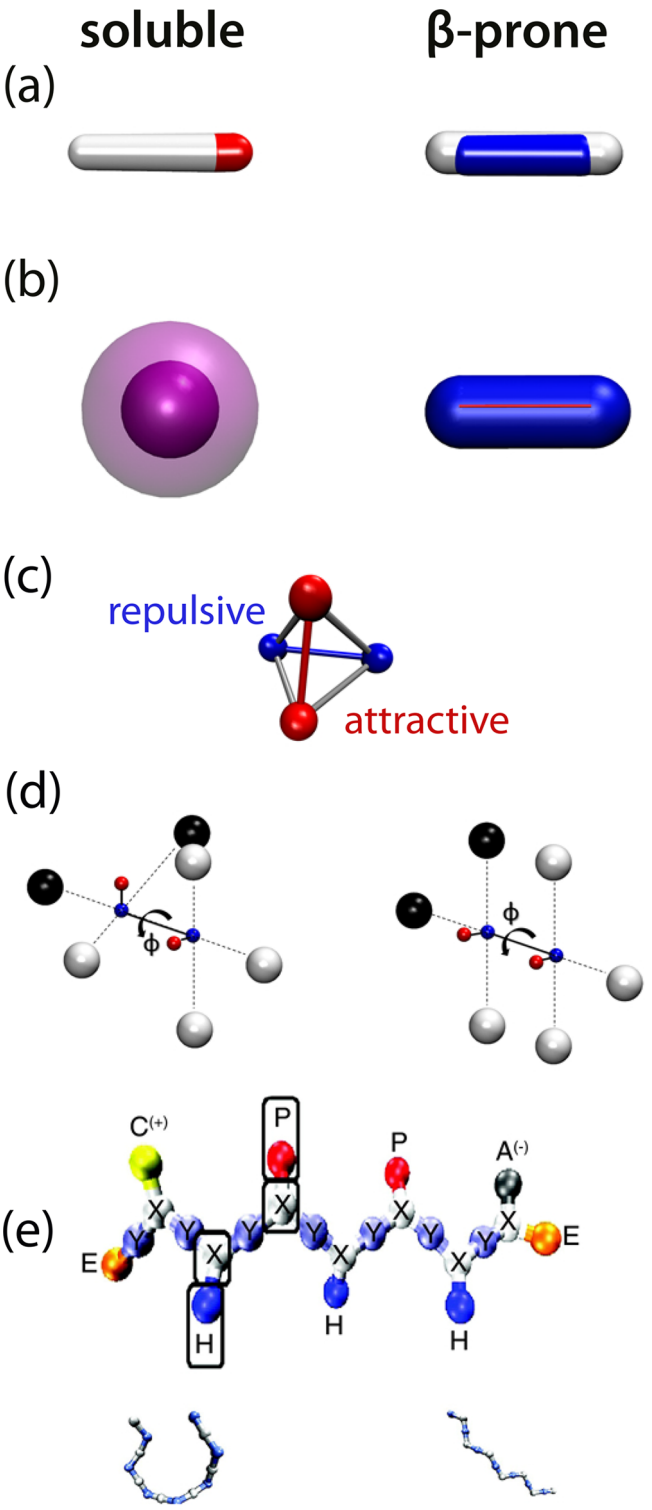

Figure 5. Coarse grained models used to study the lag phase of amyloid growth introduced in the groups of (a) Frenkel, (b) Briels, (c) Urbanc, (d) Caflisch, and (e) Shea (Adapted with permission from ref 147. Copyright 2014 American Chemical Society).

DOI: 10.1021/acs.chemrev.8b00731
Chem. Rev. XXXX, XXX, XXX−XXX

The Urbanc lab developed a rigid tetrahedron representation with two hydrophobic (attractive) and two hydrophilic (repulsive) beads (Figure 5(c)).[178] They combined it with discrete MD simulations in implicit solvent to investigate the aggregation pathways of their molecules. The beads are characterized by effective attractive and repulsive potentials. Their ratio gives rise to η, the sole model parameter used throughout the simulations. For purely attractive monomers (η = 0) the molecules simply aggregate into large oligomers, whereas at η = 0.5 the process becomes more complex. Their results showed the coexistence of two types of aggregates: quasi-spherical oligomers and elongated aggregates. The elongated aggregates grow by monomer addition, while the quasi-spherical oligomers vanish as the simulations evolve. Compared to other coarse grained models the monomer introduced here is rigid and therefore trapped in a β-prone state, and hence does not capture the conformational entropy of an amyloidogenic peptide. Nevertheless, the efficiency of the model is higher when studying fibrillar growth (Section 3.2.2).

The Caflisch group introduced a phenomenological model of an amphipathic polypeptide as a ten bead molecule with one internal dihedral degree of freedom to convert between amyloid-forming (β-prone) and amyloid-protected (soluble) states (Figure 5(d)).[179−181] In this model four beads represent the backbone of the molecule while the remaining six approximate the side chains. The switching between the two states is achieved by changing the potential of the backbone dihedral angle according to an amyloidogenicity parameter. The simulation results showed that the amyloid-protected-monomer nucleates only at concentrations larger than the critical micelle concentration, whereas the amyloid-forming-monomer nucleates even at lower concentrations. Furthermore, peptides with a high amyloidogenic tendency nucleate without intermediates, whearas low amyloidogenic peptides nucleate either through micelle-sized oligomers or transient oligomers.[179]

The Shea model contains three beads per amino acid, two for the backbone and one for the side-chain, capturing the hydrophobic, polar, or charged nature of the residue (Figure 5(e)). To regulate the β-propensity in the monomeric form, a dihedral potential is introduced to constrain all beads.[182,183] A peptide becomes more rigid, *i.e.*, more β-prone, with increasing value of the dihedral energy constant. Consistent with the other coarse-grained models, they show that the resulting aggregates depend on the affinity of the peptides to form β-rich structures. β-Prone peptides, *i.e.*, very rigid, exist mainly in fibrillar states, and very flexible molecules accumulate into amorphous aggregates. Peptides with intermediate flexibility can coexist in aggregates ranging from amorphous accumulations to β-barrels and antiparallel double- and triple-layered fibrils.

We refer the interested reader to a number of reviews focused on experimental, theoretical, and simulation aspects of the lag phase in refs 40, 93, and 184. Since lattice models[185,186] have already been reviewed in the latter, we will not discuss them again in the present review. Most of these studies refer to different proteins and peptides, yet as discussed above, the results are consistent across the different models and simulation methods emphasizing the generic behavior of amyloid forming peptides.[187] Furthermore, these studies inform on the nucleation mechanisms at lower resolutions and across time scales. Nevertheless, higher resolution models are needed in order to propose successful inhibition tools, especially in light of the current hypothesis that the oligomers may be the toxic species in neurodegenerative diseases and since the peptide sequence can affect the specific dynamics of amyloid formation.

In an attempt to elucidate the details of the lag phase at atomistic resolution, Baftizadeh et al. started from single disordered oligomers in explicit solvent and used bias-exchange metadynamics simulations to explore their transformation into amyloid like structures.[188,189] They investigated 18-mers of polyvaline (eight residues)[188] and of Aβ_{35-40} peptides,[189] both yielding similar results. They reconstructed a multidimensional conformational free energy landscape as a function of three variables, which quantify the parallel and antiparallel arrangements of β-strands within a peptide layer and the steric zipper packing of adjacent β-strands. They identified that the lowest point in the free energy landscape corresponds to disordered aggregate structures. Higher plateau regions in the free energy profile are populated by structures rich in antiparallel β-sheet aggregates followed by a small minimum, separated from the rest by a barrier, in which conformations rich in parallel β-strands are present. The path followed by the peptides in the space projected onto the collective variables is intricate. The disordered aggregate first favors the formation of antiparallel β-sheets followed by the formation of a few parallel β-sheets. Once the system has nucleated, *i.e.*, a sufficiently large number of peptides are in the parallel arrangement, the free energy decreases toward a minimum, which is separated from the other states by a free energy barrier.

3.2.1.1. Dimers. The smallest aggregates associated with cellular toxicity are dimers.[23,71] Therefore, understanding their structural and dynamic properties is of great interest. Here we present the dimerization mechanisms (Table 2) identified by molecular simulations for the reviewed peptides.

Chebaro et al. studied the dimerization thermodynamics and the structural conversions of Aβ_{16-35} by means of replica exchange molecular dynamics simulations in implicit solvent and using the OPEP coarse force-field.[190] They started from a random dimeric structure and evolved 20 replicas over a total of 12 μs. From a structural perspective, they found that the dimer is scarcely populated by α-helical or β-sheet-like structures. Next, they identified that the ^{18}VFF^{20} hydrophobic patch has a higher affinity toward attaining β-sheet-like structures than ^{31}IIGLM^{35}. The Aβ_{16-35}-dimer populates various states; there is a transition from an antiparallel β-sheet construct formed by residues ^{18}VFFA^{21} and ^{17}LVFF^{20} of the two peptides into a disordered dimer with parallel orientations of these fragments and the 31−35 sequence. This study was later extended to include the full Aβ_{42} dimer, the S8C mutant,[191,193] as well as Aβ_{40},[194,196] and the Aβ_{40} (D23N) mutant.[192] They showed that the highest number of inter- and intramolecular contacts is maintained in the region of hydrophobic patches for all mutants, *i.e.*, CHC and C-terminus.[193] The peptides record an increase in the averaged total β-strand propensity upon dimerization, with the highest increment recorded for the Aβ_{42} peptide. Additionally, they extended their protocol to understand the effect of point mutations on the propensity of Aβ_{40} homo- and heterodimers, *i.e.*, Aβ_{40}(A2V) − Aβ_{40}(A2V) and Aβ_{40} − Aβ_{40}(A2T) and Aβ_{40} − Aβ_{40}(A2V), respectively.[195,196] They identified two different dimerization pathways, a slow one for homodimers and a fast one for heterodimer. They defined the fast-pathway to be predominant when the interpeptide distance is below 0.8 nm and the peptides have a radius of gyration between 0.95 and 1.25 nm or record an interpeptide van der Waals energy below −107 kcal/mol. Furthermore, they showed that the transition from hydrophobic intrapeptide to interpep-

DOI: 10.1021/acs.chemrev.8b00731
Chem. Rev. XXXX, XXX, XXX−XXX

Table 2. Computational Studies Focusing on Dimerization[a]

Reference	Dimer	Model	Solvent	Method	Sampling[b]
Chebaro et al.[190]	$A\beta_{16-35} - A\beta_{16-35}$	OPEP	implicit	REMD	12 μs
Man et al.[191]	$A\beta_{42} - A\beta_{42}$	AMBER99SB-ILDN	TIP3P	REMD	25 μs
	$A\beta_{42}$(S8C) − $A\beta_{42}$(S8C)				25 μs
Cote et al.[192]	$A\beta_{40} - A\beta_{40}$	OPEP	implicit	HT-REMD	27.5 μs
	$A\beta_{40}$(D23N) − $A\beta_{40}$(D23N)				27.5 μs
	$A\beta_{42} - A\beta_{42}$				27.5 μs
Man et al.[193]	$A\beta_{42} - A\beta_{42}$	OPLSAA	TIP3P	REMD	36 μs
		CHARMM22*			36 μs
		AMBER99SB-ILDN			36 μs
		AMBERSB14			36 μs
Tarus et al.[194]	$A\beta_{40} - A\beta_{40}$	CHARMM22*	TIP3P	REMD	24 μs
Nguyen et al.[195]	$A\beta_{40}$(A2V) − $A\beta_{40}$(A2V)	CHARMM22*	TIP3P	REMD	24 μs
	$A\beta_{40} - A\beta_{40}$				24 μs
	$A\beta_{40} - A\beta_{40}$ (A2V)				24 μs
Nguyen et al.[196]	$A\beta_{40} - A\beta_{40}$ (A2T)	CHARMM22*	TIP3P	REMD	24 μs
Cao et al.[197]	$A\beta_{40} - A\beta_{40}$	PACE	MARTINI	REMD	2.7 ms
Sharma et al.[198]	$A\beta_{42} - A\beta_{42}$	CHARMM36	TIP3P	MD+REMD	1.5 μs
	$A\beta_{42} - A\beta_{42}$ (A2V)				1.5 μs
	$A\beta_{42}$(A2T) − $A\beta_{42}$ (A2T)				1.5 μs
	$A\beta_{42}$ (A2T) − $A\beta_{42}$(A2V)				1.5 μs
	$A\beta_{42}$ (A2V) − $A\beta_{42}$(A2V)				1.5 μs
Das et al.[199]		OPLS-AA	TIP3P	REMD	51.2 μs
	$A\beta_{42} - A\beta_{42}$ (A2T)				51.2 μs
Barz et al.[200]	$A\beta_{40} - A\beta_{40}$	OPLS/AA	GBSA	MD	2.5 μs
	$A\beta_{42} - A\beta_{42}$				2.5 μs
Zoete et al.[201,202]	$insulin^p$ − $insulin^p$	CHARMM22	TIP3P	MD	5 ns
Raghunathan et al.[203]	$insulin^p$ − $insulin^p$	CHARMM22/CMAP, CHARMM36	TIP3P	MD, TI	10, 100, 4 ns
	$insulin^p$(F24G) − $insulin^p$(F24G)				10, 100, 2 ns
	$insulin^p$(F24A) − $insulin^p$(F24A)				10, 100, 2 ns
	$insulin^p$(F24D-A) − $insulin^p$(F24D-A)				10, 100, 2 ns
	$insulin^p$(ΔF25) − $insulin^p$(ΔF25)				10, 100, 2 ns
Dupuis et al.[204]	hIAPP − hIAPP	AMBER96	GB	MD	2.4 μs
	rIAPP − rIAPP				2.4 μs
Qi et al.[205]	$hIAPP_{11-25}$ − $hIAPP_{11-25}$	OPLS-AA/L	TIP4P	MD, REMD	12, 12 μs
Qiao et al.[205]	$hIAPP_{11-25}$ − $hIAPP_{11-25}$	OPLS	TIP4P	MD	90 μs
Ilitchev et al.[206]	$hIAPP_{1-8}$ − $hIAPP_{1-8}$	OPLS-AA	TIP3P	REMD	3.6 μs
Guo et al.[207]	hIAPP − hIAPP	AMBER99SB*-ILDN	TIP3P	BE-MD	3 μs
Larini et al.[118]	$\tau_{273-284} - \tau_{273-284}$	OPLS-AA	TIP3P	REMD	7.92 μs
	$\tau_{273-284}$ΔK280 − $\tau_{273-284}$ΔK280				7.92 μs
Ganguly et al.[208]	$\tau_{273-284} - \tau_{273-284}$ΔK280	OPLS-AA	TIP3P	REMD	≈18 μs
	$\tau_{273-284} - \tau_{306-317}$				≈18 μs
	$\tau_{273-284}$ΔK280 − $\tau_{306-317}$K280				≈18 μs
	$\tau_{306-317} - \tau_{306-317}$				≈19 μs
Chebaro and Derremaux[121]	$PrP_{125-228} - PrP_{125-228}$	OPEP	implicit	MD	180 ns
	$PrP_{125-228}$(T183A) − $PrP_{125-228}$(T183A)				320 ns
Chamachi and Chakrabarty[209]	$mPrPC_{124-226} - mPrPC_{124-226}$	Gromos54a7, AMBER99SB-ILDN	SPC	REMD	38.4, 38.4 μs
Tian et al.[210]	CsgA − CsgA	ProFASi	implicit	MC	$64 \times 3 \cdot 10^6$ steps
Tian et al.[125]	CsgA − CsgA	ProFASi	implicit	MC	10^8 steps

[a]Abbreviations. MD, molecular dynamics; REMD, replica-exchange molecular dynamics; HT-REMD, Hamiltonian and temperature replica exchange molecular dynamics; TI, thermodynamic integration; MC, Monte Carlo. [b]Cumulative sampling over all replicas.

tide interactions leads the transformation from slow- to fast-pathway dimers.

Along the same lines the Belfort group performed MD and REMD simulations in explicit solvent of $A\beta_{42}$ homo- and heterodimers, *i.e.*, $A\beta_{42}$ - $A\beta_{42}$, $A\beta_{42}$ - $A\beta_{42}$(A2V), $A\beta_{42}$(A2T)-$A\beta_{42}$(A2T), $A\beta_{42}$(A2T)- $A\beta_{42}$(A2V), and $A\beta_{42}$(A2V)-$A\beta_{42}$(A2V), to understand the relationship between the N-termini and dimer toxicity.[198,199] They found that the toxic dimers (containing A2V mutation) record frequent contacts between the N-termini of the monomers, while protective dimers (A2T) have more flexible N-termini.[198] Additionally, they found that the $A\beta_{42}$ - $A\beta_{42}$(A2T) heterodimer is more disordered than the wild-type $A\beta_{42}$ homodimer, leading to a reduced secondary structure content and a weak intermolecular interface.[199]

DOI: 10.1021/acs.chemrev.8b00731
Chem. Rev. XXXX, XXX, XXX−XXX

Cao et al. investigated the mechanisms of dimerization for Aβ_{40} by using a hybrid resolution model (PACE).[197] In particular, they built a Markov state model (MSM) to investigate the formation of β-hairpins and stuctures similar to those sampled in fibrils, but in dimeric systems. Upon studying the dimerization pathways, they found that β-hairpin aggregates follow a different route than fibril-like dimers. The formation of β-hairpin dimers, comprising residues 16−35, occurs via one-step-nucleation; that is, two peptides simultaneously sample this conformation in solution, and they randomly meet and bind, preserving the β-hairpin conformation. This process occurs on a time scale of about 200 μs, which is much faster than the aggregation of fibril-like dimers (25.8 ms). These were found to form due to the binding of two monomers in random conformations followed by their structural rearrangement into the fibrillar topology, which is only marginally sampled by the soluble monomers. Their results indicate that aggregation is initiated by nonspecific hydrophobic interactions followed by a rapid replacement of intramolecular contacts with intermolecular contacts. Next, the peptides unfold while undergoing structural rearrangements. They continue to break the intramolecular contacts and start to form parallel, in-register contacts, characteristic of fibrillar structures. While additional cross-β sheets form, the peptide ensemble continues to unfold. The radius of gyration records fluctuations, which correlate with the expansion and the compression of the peptides. At the final stage, the peptides adopt the folded fibrillar conformation. The pathways by which this assembly is formed are diverse, yet in the most prominent route aggregation is initiated in the ^{16}KLVFFA^{21} region, followed by the 30−40 segment and finally the 23−29 region.

As part of their atomistic study on the early stages of aggregation of Aβ_{42} and Aβ_{40} (see Section 3.2.1.2), Barz et al. characterized the structural differences between dimers and trimers of the two alloforms.[200] They observed formation of dimers by the aggregation of free monomers in both cases, yet some difference appeared. Aβ_{42}-dimers record only little contacts between their first 10 residues, whereas for Aβ_{40} they appear to be engaged in contacts with their correspondent amino acids. The same behavior is observed for the M35-A42 sequence. They hypothesize that the increased flexibility of the N- and C-termini in Aβ_{42} may drive the association of two dimers into tetramers, this being one of the main conclusions of their study (see Section 3.2.1.2)

Zoete et al. investigated the stability of porcine insulin dimers by means of molecular dynamics simulations in explicit solvent.[201] They showed that the dimer is structurally stable with marginal deviations from the X-ray structure within a time scale of 5 ns. They calculated the binding free energy of insulin dimerization using the generalized Born MV2 approach (GB-MV2).[202] The determined binding free energy of −11.9 kcal/mol compares favorably to the experimental −7.2 kcal/mol. Raghunathan et al. extended the study of Zoete et al. to include key mutations involving residue F24 (F24G, F24A, F24D-Ala, ΔF25).[203] They used the molecular mechanics-generalized Born surface area (MM-GBSA) and thermodynamic integration (TI) to determine the binding free energy. They found that the wild-type dimer is the most stable one, with a binding free energy in the [−16; −8.4] kcal/mol interval depending on the method used, MM-GBSA or TI, respectively. Both values compare favorably to previous studies[202] and experimental measurements. Furthermore, they showed that the ΔF25 mutant is unstable, while F24G and the alanine mutants are structurally less stable than the wild type dimer; hence, they measure higher binding free energies.

Dupuis et al. performed atomistic simulations in implicit solvent on the human (hIAPP) and rat IAPP (rIAPP) to complement their experimental study on the assembly mechanisms of these peptides.[204] They found that rIAPP forms mainly coil-rich dimers while hIAPP dimers are largely populated by β-strand interfaces. Furthermore, they showed that the binding between dimers is preferred by monomers adopting the β-strand conformation. They identified the major binding mode to be side-by-side assembly of β-hairpins (comprising residues ^{11}IVLSVALN^{18} and ^{23}TPIESHQVEK^{32}) rather than their stacking. Next, their results showed that the monomers undergo structural transitions from helical to β-rich structures upon dimerization. Their binding energies revealed that hIAPP dimerization is more favorable than rIAPP binding with energies of −59.5 kcal/mol and −38.3 kcal/mol, respectively.

The thermodynamics and kinetics of hIAPP$_{11-25}$ dimerization have also been explored by atomistic simulations in explicit solvent facilitated by the construction of Markov state models and REMD simulations.[205,211] Qiao et al. found that the hIAPP$_{11-25}$ dimer populates multiple metastable states, ranging from random coil structures to small fragments rich in helical or β-rich confromations. The most visited state consists of peptides adopting elongated antiparallel cross-β structures. The dimerization process is driven by hydrophobic and electrostatic interactions, and the cross-β conformation is adopted at a later stage after the peptides have undergone large confromational reorganizations. Interestingly, they found transitions from α-helical to β-rich conformations which have been observed also for other peptides.

Recent studies in the Shea and Bower groups further investigated the importance of the disulfide bond by focusing on the first eight residues of hIAPP.[206] They used replica-exchange molecular dynamics to simulate the ^{1}KCNTATCA^{8} fragment and the influence of the C2S/C7S mutation on aggregation. Their study showed that the reduction of the disulphide bond by mutation increases the aggregation rate of the peptide. They suggested that the intact disulfide bond in the wild-type peptide may be protective against aggregation due to a reduction of interpeptide hydrogen bonding. This finding is consistent with recent experiments showing that the removal of the disulfide bond accelerates amyloid formation in solution and near membranes.[212]

Guo et al. investigated the early stages of hIAPP dimerization by means of bias-exchange metadynamics in explicit solvent.[207] They derived the dimerization pathways using the finite temperature string method and found that in the initial state disordered monomers need to overcome a free energy barrier of $7k_BT$, in order to form an intermediate β-sheet structure. This barrier depends on the distance and the orientation of the peptides with respect to each other. As more bonds form between the peptides, a second barrier emerges in the free energy profile ($\approx 2k_BT$), which is associated with the conformational adjustment of the two monomers. The free energy then decreases as the peptides undergo conformational changes from two extended chains stacked side-by-side in parallel to a compact "ribbon-like" structure exhibiting a slight twist.

Ganguly et al. investigated the binary mixtures of several tau truncations containing the segments identified to act as aggregation centers for paired helical filaments, *i.e.*, ^{275}VQIINK^{280} and ^{306}VQIVYK^{311}.[118,208] In particular, they

DOI: 10.1021/acs.chemrev.8b00731
Chem. Rev. XXXX, XXX, XXX−XXX

Table 3. Computational Studies of Oligomerization[a]

Reference	Peptide	Model	Solvent	Method	Sampling[b]
Gsponer et al.[213]	$Sup35_{7-13}$	CHARMM19	implicit	MD	20 μs
Urbanc et al.[214]	Aβ_{42}	CG	implicit	DMD	1×10^7 steps
	Aβ_{40}				1×10^7 steps
Barz et al.[200]	Aβ_{42}	OPLS-AA	GBSA	MD	2.5 μs
	Aβ_{40}				2.5 μs
Sun et al.[215]	Aβ_{16-22}	CG	EEF1	DMD	2 μs
	$hIAPP_{15-25}$				3 μs
	$hIAPP_{15-25}$(S20G)				3 μs
	$hIAPP_{19-29}$				3 μs
	$hIAPP_{19-29}$(S20G)				3 μs
	$hIAPP_{22-28}$				2 μs
	α-syn $_{68-78}$				2 μs
Sun et al.[216]	hIAPP	CG	EEF1	DMD	10−25 μs
Collu et al.[217]	ovPrP$Sc_{171-226}$	GROMOS53a6	SPC	MD	2.2 μs
Carballo-Pacheco et al.[218]	Aβ_{25-35}	OPLS-AA	TIP4P	MD	30 μs
	kassinin				30 μs
	neuromedin K				30 μs

[a]Abbreviations. MD, molecular dynamics; DMD, discrete molecular dynamics; CG, coarse-grained. [b]Cumulative sampling over all replicas.

used atomistic descriptions of R2/wt ^{273}GKVQIINKKLDL^{284}, R3/wt ^{306}VQIVYKPVDLSK^{317}, and R2/ΔK280 ^{273}GKVQIINKLDL^{284} mixtures in explicit solvent and sampled trajectories using REMD. Their study, complemented by experiment, revealed the formation of homo- and heterodimers. The R2/wt-R3/wt and R3/wt-R3/wt dimers populate both compact and extended conformations, with the latter consisting of peptides alternating between parallel and antiparallel arrangements for the heterodimer and with the homodimer preferring parallel orientations, respectively. The parallel arrangement is driven by hydrophobic interactions and hydrogen bonds in the ^{306}VQIVYKPVDLSK^{317} region. On the other hand, the R2/ΔK280-R3/wt aggregate is more flexible, rich in extended structures and antiparallel orientations of the peptides.

Chebaro and Derreumaux investigated the structural and dynamical dimerization properties of the prion globular domain $PrPC_{125-228}$. Furthermore, they looked into the effect of the T183A disease variant on the dimers by using a coarse representation of the peptides in implicit solvent at physiological and high values of the temperature.[121] They found that α_1 is structurally stable in the wild-type dimer and that intermolecular β-sheets form at positions 142−143 and 226−227. Furthermore, they showed that the T183A mutation leads to unfolding of α_2 and α_3 at high temperatures. This can result in the sporadic formation of intermolecular β-sheets localized in α_2.

Chamachi and Chakrabarty used REMD in explicit solvent to investigate the aggregation and thermodynamic stability of the mouse $PrP^c_{124-226}$ globular domain dimer.[209] They observed a spontaneous and irreversible dimerization process, mediated by salt-bridges, hydrogen bonds, and hydrophobic interactions. They identified three main interaction sites by using principal component analysis (PCA) and characterizing the three most dominant clusters. In the largest cluster, contacts between the ^{181}ITIKQHTVTTTTK^{193} residues of α_2 of one protein with ^{124}LGG^{126} and ^{181}ITIKQHTVTTTTK^{193} of the other molecule are formed. In the second case, the ^{153}MYRYPNQ^{159} and ^{187}TVTTTTKGEN^{196} sequences of one of the peptides can bind to ^{123}GLGGYML^{129} of the second peptide, occasionally forming a β-sheet. Lastly, the ^{180}NITIKQHTVTTTTK^{193} fragment forms contacts with ^{166}DQYSNQNNFVHD^{177} of the other peptide.

Tian et al. used enhanced sampling Monte Carlo simulations of CsgA dimers and trimers in implicit solvent to refine the contacts resulting from their homology model.[210] Later they extended the simulation procedure to investigate the formation of dimers consisting of the five subrepeats of the protein.[125] They determined the binding free energy of each fragment and found that the individual fragments have different dimerization tendencies. In particular, R1, R4, and R5 display a high β-content and increased dimerization preference, while R2 prefers to remain unbound and R3 adopts intermediate bound conformations. Additionally, they found that the hydrogen bonds are the stabilizing contacts within the dimers.

From the atomistic simulation studies aimed at various peptides we conclude that dimerization is driven by the hydrophobic effect (like protein folding) and stabilized structurally (i.e., kinetically) by hydrogen bonds. Furthermore, a variable degree of β-sheet content is associated with the dimerization process, yet there is no concrete evidence on how or if β-hairpin tendency in the monomeric form of the peptides contributes to dimer formation. Additionally, hardly any studies focusing on the dimerization of functional peptides exist in the current literature. We propose the exploration of the self-assembly of functional amyloids which might reveal similarities and differences with respect to pathological amyloids.

3.2.1.2. Oligomers. Oligomeric assemblies have been proposed to be intermediate (on-pathway) species toward the formation of amyloid fibrils.[23,72−74] Off-pathway oligomers have been associated with cellular toxicity and were proposed to play a role in membrane disruption and to be implicitly linked to disease pathogenesis.[79,85,87] The aggregation into oligomers has been investigated by the coarse-grained models mentioned in the previous section, yet none can inform on the conformations and plasticity of such aggregates at atomic level of detail. Therefore, in this section we focus on the simulation studies (Table 3) carried out with atomistic simulations and slightly coarse grained representations.

Gsponer et al. carried out implicit solvent molecular dynamics simulations to study the early steps of aggregation of three ^{7}GNNQQNY^{13} peptides, extracted from the N-terminal prion-determining domain of the yeast protein Sup35.[213] It emerged from the simulations that backbone hydrogen bonds favor the

DOI: 10.1021/acs.chemrev.8b00731
Chem. Rev. XXXX, XXX, XXX−XXX

antiparallel β-sheet arrangement, while side-chain hydrogen bonds and aromatic stacking stabilize the in-register parallel structure. The comparison with the sampling obtained with peptide mutants devoid of Y13 showed that aromatic residues stabilize kinetically the parallel assemblies. One of the conclusions of their study was that the dependence of aggregation and disaggregation rates on the peptide sequence might be an essential factor determining the time scale of nucleus formation. Up to that time, the general accepted hypothesis was that the peptide backbone is the main driving force of amyloid aggregation, irrespective of the primary structure.

Urbanc et al. used a four bead per residue representation to investigate the early stages of Aβ peptide oligomerization.[214] In their model four beads are used to represent each residue; three beads for the backbone atoms and one bead for the side-chain. The simulation system consisted of 32 copies of either Aβ42 or Aβ40, and discrete molecular dynamics simulations in implicit solvent were used to propagate each system. The self-assembly is initiated in the ^{36}VGV^{39} region followed, at a later stage, by the ^{21}AEDVGSNKGA^{30} sequence for both $A\beta_{42}$ and $A\beta_{40}$. Their results revealed that the shorter peptide prefers to form more dimers than $A\beta_{42}$ which, on the other hand, forms more pentamers than $A\beta_{40}$. Structurally, the stability of the pentameric core is ensured by the hydrophobic clusters ^{17}LVFFA^{21}, ^{30}AIIGLM^{35}, and ^{39}VIA^{42} whereas the first 16 residues remain solvent exposed. This result is consistent with experimental findings, which emphasize the importance of the LVFF sequence in β-sheet formation and amyloid growth,[219,220] as well as with simulations, which show that the hydrophobic segments are the ones to initiate docking and the last to detach from a preformed fibril; see Section 3.2.2. Additionally, their results inform on the formation of an internal β-strand within the N-terminus of the shorter peptide, which they correlate with the instability of $A\beta_{40}$-oligomers due to the solvent exposure of the core of the aggregate.

Along the same lines, Barz et al. investigated the early stages of aggregation of the two amyloid-β alloforms in implicit solvent by means of molecular dynamics simulations.[200] Starting from systems consisting of 20 disordered monomers, they built transition networks and defined aggregation states by means of four variables: number of peptides per oligomer, number of intermolecular salt bridges, number of intermolecular hydrophobic contacts, and the shape of the aggregate. They identified the coexistence of oligomers consisting of the same number of peptides, but which differ significantly in shape. They found that for both Aβ alloforms elongated and compact oligomers are formed. While the first appear to be involved in the assembly process, the latter are metastable and contribute little to the formation of new aggregates. Interestingly, they showed that the two alloforms populate differently sized oligomers; that is, $A\beta_{42}$ will mainly be engaged in dimers (discussed in Section 3.2.1.1), tetramers, and hexamers, while $A\beta_{40}$ will form primarily dimers, trimers, and tetramers. The major differences arise in the role of the tetramers toward the formation of higher order assemblies. In particular, $A\beta_{42}$-tetramers contribute toward the formation of bigger oligomers (pentamers, hexamers, heptamers, 10-mers, and 14-mers) while $A\beta_{40}$ oligomers appear to contribute less to the formation of 10-mers and 14-mers.

Sun et al. investigated the oligomerization dynamics of fragments extracted from Aβ, α-syn, and hIAPP by means of discrete molecular dynamics simulations.[215] Their simulation systems consisted of two to twenty copies of each hIAPP fragment ($hIAPP_{15-25}$, $hIAPP_{19-29}$, and their S20G mutants) and eight copies of $hIAPP_{22-28}$, $A\beta_{16-22}$, α-syn $_{68-78}$. Starting from random initial configurations, they found that the aggregation process is very dynamic with oligomers that can interconvert between species. They found that the monomers accumulate into intermediate β-barrel oligomers prior to transforming into cross-β aggregates.[215] They later extended their study to investigate the behavior of full length hIAPP and found that it also forms β-barrel intermediates.[216]

Collu et al. studied early stages of aggregation of ovine PrP^{Sc} (α_2 - α_3) by means of molecular dynamics simulations.[217] Starting from 18 randomly distributed peptides, they found that aggregation follows a two step process; first a nucleus consisting of five to eight monomers is formed, followed by the attachment of other free monomers. Additionally, they showed that residues T195 and T196 are indispensable in maintaining the stability of the nucleus.

Carballo-Pacheco et al. studied the aggregation of $A\beta_{25-35}$ and two tachykinin peptides (neuropeptides), kassinin and neuromedin K, using atomistic simulations in explicit solvent.[218] They started from systems consisting of six randomly distributed monomers and found that the aggregation kinetics of the neuropeptides is much faster than that of $A\beta_{25-35}$. Furthermore, the size of the aggregates also varies significantly; that is, the tachykinin peptides form hexamers on time scales of 100 ns, while $A\beta_{25-35}$ can only form tetramers on time scales three times longer. Additionally, they found that the aggregation kinetics is highly dependent on the configuration of the monomers, as hairpin-like conformations appear to reduce the aggregation kinetics for these short fragments.

We refer the reader to a review focusing on the oligomerization progess of pathologic peptides.[221] Additionally, we mention studies assessing the effects of various force fields and different water models on the aggregation of intrinsically disordered proteins[222,223] or fragments thereof.[224]

3.2.2. Growth Phase. While nucleation is a rare event, fibril elongation is a much faster process and occurs through monomer binding at fibrillar ends and other mechanisms. Most mechanisms of fibril growth depend on the concentration of monomers and aggregates:[171]

- monomer addition takes place usually at the fibrillar tips and is reversible as it involves noncovalent interactions;
- fibril breaking results in a higher effective concentration of tips which can grow by monomer addition and/or other mechanisms;
- secondary nucleation gives rise to additional aggregates on the surface of the fibril which may act as catalysts in the generation of new filaments;
- fibril merging gives rise to larger fibrillar aggregates by joining the ends of two fibrils that meet in properly aligned orientations.

In the coming sections we will not elaborate on the kinetic theory behind fibrillar growth but rather emphasize the different models and simulation techniques used to study the distinct processes.

3.2.2.1. Monomer Addition. At higher resolutions, the experimental "stop-and-go" growth mechanism is defined in simulations as a "dock–lock" mechanism, in which a monomer first attaches to the fibril surface ("dock") and then undergoes structural rearrangements to adopt the template of the fibril ("lock"), enabling the attachment of further monomers (Figure 2 inset B).[109,225−230] While coarse-grained models are highly

DOI: 10.1021/acs.chemrev.8b00731
Chem. Rev. XXXX, XXX, XXX−XXX

Table 4. Computational Studies Focusing on Fibril Elongation[a]

Reference	Peptide	Model	PDB ID	Solvent	Method	Sampling[b]
Association simulations						
Nguyen et al.[226]	$A\beta_{16-22}$	GROMOS96 43a1	1HZ3[231]	SPC	MD	2.1 μs
Reddy et al.[229]	$Sup35_{7-13}$	CHARMM22	1YJP[244]	TIP3P	MD	0.8 μs
	$A\beta_{37-42}$		2ONV[245]			0.23 μs
O'Brien et al.[227]	$A\beta_{35-40}$	CHARMM22/CMAP	2OKZ[245]	GBSW	LD + MhREX	1.03 μs
		CHARMM22		TIP3P	MD	≈ 180 ns
Takeda and Klimov[233,234]	$A\beta_{10-40}$	CHARMM19	2LMN[232]	SASA	REMD	48 μs
Han and Hansmann[236]	$A\beta_{17-42}$	AMBER99SB	2BEW[235]	GB	REMD	5.94 μs
Gurry and Stultz[237]	$A\beta_{17-42}$	CHARMM19	2BEG[235]	EEF1	US	33 μs
	$A\beta_{9-40}$		2LMN,2LMO [232]			66 μs
Han and Schulten[228]	$A\beta_{17-42}$	PACE	2BEG[235]	Martini	US+REMD	1.3 ms
Schwierz et al.[241]	$A\beta_{9-40}$	CHARMM-C27	2LMN[232]	TIP3P	US	0.5 μs
Sasmal et al.[246]	$A\beta_{12-40}$	CG	2M4J[247]	implicit	LD	1.5 s
Ilie et al.[248]	α-syn_{30-90}	HCG	toy-model	implicit	constrained BD	94 μs
Roeder and Wales[133]	$A\beta_{17-42}$	AMBER ff14SB	2BEG[235]	GB	DPS	
Dissociation simulations						
Buchete et al.[249]	$A\beta_{9-40}$	CHARMM27,AMBER94	2LMN[232]	TIP3P	MD	126 ns
Baumketner et al.[250]	$A\beta_{9-40}$	OPLS/AA	2LMN[232]	TIP3P	MD	50 ns
Schor et al.[251]	$insulin_{11-17}$	GROMOS96	3HYD[252]	SPC	SMD + TPS	750 ns
	$TTR_{105-115}$		2M5N[57]			5 μs[d]
Lemkul and Bevan[253]	$A\beta_{17-42}$	GROMOS96 53A6	2BEG[235]	SPC	MD + SMD + US	310 ns
Bacci et al.[243]	Aβ42	CHARMM36	2BEG[235]	TIP3P	PIGS	10 μs
Rodriguez et al.[254]	$A\beta_{17-42}$	CHARMM36	2MPZ[255]	TIP3P	SMD	
Davidson et al.[256]	$\tau_{306-378}$	CHARMM36m	5O3L,5O3T[257]	TIP3P	MD	1.7 μs
	$A\beta_{11-42}$		5KK3[132]			2 μs
	$hIAPP_{21-27}$		3KIB[258]			2 μs
Ilie and Caflisch[259]	$A\beta_{42}$	CHARMM36m	5KK3[132]	TIP3P	MD	15 μs
Tofoleanu et al.[260]	hIAPP	CHARMM36	[261]	TIP3P	MD	250 ns

[a]Abbreviations. MD, molecular dynamics; LD, Langevin dynamics; CG, coarse-grained; HCG, highly coarse-grained MhREX, multiplexed Hamiltonian replica exchange; REMD, replica-exchange molecular dynamics; US, umbrella sampling; BD, Brownian dynamics; DPS, discrete path sampling; SMD, steered MD; TPS, transition path sampling; PIGS, progress-index guided sampling. [b]Cumulative sampling over all replicas. [c]The studies are presented in chronological order. [d]For each value of pH.

efficient in recovering the low-resolution process, atomistic simulations are more adequate in elucidating the molecular details underlying this process. The complexity, conformational flexibility, and large number of states that amyloidogenic peptides can adopt, as well as the millisecond to hours fibril elongation time scales, require a large computational power to enable monomer characterization upon binding to preformed nuclei. Therefore enhanced sampling techniques have been widely applied to elucidate the mysteries of the dock−lock mechanism. Furthermore, many groups studied the growth of truncated fibrils containing key residues for the elongation (Table 4). In the following paragraphs, we direct our attention toward these methods in relation to monomer attachment. We start by describing simulations studying the attachment of a monomer to the fibrillar tip and then proceed with studies focused on the dissociation of the tip peptide.

In one of the pioneering studies of the dock−lock mechanism Straub, Thirumalai, and co-workers performed molecular dynamics simulations in explicit solvent on an $A\beta_{16-22}$ (^{16}KLVFFAE^{22}) hexamer extracted from solution NMR (PDB ID: 1HZ3[231]).[226] Their results showed that upon elongation the peptide is absorbed on the fibrillar surface and then undergoes structural rearrangements with a stepwise growth in β-content. In particular, upon docking they observed a significant increase in β-content as compared to the soluble state, followed by large structural rearrangements in the slower locking stage. They showed that during locking the monomer conformation resembles the one of the fibrillar template. Additionally, their results revealed that the rate-limiting step in fibrillar growth is the locking step. Later they extended the study to fragments from the yeast prion Sup35 (^{7}GNNQQNY^{13}), the $A\beta_{37-42}$ (^{37}GGVVIA^{42}) peptide[229], and $A\beta_{35-40}$ (^{35}MVGGVV^{40}).[227] Their results showed that during fibril elongation the attaching monomer undergoes several docking/undocking events before being absorbed onto the fibril. Furthermore, the locking stage is highly sensitive to the conformation that the docked monomer adopts; that is, only the peptides that form at least one native contact with the fibril lock rapidly to the fibril and adopt the template. During the locking stage the monomer forms hydrogen bonds with the water molecules which gradually get replaced by in-register interactions with the fibril tip. Nevertheless, a number of non-native contacts form between the attaching monomer and the template which are perceived as kinetic traps that hamper the efficient locking.

Takeda and Klimov studied the attachment of $A\beta_{10-40}$ peptides onto fibrils (PDB ID: 2LMN[232]) consisting of single and double protofilaments by REMD.[233,234] They found the ^{10}EVHHQKLVFF^{20} sequence to be the most aggregation prone. Additionally, they tested the role of the side-chain interactions to fibrillar growth by partially deleting contacts between individual residues. They found that this partial deletion stabilizes the locked amyloid state, yet complete elimination of these interactions may hamper fibrillar growth.[233]

DOI: 10.1021/acs.chemrev.8b00731
Chem. Rev. XXXX, XXX, XXX−XXX

Table 5. Thermodynamics and Kinetics from Association and Dissociation Simulations

Reference	Peptide	Model	Details[a]	ΔG_{bind} (k_BT)	τ_{dock}	τ_{lock}	temp (K)
Association simulations							
Schor et al.[262]	$TTR_{105-115}$	AMBER99SB-ILDN	low pH			22 μs	300
			neutral pH			56 μs	
Han and Schulten[228]	$A\beta_{17-42}$	PACE	dis (odd)	6.8	1 μs	100 ms	332
			dis (even)	7.2	0.5 μs	2.5 ms	
Schwierz et al.[241]	$A\beta_{9-40}$	CHARMM27	dis (odd)	24.9	$\tau bind$ = 2.3 μs		310
			dis (even)	22.8	$\tau bind$ = 9.9 μs		
Sasmal et al.[246]	$A\beta_{12-40}$	CG	dis (Cter)	14.3	40 μs	0.44−1.2 ms	337
			dis (Nter)	13.6 - 14.2	60 μs	0.48−1.4 ms	
			fib (Cter)	13.6	20 μs	0.56−1.2 ms	
			fib (Nter)	13.5	60 μs	0.5−1.3 ms	
Ilie et al.[248]	α-syn_{30-90}	HCG	dis	64			310
Dissociation simulations							
Ilie et al. [109]	α-syn_{35-97}	CHARMM27/CMAP	dis	31			310
Lemkul and Bevan[253]	$A\beta_{17-42}$	GROMOS96 53a6	ord (odd)	84			310
	$A\beta_{17-42}$(F19G)			85			
	$A\beta_{17-42}$(D23A)			75			
	$A\beta_{17-42}$(I32G-L34G)			72			
	$A\beta_{17-42}$(K28A)			62			
Rodriguez et al.[254]	$A\beta_{17-42}$	CHARMM36	ord (odd)	14.7			298

[a]Conformation of the attaching monomer: dis, disordered; fib, in the fibrillar state.

Han and Hansmann investigated the thermodynamics of the $A\beta_{17-42}$ fibril (PDB ID: 2BEG[235]) by means of atomistic REMD in implicit solvent.[236] They found that docking is initiated by the ^{31}IIGLMVGGVVIA^{42} segment, which attaches to the preformed fibril in a random-coil conformation. The monomer then undergoes structural rearrangements to form a β-sheet with residues 31−42 of the edge peptide of the fibril, followed by a reorganization into conformations characteristic to the template.

Gurry and Stultz investigated the elongation of $A\beta_{17-42}$ and two $A\beta_{9-40}$ polymorphs by using umbrella sampling in implicit solvent.[237] They showed that both peptides follow a similar elongation pathway in which the monomer evolves according to a downhill free energy path with the global minimum corresponding to the ideal fibrillar state. First, the peptide docks onto the fibril localized around the ^{17}LVFF^{20} patch. An intermediate state is sampled in which the peptide adopts the monomeric β-hairpin conformation. Finally, the intramolecular hairpin bonds are disrupted and intermolecular hydrogen bonds are formed, while the monomer adopts the fibrillar template. They proposed that the β-hairpin is a required intermediate conformation upon binding to the fibrillar tip.

Han and Schulten combined umbrella sampling[238−240] with a hybrid resolution model and replica exchange molecular dynamics to study the elongation of the $A\beta_{17-42}$ polymorph as extracted from solution NMR (PDB ID: 2BEG[235]).[228] In their simulations they used PACE[142] for the representation of the peptide in a coarse Martini solvent[143] to explore the thermodynamics and the kinetics of fibril elongation. Their results showed that the hydrophobic patches, ^{17}LVFF^{20} and ^{37}GGVVIA^{42}, may be the ones initiating contacts of the monomer with the fibril (docking). Furthermore, upon attachment they identified structures rich in β-hairpin conformations similar to those observed for the monomers in solution. They hypothesize that the contacts formed in the monomeric structure are lost upon attachment as the peptide first breaks the monomeric native contacts and then attaches and rearranges on the fibrillar tip, suggesting that the hairpin arrangement is an on-pathway conformation in fibril elongation. This result is consistent with the observations of Gurry and Stultz.[237] Additionally, they showed that fibril elongation is much slower at the odd end as compared to the even end; see Table 5.

A different transfer from intra- to intermolecular contacts upon attachment has been observed in a later study by Schwierz et al.[241] They used umbrella sampling simulations in explicit solvent to study the association/dissociation pathways of the $A\beta_{9-40}$ monomer onto the solid state NMR protofilament (PDB ID: 2LMN[232]). They showed that the initial interactions are driven mainly by non-native hydrogen bonds of the free monomer with the fibril. The docking is then followed by an increase in the number of native hydrogen bonds, which form by sacrificing multiple non-native ones, consistent with the results on smaller fragments.[115,229] Additionally, the formation of long-lived non-native contacts leads to kinetic trapping of intermediate conformations that slow down and implicitly hamper the elongation process.

Contrary to previous studies, Roeder and Wales documented no intermediate hairpins upon $A\beta_{17-42}$ attachment (PDB ID: 2BEG[235]) in their atomistic simulations in implicit solvent.[133] They used discrete path sampling[242] to explore the kinetic pathways of aggregation and focused on characterizing the kinetic traps occurring during the locking stage. They identified trapping due to misaligned interactions, such as out-of register stacking of residues F19 and F20, or twisting, which has as a natural consequence a misalignment between peptide layers. Their study confirms previous simulations studies[243] (see Section 3.2.2.2) regarding the increased disorder at the tip as a rate-limiting step during the locking stage.

Sasmal et al. sacrificed the atomistic detail to reach longer simulation times and recover the time scales characteristic to fibrilar growth (ms to min).[246] They used a coarse grained model, with one bead per residue, combined with Langevin dynamics and complemented by explicit solvent molecular dynamics simulation to study the influence of the conformation of the attachment $A\beta_{12-40}$ on fibril elongation. They populated

DOI: 10.1021/acs.chemrev.8b00731
Chem. Rev. XXXX, XXX, XXX−XXX

a simulation box with a stable fibril and soluble monomers, which could freely attach to the nucleus, to determine the thermodynamics and kinetics of fibril elongation. Their results showed that the docking of a monomer is up to 30 times faster than the locking step depending on the conformation of the attaching peptide. A disordered peptide will lock onto the fibrillar template more slowly than one that is preformed to attach (see Table 5), consistent with the coarse grained simulations introduced in Section 3.2.1. Additionally, they did not record significant differences between the docking and locking time scales at the two ends.

Ilie et al. used a highly coarse grained model in implicit solvent for the truncated α-synuclein (residues 30−90) to study its attachment and detachment to and from a fibril model inspired by the fold proposed by Vilar et al.[54] by means of distance constrained Brownian dynamics simulations.[177,248] They endowed five particles connected by springs with internal degrees of freedom such that they capture the agility of the protein to adapt its secondary structure in response to the environment. Each "chameleon" particle[176] (see the Briels model in Section 3.2.1) consists of about 12 residues. A protein in the disordered conformation is represented as a chain of soft spheres. By transformations of the particles into spherocylinders with directional binding affinities and by their rearrangement into a planar configuration, the protein can adopt an ordered state capable of forming fibrils. They found that upon gradually approaching a disordered peptide toward a preformed fibril the attaching monomer easily gets trapped in suboptimal configurations that hamper fibrillar growth. The nature of this contacts can, however, not be probed using low resolution models. Furthermore, they measured the attachment free energy of a free monomer which is slightly higher than the experimentally measured one; see Table 5 for the exact values. They also studied the dissociation process, which revealed a stepwise detachment of the monomer, by gradual dissociation of each bead with increasing distance. They later complemented the highly coarse grained study with atomistic representations in explicit solvent to calculate the binding free energies starting from the Greek key fibril template (PDB ID: 2N0A[141]).[109] They treated each fragment involved in the fibrillar core separately and derived the theoretical framework to calculate the binding free energy of α-syn$_{35-97}$ attachment. Their results yielded a total favorable attachment free energy of 77 kJ/mol, which is comparable to experimental measurements.[62]

3.2.2.2. Fibril Stability and Dissociation. As described in the previous section, it is computationally very challenging to study the attachment of a protein or peptide to a mature fibril. For this reason several studies focused on the reverse process, *i.e.*, the detachment of a tip monomer to analyze the structural stability.

Buchete et al. investigated the structural stability of multiple C_2 symmetric Aβ_{9-40} fibril topologies by means of atomistic molecular dynamics simulations in explicit solvent.[249] They showed that the fibrils are structurally stable on a time-scale of 10−20 ns, which is relatively short for current computational performances but still very informative. The D23-K28 intramolecular salt bridge contributes largely to fibrillar stability. In addition, residues close to the ^{22}EDVGSNKG^{29}-loop are rigid and do not record any significant structural motion. Later they extended their study to explore the behavior of fibrils at elevated temperatures.[263] They found that the dissociation of the tip peptides is initiated in the 24−30 region, followed by residues 9−23, resulting in the breakage of the D23-K28 salt bridge . Furthermore, the ^{22}EDVGSNKG^{29} loop region becomes disordered and the two β-strands slide on top of each other. On the other hand, the 32−40 fragment remains closely attached to the fibril, suggesting that in the reverse process these residues may be the ones initiating the contact between an incoming monomer and the fibril.

Baumketner et al. used a rigid template for the Aβ_{9-40} and E22Q mutant fibril (PDB ID: 2LMN[232]) in explicit solvent to study the dissociation of the tip peptide.[250] They show that, upon unbinding, residues ^{17}LVFF^{20} are the last to break from the fibrillar template, suggesting that in the reverse process they may be the first ones to dock. This result is consistent across most Aβ simulation studies addressing fibrillization and even oligomerization. Furthermore, they showed that the 9−14 fragment behaves similarly for both peptides. A closer analysis of fragment 15−28 reveals that the mutant is 1.4 times faster than the wt peptide to successfully lock onto the fibrillar template. The activation free energy of the two mutants is 5.4 and 4.6 kJ/mol for the wild-type and the E22Q mutant, respectively.

Schor et al. investigated the molecular mechanisms underlying the growth of the amyloidogenic region of the insulin B-chain (^{11}LVEALYL^{17} PDB ID: 3HYD[252]) by using steered molecular dynamics (SMD) simulations in explicit solvent combined with transition path sampling.[251] The monomer center of mass pulling simulations resulted in a free energy loss of about 42k_BT per peptide. They identified L17 and Y16 as the last to detach from the mature fibril, which stands as an indication that they may be the first to dock. They then used docked conformations from SMD as starting point for the TPS sampling and focused on the rate limiting transition from a docked stage to the locked arrangement. They identified several metastable misfolded states characterized by misalignment, *i.e.*, antiparallel attachment of the peptide and register shift upon locking. Nevertheless, they described two locking pathways: the peptide can either first form a majority of the backbone hydrogen bonds with the tip of the fibril followed by the reorientation of the E13 sides chain to complete the hydrogen bond pattern with the template or the orientation of the E13 side chain occurs before the building of the appropriate H-bond network.

They later applied a similar protocol to study the locking of a transthyretin TTR amyloidogenic fragment (^{105}SPFHEHAEVVF^{115}) to a fibril at low and neutral pH.[262] First, they heated up the system to 900 K, to stimulate detachment, and then they chose docked conformations as starting points for their time-lagged independent component analysis (TICA) and constructed Markov state models to extract the locking time scales. They found multiple trapped states that contribute unfavorably to the locking of the incoming peptide and that the escape rates from these metastable states are slower at low pH than at neutral pH. Furthermore, they identified that at low pH the aggregation pathways are driven by the hydrophobic residues whereas at neutral pH the mechanisms are more intricate. The new effect is reflected on the locking time scale which is almost three times slower at neutral pH as compared to low pH; see Table 5.

Lemkul and Bevan performed both explicit solvent conventional MD, steered MD, and umbrella sampling simulations to investigate the dissociation thermodynamics of the wild-type Aβ_{17-42} peptide and some mutations (F19G, I32G/L34G, K28A, and D23A) from a single filament fibril (PDB ID: 2BEG[235]).[253] They started by relaxing each system for 100 ns followed by sampling with restraints applied on the center of mass of the dissociating peptides. Their initial simulations

DOI: 10.1021/acs.chemrev.8b00731
Chem. Rev. XXXX, XXX, XXX−XXX

showed structural distortions of the mutated protofilaments, with maximal deformations created by the K28A mutation, due to the absence of the salt bridge characteristic to the fibril polymorph. The F19G and I32G/L34G mutants follow similar dissociation pathways; the ^{31}IIGLMVGGVVIA^{42} residues are the first to detach, followed by the loop region and finally ^{18}VFFAEDVGS^{26}. The mutants with the missing salt bridge (D23A and K28A) follow a different pathway; the dissociation is initiated in the loop region comprising residues ^{25}SNKGA^{30} succeeded by a simultaneous detachment of the rest of the peptide. The dissociation of wild-type peptide is initiated by the solvent exposure of the salt-bridge upon pulling which results in the destabilization of residues ^{32}IGLM^{35}. Additionally, they calculated the binding free energies of each monomer showing that the Aβ_{17-42} and the F19G mutant have comparable binding energies, while K28A has the least preference toward binding; see Table 5.

Okumura and Itoh investigated the structural and fluctuational differences between fibrillar ends for Aβ_{42} in explicit solvent by using molecular dynamics simulations.[264] Starting from the 2BEG[235] fibril polymorph, they showed that the tip peptides adopt different conformations at the two ends over a run length of 200 ns. In particular, they found that at the even end the tip monomer records little fluctuations and scarce deviations from the its original U-shape maintaining its closed conformation. At the opposite end, the peptide can adopt an open conformation which deviates from the NMR structure and is far more flexible than its opposite adjacent. Taking this into consideration, they speculated that the even end would extend faster due to the reduced flexibility and conformation of the tip monomer. This is consistent with the results of Han and Schulten, who calculated lower locking rates at the even end.[228]

Bacci et al. investigated the dock−lock mechanism of the solution NMR Aβ_{42} pentamer (PDB ID: 2BEG[235]) in explicit solvent by using the progress index guided sampling simulation protocol (PIGS).[243] They explored the transient states encountered during fibril elongation and investigated the disorder-to-order transition equivalent to the locking stage. They built a Markov state model for aggregation, and their results show transitions to the locked state on the microsecond time scale. Similar to previous studies,[228,241] they found that the hydrophobic ^{17}LVFF^{20} patch is often involved in non-native conformations with the preformed fibril. An important addition to the literature is the characterization of the N-termini, which appear to shield the lateral interfaces of the growing fibril acting as polymer brushes. Furthermore, their findings suggest that a certain degree of disorder in the penultimate peptide layer of the fibril contributes favorably to the binding of free monomers from solution, therefore introducing the hypothesis that the rate-limiting step may be regulated by the degree of disorder at the tip. Contrary to previous studies, in which the β-hairpin was proposed to be a crucial step in fibril elongation, Bacci et al. have not recorded any clear evidence that the presence of β-hairpins is mandatory.

Rodriguez et al. studied the unbinding of the Aβ_{15-40} D23N mutant from the odd end of a single filament fibril (extracted from PDB ID: 2MPZ[255]) in explicit solvent by using steered molecular dynamics simulations.[254] They calculated an activation free energy barrier of about 36.4 kJ/mol for the tip monomer and, consistent with previous studies, they identified three elongation stages driven by the hydrophobic residues. The ^{30}AII^{32} fragment detaches from the fibril, followed by a simultaneous dissociation of residues A21, A30, and I32 and finally a disruption of amino acids L34, M45, V36, V39, and V40. Furthermore, they found that the penultimate peptide layer undergoes structural rearrangements upon the dissociation of the tip. This observation is consistent with the hypothesis introduced by Bacci et al.,[243] which assumes that monomer attachment requires a certain degree of disorder at the tip.

Davidson et al. investigated the stability of various amyloid fibrils and the structural similarities between them by means of molecular dynamics simulations with a polarizable force field in explicit solvent.[256] As starting structures they used the new alloforms of Aβ_{11-42} (PDB ID: 5KK3[132]), $\tau_{306-378}$ (PDB ID: 5O3L and 5O3T[257]), and hIAPP$_{21-27}$ (PDB ID: 2KIB[258]). They showed that both tau alloforms and the Aβ_{42} double-horseshoe form water channels in their structures that exchange water molecules with the surrounding solution throughout the simulations. While for the tau fibrils on average five water molecules are bound in the hydrophobic turn of each filament, the Aβ_{42} fibril forms large channels of about 50 water molecules. The similarity between the fibrils lies in the slight asymmetry in the number of water molecules in the channels of each protofilament forming the fibrils. Furthermore, they showed that the architecture of the fibrils is stabilized by salt bridges that naturally differ from the ones identified for older polymorphs of the peptides. Next, they investigated the hydration of two hIAPP(21−27) alloforms, with parallel and with antiparallel β-sheets. They found that the parallel fibril is more hydrated than the antiparallel one. This occurs due to the structural instability of the antiparallel fibril, which distorts in an attempt to form parallel layers.

The authors of this review investigated the structural stability of the tip peptides of the full length double-horseshoe Aβ_{42} fibril polymorph (PDB ID: 5KK3[132]) by multiple explicit solvent molecular dynamics simulations.[259] They showed that the central five peptide layers are structurally stable despite an increase in the twist between consecutive layers of about three degrees, which is consistent with experimental findings.[265,266] They found that the tip peptides dissociate at both ends and the detachment is localized around residues ^{21}AEDVGSNKG^{29}. Furthermore, residues ^{17}LVFF^{20} and ^{35}MVGGVVI^{41} remain closely attached to their neighbors. The preference of the hydrophobic sequences to remain attached to their corresponding neighbors is a common feature throughout all the presented studies, independently of the fibril polymorph. In addition, they showed that the tip N-termini occasionally form transient contacts with the adjacent neighbors in an ordered fashion but prefer to be largely disordered. The ordered attachment of the N-terminus to the core of the adjacent peptide may hamper the docking of a free peptide to the fibril and hence contribute to the stop phase of fibrillar growth.

Tofoleanu et al. simulated the hIAPP fibril and multiple mutants in explicit solvent, starting from the refined structure proposed by Luca et al.,[261] to study the effects of sequence alteration on the dynamics of the aggregates.[260] They found that mutations contribute both favorably and unfavorably to the fibrillar stability. Fibrils consisting of S28P, S29P, N31K, pramlintide, or rIAPP mutants show a decrease in β-sheet content along the simulations. This is consistent with the monomeric studies of Chiu et al. reporting on the effect of proline mutation on structure alterations.[116] On the other hand, mutations to hydrophobic or charged residues such as V17I, S20R, I26V, or L27F enhance the β-sheet content and contribute favorably to fibrillar stability. Their results indicated

DOI: 10.1021/acs.chemrev.8b00731
Chem. Rev. XXXX, XXX, XXX−XXX

that A25T and N31K are the most structure disruptive mutations that contribute to fibril solubility.

As for protein folding, the hydrophobic effect is the main contribution to monomer attachment to the fibrillar tip. Hydrogen bonds have both a favorable and unfavorable contribution to fibril elongation: they efficiently lock the monomer on the surface, yet they can also trap the peptide in non-native configurations on the fibrillar surface. As a result of their study Ilie et al. showed that the binding free energy of a monomer on the fibrillar surface can be split in several key terms.[109] Two large opposing components result from the favorable hydrogen bonding effects and the loss in conformational entropy of a monomer upon binding to the fibrillar template, modulated by weaker hydrophobic terms. Overall fibril elongation is a complex process which results from the competition between native/non-native hydrophobic contacts and hydrogen bonds outweighed by the loss in conformational disorder of the monomer and the fibrillar tip.

3.2.2.3. Fibril Growth. Once the structural details of the rate limiting step have been elucidated, one can study fibril elongation from a different perspective. In particular, the coarse-grained models introduced in Section 3.2.1 have been employed to simulate the fibril elongation process by incorporating the fine details in single parameters.

The ten bead per protein model introduced by Pellarin and Caflisch (Figure 5(d)) has a single free parameter that modulates the tendency for fibril formation. This phenomenological coarse grained model captures a broad range of aggregation kinetics and was used to describe the heterogeneity of pathways of self-assembly and fibril polymorphs.[179−181] The elongation rate was shown to be up to 4 orders of magnitude slower for the β-amyloid-protected monomer as compared to the β-amyloid-forming monomer.[179] Furthermore, the elongation rate is highly dependent on the monomer concentration for the β-prone, but not for the β-protected, for which the formation of on-pathway oligomeric intermediates results in a constant concentration of monomers. In the final equilibrium, the fibrils consist of bundles of four intertwined filaments, with disordered peptides at the tips.[179] The latter result is consistent with recent atomistic simulations which have provided evidence of disorder at the fibrillar tips.[243,259] In a later study, Pellarin et al. employed the same model to gain insight into the elongation mechanisms and to determine the association rates of a monomer to a preformed fibril.[180] In particular, the amyloid-protected-monomer can access oligomeric states before it fully associates with the four intertwined filament arrangement. Most of these intermediate states consist of only two or three protofilaments. They found wide transition regions from two- to three-protofilament fibrils and from the three- to the final protofilament state. Next, they observed the β-monomer to be almost twice as efficient as the protected monomer in attaching to a mature fibril. Additionally, they investigated the relation between the amyloidogenic capabilities of the monomer and the fibril polymorphism.[181] They showed that the amyloid-competent monomers aggregate in the fibril that has the highest stability (thermodynamic control), while the amyloid-protected monomers self-assemble into metastable fibrils and form the energetically most favorable fibril with a lower probability (kinetic control). The kinetic control of amyloid aggregation had been suggested earlier by Karplus and co-workers on the basis of atomistic simulations of peptide dimerization.[267]

The rigid tetrahedron model developed in the Urbanc lab (Figure 5(c)) captures similar aggregation patterns.[178] In particular, for η = 0.75 fibrillar growth is characterized by a mix of fast and slow processes involving either oligomer addition or monomer association and dissociation, respectively. The quasi-spherical oligomers formed during the nucleation phase evolve into curviliniar protofilaments and finally into even larger aggregates consisting of multiple domains, generally separated by kinks.

The polymorph patchy particle representation of Ilie et al. (Figure 5(b)) suggests that fibril merging is an additional mechanism of fibril growth.[176] In this model, merging is possible only when the ends of two fibrils are in the correct orientation, *i.e.*, the patches mimicking hydrogen-bonding face each other.

3.2.2.4. Secondary Nucleation. The one particle coarse models for Aβ and α-synuclein are efficient in capturing fibril self-replication.[176,268] The model introduced by Ilie et al. captured the interaction of α-syn oligomers with mature fibrils.[176] In particular, they observed the simultaneous binding of several monomers onto the surface of a fibril, followed by a rapid interconversion of the oligomer's constituents into elongated β-conformations and simultaneous binding to form a child fibril, which detaches from the parent-fibril; see Figure 3. Saric et al. extended their model for Aβ to include a third intermediate state, in which a soluble monomer can interact with a fibril, to investigate the self-replication regime of fibrillar assemblies.[268] They varied the protein concentration and the interactions between peptides to measure the primary and secondary nucleation rates. They found that self-replication occurs in a very narrow regime, at low protein concentrations and weak interactions between the peptides, where it dominates significantly over the primary nucleation mechanism. A necessary requirement in this case is that the secondary nucleus is different than the primary one. Later they extended the study to investigate the effect of temperature on secondary nucleation.[175] Opposite to primary nucleation, they found that secondary nucleation is hindered at high temperatures due to the fact that fewer monomers attach to the fibrillar surface, therefore inhibiting the formation of oligomers. Additionally, they identified a higher free energy barrier for oligomer conversion than for oligomerization on the fibril surface.

Schwierz et al. used REMD simulations in explicit solvent to elucidate the structural information and the kinetic details of secondary nucleation of Aβ_{9-40}.[269] They set up four systems, each consisting of a parent 12-mer fibril (PDB ID: 2LMN[232]) and a child fibril, of 1 to 4 monomers, oriented perpendicular to the long axis of the first filament. The association/dissociation was monitored along the center of mass of the two entities, *i.e.*, restrained parent and mobile child fibril. Their results showed that for all systems the binding of the child fibril is favorable. They found that the monomer has a binding affinity ($25.3k_BT$) comparable to the binding free energy of monomer attachment to the tips; see Table 5. Interestingly, the dimer has the lowest binding affinity ($19.7k_BT$), the trimer is higher than the monomer ($35.1k_BT$), and the tetramer records the highest binding preference ($63.7k_BT$). In the detached state the monomer is mainly disordered, while the other aggregates preserve their cross-β-conformations. The attachment of the child fibril(s) is driven by the hydrophobic interactions with the parent, while the hydrogen bonds contribute very little to the process. The monomer attaches in stretched conformations with initial non-native contacts followed by a collapse of the monomer on the surface. The dimer is ordered with a slightly disordered C-terminus disrupting the cross-β-conformation, yet binding is initiated between the dimeric G9-A21 residues and

DOI: 10.1021/acs.chemrev.8b00731
Chem. Rev. XXXX, XXX, XXX−XXX

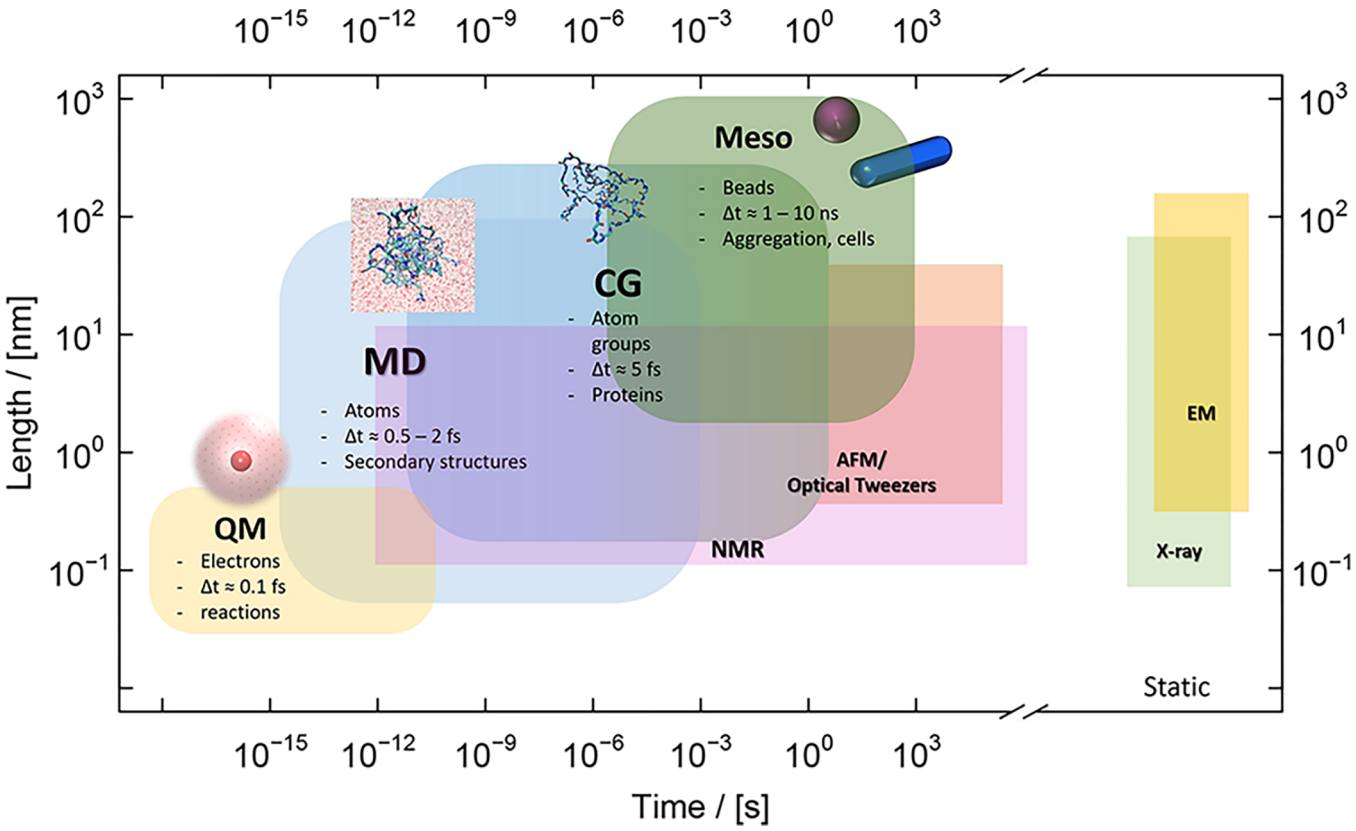

Figure 6. Schematic representation of the spatiotemporal scales of simulation protocols (round boxes) and experimental methods (rectangles). Δt, time step of the simulation technique; QM, quantum mechanics; MD, molecular dynamics; CG, coarse grained; Meso, mesoscale models; NMR, nuclear magnetic resonance spectroscopy; AFM, atomic force microscopy; EM, electron microscopy; X-ray, protein crystallography. Adapted with permission from ref 276. Copyright 2012 Annual Reviews.

the fibril A30-A40 fragment. The cross-β-conformation is kept throughout the simulations involving trimers and tetramers, and contacts with the fibril are concentrated at the C-termini but also with residues G9-A21 of the fibril.

Bellaiche and Best explored the thermodynamics of Aβ_{42} adsorption on the surface of a mature fibril by means of Hamiltonian replica exchange molecular dynamics simulations in explicit solvent.[270] They set up 16 copies of their system consisting of a mature fibril (PDB ID: 2MXU[271]) and a monomer in various initial configurations, *i.e.*, attached or completely detached from the parent. They determined a favorable adsorption free energy of the monomer on the fibrillar surface of about 19 kJ/mol, which is comparable to experimental findings and coarse-grain simulations[272] but smaller than the one obtained by Schwierz et al. for Aβ_{9-40}.[269] Additionally, they identified frequent contacts of E22 and D23 of the monomer with the fibrillar Q16, suggesting monomer adsorption is driven by polar interactions.

Most of the amyloidogenic peptides have been experimentally shown to self-replicate under certain conditions. As an example, α-synuclein undergoes secondary nucleation at mildly acidic pH, *i.e.*, at pH below six.[24,25] It has been proposed that the efficiency of the secondary nucleation of the prion protein could be one of the factors that influences the pathology of prion diseases.[77] The generic dependence of the secondary nucleation on the fibril concentration has been demonstrated also for hIAPP.[78]

Despite experimental evidence and extensive derivation of the theoretical framework, secondary nucleation is far from being explored from a simulation perspective. Simulations of secondary nucleation are computationally expensive because of the large size of the system. An interesting question is if different fibril polymorphs form or rather the child fibrils adopt the template of the parent-fibril despite nucleating on the surface. A related question is whether oligomers formed during secondary nucleation are toxic. Secondary nucleation is not limited to amyloidogenic peptides, but it applies to a vast number of nucleating systems, including organic crystals, inorganic crystals,[273] and polymers.[274] In contrast, no clear evidence of fibril-surface-catalyzed secondary nucleation exists in the case of functional amyloids.[12]

3.2.2.5. Fragmentation. The coarse-grained models discussed in the previous sections do not report on fibril breakage except for the four bead model developed in the Urbanc lab.[178] They found that upon increasing the repulsive potential, fibril breakage dominates the systems therefore reducing the size of the largest aggregates to about 120 monomers per fibril.

From an atomistic perspective Schwierz et al. examined both fragmentation and association of two Aβ_{9-40} hexamers by using umbrella sampling and generating intermediate states along the axis separating centers of mass of the aggregates.[241] They found that the association free energy is about 47.3k_BT, which is almost twice as much as the binding free energy of a monomer to any of the tips; see Table 5. Additionally, they measured an unbinding time of 3×10^{12} s, which indicates that compared to both locking and docking fragmentation is a much slower process. On the other hand, the association times are within the same order of magnitude as the monomer association times, i.e., 1.4×10^{-6} s.

DOI: 10.1021/acs.chemrev.8b00731
Chem. Rev. XXXX, XXX, XXX−XXX

Ndlovu et al. investigated the fragmentation of several IAPP fibrils in explicit solvent by using steered molecular dynamics simulations.[275] They reconstructed the double filament ^{20}SNNFGAILSS^{29} wild-type human fibril and five mutations thereof, *i.e.*, F24L, A26P, I27V, F24L-A26P, F24L-A26P-I27V, and rIAPP. They equilibrated the systems and subsequently applied four deformation protocols on each of the polymorphs independently: along the direction of fibrillar growth (stretch), perpendicular to the filament interface to pull these apart (peel), perpendicular to the fibril axis by shear (shear), dragging of a β-sheeet across another by pulling it parallel to the fibril growth axis (slide). They found that all aggregates are the most resistant to the stretch deformation, which becomes stronger as the number of hydrogen bonds between the layers is increased, contrary to shear. Peel and slide act on the hydrophobic core and experience hydrophobic resistance, as the hydrophobic interactions are primary responsible for keeping the protofilaments together. Structurally, the rIAPP is the least stable and it already destabilizes during the equilibration phase. The substitution of residues leads to a reduced degree of order in the fibrils which become more susceptible to deformation as compared to the wild-type.

There are few simulation studies of fibril breaking. Given the contribution of this process to creating new and fast growing fibrils, it is important to understand the mechanisms underlying fibril breakage at molecular or even atomistic level. It does not suffice to match experimental and theoretical kinetic rates to obtain a detailed picture which can be used to predict new experiments. Comparison of atomistic simulations and experimental data on fibril fragmentation would provide confidence in the models and simulation protocols and/or reveal weaknesses in the simulation methodologies.

4. SYNERGIES WITH EXPERIMENTS

The goal of the simulation studies is to shed light into the structure, dynamics, and interaction mechanisms within and between amyloidogenic peptides, and their potential involvement in pathology and/or functionality.[277] Computer simulations and experiments are complementary methods because of the inherent differences in spatiotemporal scales and resolutions (Figure 6). Simulations can reach very high temporal resolution (1 fs) and essentially unlimited spatial resolution which are not accessible by conventional biophysical techniques. On the other hand, simulations are hampered by the approximations required to access physiologically and pathologically relevant time and length scales. The atomic level of detail is sacrificed in the coarse grained and mesoscale simulation models, which can reach the time scales required for capturing the self-assembly process (Figure 6).

4.1. Challenges in Comparing Simulations and Experiments

Quantum mechanical (QM) methods capture the electronic properties, which enable the study of reaction mechanisms, charge distribution, and transition states in chemical reactions[277] (Figure 6). Nevertheless, they require a lot of computational resources and can thus only address small systems ($\leqslant 10^4$ atoms) over short time scales (fs to ps).[278] Most QM methods scale with the third power (or higher) of the number of electrons so that their application even to a short peptide is computationally prohibitive for time scales longer than nanoseconds.

In simulations based on classical mechanics (here referring to all types of atomistic simulations: MD, Monte Carlo, umbrella sampling, etc.) electronic degrees of freedom are not taken into account explicitly. Thus the atomic nuclei behave as particles (spheres) that follow the laws of classical physics, e.g., the Newton equation of motion in MD of proteins.[279] This enables the characterization of systems, usually consisting of up to 10^6 atoms over μs time scales see Figure 6. Thus classical simulations, without sacrificing the atomic detail, can reach length and time scales that are sufficient to describe the monomeric and oligomeric state for peptides with less than about 50 residues.

Frequently the structural information extracted from small-angle X-ray scattering, nuclear magnetic resonance spectroscopy, and X-ray diffraction is used to validate simulation results. Additionally, quantities derived from electron paramagnetic resonance (a spectroscopy technique for the analysis of molecules that have one or more unpaired electrons), circular dichroism, infrared, Raman spectroscopy, fluorescence microscopy, and response from atomic force microscopy experiments aids in the comparison to simulation results.[277,280] Examples include NMR derived distances, distances probed via nuclear Overhauser effect, J-couplings, chemical shifts, and binding energies. We refer the reader to the reviews that deal with potential problems when comparing simulation and experimental results[277,278,280,281] and just list these problems here. First, the quantities extracted from most experimental techniques are averaged over multiple molecules and over long time-scales. A direct comparison of simulation results and experimental data is possible for mainly rigid molecules or flexible (macro)molecules in a well defined state, *e.g.*, a globular protein in its folded state. In the case of dynamical systems, such as unstructured (poly)peptides and amyloids, different averaging techniques need to be employed.[277] Second, comparison to quantities derived from experiments, *i.e.*, not directly measured, may be erroneous and can introduce noise, as they rely on approximations and assumptions.[280,282] Therefore, one should be careful when comparing with experimental data, but also when using experimental information to bias simulation studies. Third, simulations generally emulate experimental arrangements reduced to a finite system and, hence, constrained in space by boundary conditions. Fourth, atomistic simulations of fibrillar aggregates frequently use as starting configurations structures extracted from NMR measurements or cryo-EM experiments. One has to be careful to remove any potential bias introduced by the initial configuration. In other words, averages taken over trajectories are representative if the sampling time is much longer than the relaxation time. Furthermore, in order to sample the statistically significant dynamics of a system, one should simulate at least 1 order of magnitude longer than the process one is interested in.[283] In this context it is important to note that convergence is rarely reached either due to the complexity and diversity of phase space or because it is poorly probed.[284] Some of the studies described in the present review combined experimental and computational techniques to explore different spatiotemporal resolutions. Examples include, probing of the aggregation tendency of mutated peptides[204,206] and/or analysis of oligomer size and shape distributions,[200] fibril length and pitch,[259] and binding affinities.[133,241] With recent computational advances and the abundance of high-resolution data, coarse grained models are becoming more descriptive. They usually exceed atomistic time- and length-scales by several orders of magnitude so that some of the difficulties mentioned above are alleviated, *e.g.,* dependence on starting structure. One critical aspect of coarse-grained models is the danger to steer the

DOI: 10.1021/acs.chemrev.8b00731
Chem. Rev. XXXX, XXX, XXX−XXX

simulation in a desired direction. To circumvent this problem, the Boltzmann distribution should be sampled. As discussed in Section 3.2.1 coarse grained models are highly efficient in capturing the generic mechanisms of protein aggregation.[174,176,178,181] They have been efficiently tuned to capture the experimental elongation rates[285] and fibril self-replication.[268] They can efficiently predict binding free energies and elongation mechanisms at low resolutions.[248] Combined with reaction rate theories, they showed that the conformational conversion drives primary nucleation at high temperatures, whereas secondary nucleation is hampered by the adsorption and oligomerization on the fibril surface.[175] Additionally, they have been successful in determining the activation energies and entropies for primary and secondary nucleation,[272] later probed also by atomistic simulations.[270]

Different protocols and models not only enable reaching of relevant experimental time-scales but also facilitate the visiting of important states that are hard to access via conventional methods. Markov state models enable the extraction of kinetics from multiple (short) simulations exploring statistically relevant states[286,287] or upon biased sampling,[288] and have been successfully used to calculate elongation time-scales.[243,262] Transition path sampling aids in overcoming the barriers when dealing with rare events such as nucleation[289] and enables the calculation of rate constants.[251,262] Enhanced sampling techniques such as replica exchange molecular dynamics simulations, umbrella sampling, or metadynamics enable access to states otherwise inaccessible and allow the recovering of the thermodynamics of the aggregation process being analyzed. Combinations of simplified models and enhanced-sampling simulation protocols enable access to time- and length-scales to reduce the gap with experimental studies.

4.2. Mechanisms and Rates

The mechanisms of fibril nucleation and elongation have been characterized by AFM,[42,290] internal reflection fluorescence microscopy,[88−90,290] and direct stochastic optical reconstruction microscopy.[91] On mica substrates α-synuclein can form fibrils directly, while in the presence of polyamines (*e.g.*, spermidine and spermine) it forms spheroidal oligomers as intermediate along the pathway of fibril formation.[42] These processes are now referred to as primary and secondary nucleation, respectively. Fibril elongation has been observed to occur in two stages, an actively growing phase hampered by long pauses, a process experimentally referred to as: stop-and-go".[42,88−91,290] From a simulation perspective, the "dock−lock" mechanism has been analyzed at atomic resolution.[109,225−230] At a lower resolution (Figure 6), atomic force microscopy has shed light onto the mechanisms that contribute to fibril elongation. Briefly, ultrasonication or shaking can accelerate the nucleation process, fibril elongation can occur via templated-dependent propagation, and fibrils can transform from one type to another.[41,290]

The mechanisms involved in fibril elongation have been included in kinetic theories[169,291,292] and thermodynamic models[109,248] to enable interpretation, comparison, and validation of experimental and simulation findings. The thermodynamic stability of amyloid fibrils has been determined by *in vitro* measurements of the free energy difference between a protein in solution and in the fibril.[62] The values of the elongation free energy determined by experiments (Table 1 of ref 62) are within the same order of magnitude as those calculated from the simulation studies described here (~10−100k_BT, Table 5). The free energy barrier associated with fibrillar growth consists of large and opposing terms, *viz.*, a favorable enthalpic term and a large entropic penalty of the solute.[65] The burial of hydrophobic side chains at the fibrillar tip contributes favorably because of the hydrophobic effect as in protein folding. There is little information on the saturation phase of fibrillar aggregates which is the final equilibrium between the remaining free monomers and the fibrillar species. A recent study reports on the existence of a maturation process during fibril saturation; that is, fibrils undergo structural rearrangements over a very long period of time (up to 1 year) to attain the thermodynamically favorable state.[293] On time scales of 20 to 40 μs, the coarse grained model of Pellarin et al. has captured the process of transformation from one fibril polymorph to another.[181] The much faster kinetics in the simulations are due to finite size effects and lack of friction with the solvent which is not considered explicitly.

The growth rate of amyloid fibrils depends on peptide sequence, fibrillar morphology, monomer concentration, and external parameters such as temperature and pH. The experimentally calculated monomer binding rates at the fibril ends are up to 2 orders of magnitude slower for tau (9.5×10^4 M^{-1} s^{-1}[294]) and α-synuclein (1.3×10^3 M^{-1} s^{-1}[141] to 2×10^3 M^{-1} s^{-1}[124]) than for the prion protein (2×10^5 M^{-1} s^{-1}[295]) and insulin (1.8×10^5 M^{-1} s^{-1}[296]). The growth rate of fibrils consisting of long polypeptide chains depends, at least in part, on the number of conformations that are accessible in solution and the aggregation tendency of the most populated states. It is difficult to achieve time scales of fibril growth by atomistic simulations even with enhanced sampling protocols and Markov state models[243,262] (see the locking rates in Table 5). On the other hand, nucleation kinetics have been investigated by coarse grained models.[175,268,285]

4.3. Pore Hypothesis

The controversies around the disruptive nature of fibrils and/or oligomers have brought a number of questions to our attention. On the one hand, fibrillar aggregates have been linked to cellular toxicity,[83,84] while on the other hand, a plethora of experimental data indicate that oligomeric aggregates can be pathogenic.[297] Atomistic simulations of polythiophene binding to a simplified model of the prion fibril (see Section 4.4) have revealed that fibril stabilization by small-molecule binders can be beneficial.[298] Various peptides share the ability to induce disruption in cellular membranes and lipid bilayers, resulting in dysfunction and neurodegeneration, yet the detailed mechanisms are still elusive.[299,301] Three main models have been introduced to explain membrane disruption induced by amyloid peptides: the carpeting model, the detergent-like model, and the pore model.[302] In the carpeting model, the interaction of the peptides with the membrane leads to an asymmetric pressure between the two lipid layers of the membrane, inducing leakage of small molecules.[302,303] In the detergent-like model, the peptides introduce defects in the membrane by producing micelle-like structures on the surface.[302,304] In the third model, the peptides aggregate into pore-like structures on the membrane surface, enabling ion passage.[302]

Here we will focus on the formation of pores as the primary cause of membrane induced leakage and will not discuss the other two models as these have been covered in ref 302. Briefly, calcium ions regulate the function of neuronal cells; that is, Ca^{2+} ions are involved in neuronal firing.[305] Calcium ions are present both inside and outside the cell, yet in different concentrations, *i.e.*, 10^{-7} M and 10^{-3} M, respectively.[305] The high difference

DOI: 10.1021/acs.chemrev.8b00731
Chem. Rev. XXXX, XXX, XXX−XXX

gives rise to a gradient in Ca^{2+} concentration. The transfer of ions across the cell membrane is regulated by specific ion channels, which allow passage of a controlled amount of Ca^{2+}. Increasing the intracellular concentration of Ca^{2+} ions by as little as 1 order of magnitude leads to apoptosis.[306] It has been proposed that amyloid pores form in the cellular membrane and alter the Ca^{2+} concentration in the cytosol ultimately contributing to neuronal death.[300,307,308]

The mechanisms of membrane permeation and disruption are poorly understood. Experimentally, single point mutations have been shown to influence binding to a membrane and regulate its disruption.[81] For example, the H50Q and G51D mutations in α-synuclein have been associated with increased progression of Parkinson's disease.[309] Small angle X-ray scattering studies showed that oligomers of α-synuclein and mutants thereof bind to negatively charged bilayers, and despite the similarities in aggregation number and membrane lipids, differences arise in membrane permeabilization as the G51D oligomers do not induce leakage, unlike H50Q.[81] Furthermore, the A30P and A53T mutations were shown to induce leakage more than the wild-type protein.[310] The latter was shown to allow only molecules of specific size to permeate vesicles through pores with inner diameters of up to 2.5 nm. $A\beta_{42}$ and fragments thereof were shown to form membrane pores that could facilitate Ca^{2+} passage.[82,308] The E22G mutation can also form membrane pores consisting of 40−60 monomers.[311] Furthermore, hIAPP and fragments thereof were observed to permeabilize membranes by a pore-like mechanism.[312−314] Differential scanning calorimetry, thioflavine-T fluorescence assay,[312] and circular dichroism spectroscopy[315] have revealed that fragments prone to form fibrils (i.e., $hIAPP_{12-18}$) have less membrane damaging effect than segments that do not form fibrils (i.e., $hIAPP_{1-19}$ and $hIAPP_{21-27}$). This finding suggests that amyloid formation and membrane disruption are process driven by distinct sequences of the peptide. Interestingly, the CsgG lipoprotein (required for curli production and the assembly of CsgA and CsgB) can form pore-like structures.[316]

Several simulations studies have investigated the interaction of amyloidogenic peptides with lipid membranes, yet few have focused on the "pore hypothesis". Simulations with coarse-grained models have shown that the surface of a lipid bilayer can induce the formation of β-rich fibrillar aggregates.[317] Furthermore, united atom representations have revealed that $A\beta_{42}$ inserts into a lipid bilayer from residue 17 onward and forms a β-hairpin at the segment 17−36 of its sequence.[318] For more details we refer the reader to reviews addressing the interactions with membranes.[302,319]

4.4. The Gap to *in Vivo*

The cell is a highly complex and crowded environment, rich in water, ions, carbohydrates, proteins, lipids, and nucleic acids. Each of these (macro)molecules contributes to cellular functionality, and their combination in different concentrations gives rise to rich structural and functional diversity. Biophysical and biochemical experiments and simulations are based on assumptions that reduce the complexity of a cellular system in order to apply simple analytical models or numerical approaches with a predictive role.[320] They usually rely on idealization and homogeneity of the system; that is, the system is dilute enough to ensure no interaction between the molecules and homogeneous enough to assume the composition is everywhere the same. Yet in the living cell this is rarely the case as the environment is rich in constituents and therefore crowded. In other words, crowding affects the thermodynamics and kinetics of the system, *i.e.*, equilibrium, folding, aggregation, *etc.* First, crowding influences the binding curves determined by statistical mechanics in idealized systems, as entropic effects are induced by the crowding agents.[320] Examples include the structural reordering induced by entropy in systems dealing with patchy particles.[321,322] Second, the dynamics of a system is physically different in crowded environments as compared to diluted systems. The highest impact is on the diffusion of the molecules, which will experience more collisions in a highly dense and complex medium. As a consequence, the reaction rate can also be affected. Furthermore, the folding of certain proteins is modulated by various aiding agents in the cell, *e.g.,* chaperones, which can prevent the formation of misfolded intermediates. Additionally, protein concentrations used for *in vitro* experiments (*e.g.,* of aggregation) are frequently higher than those in the cell, which may lead to inconsistent results.

Computer simulations use simplified representations of such crowded environments, which try to reproduce the chemical and physical conditions of the cell. It is both computationally and experimentally more feasible to investigate individual processes independently from each other depending on the addressed question. This divide-and-conquer strategy may influence the significance of the results and their comparison with *in vivo* systems. As an example, experimental and computational studies of amyloid fibril nucleation and growth are usually carried out in the absence of cellular membranes (exceptions, *e.g.,* refs 42, 323, 324). The lack of the membrane prevents any insight on potential toxicity, *e.g.,* due to membrane defects and leakage. Thus, it comes as no surprise that even *in vitro* and *in vivo* experiments do not always provide a consistent description. α-Synuclein, for example, was shown by both *in vitro* experiments and simulation studies to transiently adopt well defined secondary structures and fold upon interaction with other molecules.[109−111,140] Nevertheless, recent *in vivo* findings revealed that in cells the protein can both preserve the disordered nature observed *in vitro*[325−327] and sample ordered structures.[325,328]

On the computational side, recent efforts have focused on the improvement of force fields and simulation protocols.[46,47] At the atomistic level, classical transferable force fields enable the accurate description of structural ensembles of peptides and their aggregates as observed *in vitro*.[222] In the attempt to reproduce interactions with membranes and capture the pH sensitivity of peptides, Roux and collaborators have developed a constant-pH simulation protocol which is based on non-equilibrium MD/Monte Carlo sampling.[329] Furthermore, Harada et al. explored the effects of the crowding effect on water using explicit solvent molecular dynamics simulations of dense protein solutions.[330] While at low concentrations both structure and dynamics remain unaffected, at high concentrations the diffusion rates and dielectric constants of water beyond the first solvation shell are reduced.

In a translational study, atomistic simulations of a reduced fibrillar structure were used to make predictions of antiprion agents for direct *in vivo* validation.[298] Briefly, a simplified model of a prion fibril was constructed on the basis of solid-state NMR data, and the model was employed for umbrella-sampling MD simulations of ligand unbinding. The simulations revealed that negatively charged functional groups on polythiophene-based ligands form favorable ionic interactions with complementary, regularly spaced lysine side chains on the model of the prion fibril. The potential of mean force for unbinding (calculated

DOI: 10.1021/acs.chemrev.8b00731
Chem. Rev. XXXX, XXX, XXX−XXX

from the simulations) was used to design new polythiophene derivatives which showed substantial prophylactic and therapeutic potency in prion-infected mice. Notably, the most potent polythiophene derivative extended survival of mice (infected by hamster or mice prions) by more than 80%. The success of this *in silico* to *in vivo* study provides evidence of the usefulness of atomistic simulations with classical force fields for the design of compounds that may prevent neuronal injuries caused by aberrant protein aggregation.[298]

5. OUTLOOK AND FUTURE OPPORTUNITIES

5.1. Lack of Therapies

With an increasing number of patients affected by Alzheimer's disease and other neurodegenerative diseases, the need for novel therapeutic treatments is adamant. While the few current therapies can alleviate the initial symptoms, there is no treatment to reverse or just block the progress of amyloid diseases. As a matter of fact, a large number of small molecules and antibodies targeting Alzheimer's disease developed in the past 15 years have failed in clinical trials.[331−333] Only five molecules are approved by the FDA for Alzheimer's disease, and their efficacy for alleviating the symptoms is debated. We refer the reader to detailed reviews of the molecules that have been developed to modulate the pathogenic factors of Alzheimer's disease, Parkinson's disease, amyotrophic lateral sclerosis,[334] and type II diabetes.[335]

The biggest drawback encountered in the development of new therapeutic approaches is the lack of understanding of the pathological species. The most accepted hypothesis is that protein aggregates are the primary culprits, but the mechanisms of formation and their exact implication on neurotoxicity are unclear. Despite extensive efforts, it remains unknown which types of aggregate contribute to cytotoxicity, whether intra- or extracellular accumulations lead to apoptosis, and whether specific conversion mechanisms into aggregate structures are damaging or protective.[336] Current strategies target protein aggregation and focus mainly on protein reduction (organ transplantation in non-neuronal amyloidoses,[337,338] small-molecule inhibitors,[336] anti-inflammatory treatment[338]), protein stabilization (kinetic control of a desired aggregate species,[339] small-molecules[298,340,341]), protein quality control, or proteolysis.[336] Strategies targeting specifically amyloid fibrils aim to reduce the propagation of these aggregates by amyloid remodeling, minimization of the production of prefibrillar oligomers, isolation of amyloids within membrane bound organelles,[341] amyloid removal by immunization, and inhibition of cell-to-cell signaling.[336] Other promising therapies aim to modulate neuroinflammation and synaptic transmission.[342,343] References 336, 342, and 343 review all these strategies in detail and will not be rediscussed here.

5.2. Functional Amyloids and Coexistence

The present literature is highly focused on the pathological aspects related to amyloidogenic peptides and their aggregation. However, under nonpathological conditions cells have the ability to regulate the production and localization of amyloidogenic peptides so that they can carry out their physiological function. For instance, Aβ may be involved in controlling synaptic activity[344] as its production is required for neuronal activity.[345] Furthermore, it has been suggested to act as a protective agent against infections or as a repairing assistant of the blood−brain barrier.[346] α-Synuclein may play a role in the regulation of neurotransmitter release, synaptic function, and plasticity.[347,348] Amylin is a regulatory peptide for insulin and glucagon secretion, with binding sites in the brain and has been proposed to promote satiety and inhibit gastric emptying.[349] Tau is implicated in microtubule stabilization, in the morphological differentiation and synaptic integration of new neurons.[350] Among the potential physiological roles of PrP^c are synaptic transmission and plasticity, memory formation, calcium homeostasis, neuroprotection, and peripheral myelin maintenance.[351] Given the abundance of functional activities of these (poly)peptides, we propose a redirection of focus toward the exploration of the structural and dynamic properties related to their nonpathological roles. For instance, simulations of their soluble monomeric state in proximity of membranes, receptors (e.g., the G protein-coupled receptor Adgrg6 for PrP^c[352]), or microtubules (for tau) could be carried out first with coarse grained models to sample a large variety of relative positions and orientations. These complexes could be used as starting structures for enhanced sampling by atomistic simulations.

Functional amyloids are gradually attracting more interest due to their properties and similarities to disease-related amyloids. In healthy cells they fulfill a range of tasks both intra- and extracellularly; that is, they act as agents for pigmentation, hormone storage, cell regulation, epigenetic inheritance, signal transductions, and memory.[10,13,353,354] Furthermore, it has been recently shown that part of the functional cytoplasmic polyadenylation element binding protein (CPEB) can form toxic oligomers, which is prevented by rapid formation of innocuous species.[355] A number of questions arise in the context of functional amyloids. Why are functional and pathological amyloids so similar in overall structure and yet so different in phenotype? Are there substantial differences in their aggregation mechanisms? How does the cell regulate the production of functional amyloids? Are functional amyloids able to penetrate cellular membranes in a similar way as disease-related ones? And more importantly, what can one learn from functional amyloids and how can it be deciphered in a toxic context? Given the time scales involved in the formation of functional amyloids, phenomenological or bottom-up coarse-grained models seem more appropriate than atomistic simulations to investigate differences in aggregation mechanisms.

Collective interactions between amyloidogenic peptides can have a functional or pathological role. For example, PrP^c appears to scavenge amyloid-β aggregates[351] or bind to α-synuclein fibrils modulating their effect[356] and inhibit the elongation of $A\beta_{42}$ fibrils.[357] Furthermore, PrP^c was shown to aid in the transport of Aβ across the brain−blood barrier.[358] *In vivo* experiments show that interactions between Aβ, tau, and α-synuclein promote protein aggregation and accelerate cognitive dysfunction.[359] Aβ and α-synuclein have been proposed to collectively form ion channels which may contribute to neurodegeneration.[360,361] Interactions between α-synuclein fibrils and tau were shown to inhibit microtubule assembly and stimulate tau aggregation.[362] Interestingly, exposure of bacterial amyloid was shown to enhance α-synuclein aggregation and stimulate the innate immune system.[363] The mechanisms of interaction between distinct peptide species remain elusive. It is, to date, unclear how cross-binding of peptide species can influence each other's aggregation and regulate neurodegeneration. While from an experimental perspective some aspects have been explored, from a simulation view there are, to our knowledge, few studies examining coexistence and cross-interactions between different amyloidogenic peptide species.[364,365] We propose to study the formation

DOI: 10.1021/acs.chemrev.8b00731
Chem. Rev. XXXX, XXX, XXX−XXX

of mixed oligomeric states and fibrils by grand-canonical Monte Carlo sampling which can treat a variable number of peptide molecules (at a constant chemical potential). The grand-canonical Monte Carlo sampling has to be combined with MD simulations to relax the system upon each insertion or deletion of peptide(s).

5.3. Emerging Techniques

5.3.1. Cryo-EM. Recent advancements in cryo-electron microscopy (cryo-EM)[366−368] have enabled the determination of three-dimensional (3D) structures of new fibrillar polymorphs at atomic resolution. These 3D structures represent new avenues toward the development of therapeutic interventions for Aβ_{42},[369] tau,[257,370] and α-synuclein.[371,372] Despite the variety in their sequence all fibrils follow the common amyloid fold with parallel β-sheets ordered along the fibrillar axis, and thus β-strands perpendicular to the axis (Figure 1). Furthermore, they consist of two filaments wrapped around each other and stabilized at the interfacee by hydrophobic steric zippers and/or salt bridges (see Figure 5 in ref 373).

The structural polymorphism of amyloid fibrils and its influence in disease onset and progression are poorly understood. With cryo-EM being an emerging field, an increasing number of fibrillar structures at atomic resolution will be determined in the coming years. They will be valuable candidates to investigate by atomistic simulations, which, combined with experimental biophysical approaches, would provide insight into the role of fibril polymorphism not only in disease but also in functionality. Cryo-EM aids in the identification of possible similarities between fibril polymorphs and, combined with molecular simulations, can lead to the recognition of metastable druggable states.[368] Future directions of cryo-EM may even provide a platform for direct comparison and/or validation against simulations. In particular, full resolution imaging of dynamic states of biological molecules would enable a better understanding of the relationship between structure, dynamics, and function. The imaging of short-lived states of biological molecules has been reported by introducing the time component into cryo-EM, and it could recover a continuum of coexisting states.[374−376] This appears to be a promising technique to connect experiment and simulations, particularly for protein targets that are difficult to treat by X-ray crystallography and NMR spectroscopy. Nevertheless, it encounters some drawbacks, *e.g.,* radiation damage and image quality, which will most probably be open to discussion and clarification in the coming years.

5.3.2. Machine Learning. Machine learning is a subfield of computer science that has experienced a boom for about a decade because of the large amount of data to train neural networks (*e.g.,* for object classification) and the availability of GPUs for efficient training. With a proven record in various fields (*e.g.,* image and voice recognition) and broad applicability including super-resolution microscopy data,[377] machine learning is finding its utility in drug discovery[378,379] and gradually in prediction of protein structure, binding, or phosphorylation sites.[380−382] Recently, machine learning software has been developed to try to classify intrinsically disordered proteins into soluble and insoluble categories (reviewed in ref 381).

For high precision output, the training data set needs to contain a large quantity of high quality information. Here a number of challenges arise in the prediction of the behavior of amyloidogenic peptides and/or their aggregates. The amount of data determined experimentally and computationally is too small and often contradicting, making it difficult to evaluate the accuracy of the training data. The molecular mechanisms underlying protein aggregation are to date unclear; therefore, the choice of representation for the proteins is intricate and limited to biochemical properties.[382]

Future applications of machine learning algorithms will require a large amount of input data, e.g., for the prediction of amyloidogenic (poly)peptide sequences or the design of small-molecule modulators of self-assembly. It will be necessary to acquire large data sets for peptides and protein fragments from simulations and experiments using combined approaches based on biophysical and biochemical methods. This will enable the extrapolation to larger peptide sequences or aggregates. Furthermore, similarities in sequence and propensity for regular elements of secondary structures (*e.g.,* β-hairpin formation and/or cross-β arrangement) could be used as additional representations to describe the generic amyloid state. We would like to close this subsection by noting that for the prediction of aggregation rates (linear) analytical models fitted on experimental data can also be considered machine learning tools even if they were not classified as such by their developers. Predictive models trained on experimental data of lag times and elongation rates, and/or atomistic simulations of ordered aggregation, have existed for more than 15 years.[383,384]

5.3.3. Progress in Hardware Technology and Simulation Techniques. The past two decades have witnessed major progress in computational methods for simulations of biological (macro)molecules. The improvements in hardware include graphics processing units, special-purpose parallel architectures, and parallelization across general-purpose computer chips, while the main advancements in simulation methodology are enhanced sampling, coarse graining, and force field development.[49,276,385,386] These progresses enable the access to longer time- and length-scales, and in turn to conformations otherwise unreachable by conventional methods. Nevertheless, they are not sufficient to reach a more direct comparison to experiment. While it is expected that computational methods will improve further in the coming years, multiscale approaches will equally facilitate the connection between experiment and simulations. Here we mention integrative methods, which combine information from experimental techniques (*e.g.,* small-angle X-ray spectroscopy, NMR spectroscopy, X-ray crystallography, electron and atomic force microscopy) with physical theories (*e.g.,* statistical mechanics) and statistical analysis (*e.g.,* Bayesian statistics) to compute integrative or hybrid models of protein assembly.[387,388] Examples include the use of chemical shifts as restrains to explore the conformational space of disordered peptides[389] and characterization of binding sites.[390] Reviews addressing the most commonly used techniques in the context of integrative methods can be found in refs 387, 391, 392. Additionally, the development of new integrative modeling platforms (*e.g.,* refs 393−395) facilitate the processing of a large amount of data at atomic resolution into three-dimensional macromolecular assemblies[396] or even models of cells.[397] Potentially interesting are the multiscale models that integrate atomistic representations with coarse-grain models.[45] Hybrid atomistic/coarse-grain representations are a mix of all-atom force-fields with coarse representations within the same molecule. For example, a recent combination of the all-atom CHARMM force field and coarse-grained PRIMO model[398] was used to calculate the free energy profile for the transition from the closed to the open state of adenylate kinase.[399] The PACE force-field uses a united-atom

DOI: 10.1021/acs.chemrev.8b00731
Chem. Rev. XXXX, XXX, XXX−XXX

representation coupled to a coarse MARTINI water model[142] and was employed to study the early oligomerization pathways of $A\beta_{40}$[197] and studying fibril elongation.[228] Furthermore, the UNRES model,[400] in which a protein is represented as a chain of C_α atoms with united peptide groups and side-chains attached to them, can provide insight into the mechanisms of $A\beta$ fibril elongation[401] or cross-binding between different peptides.[365] From a coarser perspective we mention the self-organized polymer model (SOP-SC), in which each residue is represented by two interaction centers, i.e., one located at C_α and one at the center of mass of the side chain. This model demonstrated that the application of mechanical force enhances the population of the otherwise rarely populated aggregation-prone states.[187] Additionally, it was recently used to show that cosolvents can modulate the elongation kinetics of $A\beta_{9-40}$.[402] Furthermore, its implementation on GPUs enables access to time scales up to centiseconds.[403]

5.4. New Directions in Simulations

Despite major progress in experimental and simulation studies of amyloidogenic polypeptides, a series of questions remain unanswered. These questions offer the opportunity to explore new directions from a simulation perspective, which can add to the current limited understanding of the toxic species and mechanisms of neuronal injury. We propose that coarse grained and multiscale models would be suitable in exploring the molecular mechanisms underlying pore formation. Furthermore, atomistic simulations could be used to investigate the monomeric and/or aggregated forms of peptides that interact with membrane-anchored proteins *in vivo* and modulate their activity.[404] With this in mind, we suggest that a complete analysis of the interaction of amyloidogenic species with distinct cell surface receptors would reveal further permeation mechanisms, which may lead to therapeutic intervention (*e.g.,* development of channel blockers). Atomistic studies addressing the full pallette of amyloidogenic peptides would aid in differentiating between the selectivity of receptors for certain species; as an example good receptors for $A\beta$ promote its transcytosis out of the brain, and bad receptors bind to oligomers and contribute to synaptic loss.[404]

Furthermore, a change in direction from the frequently analyzed proteins and peptides such as amyloid-β and amylin to, the less investigated, tau, α-synuclein, and functional amyloidogenic peptides could inform on (common) mechanisms of membrane permeation. Next, the investigation of the structural differences between pore-like oligomers and other types of oligomers (e.g., on- and off-pathway) using enhanced sampling techniques at high resolution may reveal key aspects that contribute to the evolution of these aggregates into other species. Lower resolution models are efficient in capturing processes such as secondary nucleation and fibril fragmentation, which contribute significantly to the generation of new nuclei.[176,178,268] Starting from pathways obtained by coarse grained models, umbrella sampling and atomistic MD could be used to shed light on the energetics and pathways of nucleus formation which would help for the design of small-molecule modulators. Furthermore, atomistic simulations can inform on the coexistence and cross-interactions between amyloidogenic (poly)peptides in the cell.

6. CONCLUSIONS

We have reviewed simulation studies of amyloidogenic (poly)-peptides in the monomeric state, their nucleation, and fibril propagation. Coarse grained models capture the self-assembly of amyloidogenic peptides and proteins into oligomeric states and fibrillar structures, but it is difficult to use the results obtained with simplified models to suggest new experiments because they lack atomic detail. Atomistic simulations face difficulties in reaching the time scales of nucleation and fibril elongation. Thus several computational studies of amyloid aggregation have made use of implicit solvent and enhanced sampling techniques and/or have tried to infer from simulations of detachment the mechanisms of monomer association to the fibrillar tips. These studies have been successful in shedding light on the pathways and kinetics of oligomerization and fibril formation.

Despite intensive experimental efforts and a large number of computational studies, several questions on amyloid aggregation remain unanswered. Very little is known on the toxic species *in vivo* and the mechanism(s) of neuronal injury. Is it beneficial to design molecules that block or hinder fibril formation, the so-called β-sheet breakers? This question is relevant because of recent evidence that small molecules (more precisely linear conjugated polythiophenes) that stabilize cross-β aggregates show prophylactic and therapeutic efficacy in prion-infected mice.[298] Thus, β-sheet breakers could increase the amount of toxic (oligomeric) species.

Evidence has accumulated on amyloid-like aggregates with physiological properties. As an example, a functional amyloid seems to be involved in memory consolidation in a broad range of living organisms from marine snails to mice.[16] In contrast, the knowledge on the spatial and temporal regulation of functional amyloids is rather limited. It is not clear what are the differences in aggregation pathways and kinetics between pathological and functional amyloids. The understanding of these differences at atomic level of detail may help in designing drugs against neurodegenerative diseases for which there are currently no cures. We hope that this review will inspire and motivate computational structural biologists to collaborate with experimentalists to shed light onto the molecular details of amyloid disorders. The failure of the many clinical trials of potential medicines for Alzheimer's disease[331−333] is due not only to the complexity of the human brain but also to the limited knowledge of the molecular aspects of amyloid diseases.

AUTHOR INFORMATION

Corresponding Authors

E-mail: i.ilie@bioc.uzh.ch.
E-mail: caflisch@bioc.uzh.ch.

ORCID

Ioana M. Ilie: 0000-0002-5935-3332
Amedeo Caflisch: 0000-0002-2317-6792

Notes

The authors declare no competing financial interest.

Biographies

Ioana-Măriuca Ilie received a Ph.D. in Computational Biophysics from the University of Twente in The Netherlands under the direction of Profs. Wim Briels and Wouter den Otter. During her graduate work she focused on developing novel simulation methods and coarse-grained models to study protein aggregation. Her academic career continued with a postdoc mentored by Profs. Nico van der Vegt and Wim Briels at the Universities of Darmstadt in Germany and Twente in The Netherlands, where she explored the mechanisms behind α-synuclein fibril stability from an atomistic perspective. Since 2017 she has been a

DOI: 10.1021/acs.chemrev.8b00731
Chem. Rev. XXXX, XXX, XXX−XXX

postdoctoral research fellow in the group of Prof. Amedeo Caflisch at the University of Zurich in Switzerland. Her postdoctoral work is funded by the Peter and Traudl Engelhorn Foundation and focuses on exploring the structural details of amyloid-β fibril elongation by means of molecular dynamics simulations.

Amedeo Caflisch studied theoretical physics at the ETH in Zurich. During 1992−1994 he was a postdoctoral fellow in the group of Martin Karplus at Harvard University. In 1995 he was offered an assistant professorship position at the Department of Biochemistry of the University of Zurich, and he was promoted to full professor in 2001. His research group has developed methods for enhanced sampling molecular dynamics and data-driven analysis of simulations of protein folding, amyloid aggregation, and ligand binding. The group has also developed virtual screening procedures based on fragment docking, which have been applied to enzymes and protein−protein recognition domains of pharmaceutical relevance. In 2013, at the age of 50, he decided to start gene-to-structure experimental activities in his group, which have resulted in the crystal structures of nearly 50 enzyme/inhibitor complexes and about 150 bromodomain/ligand complexes. Most of the ligands in these complexes originate from docking. Some of these hit compounds have been optimized into leads that show antiproliferative activity in mouse models of cancer.

ACKNOWLEDGMENTS

We thank Mireille Claessens, Slav Semerdzhiev, Jean-Rémy Marchand, and Karthik Ramanadane for interesting discussions. Ioana M. Ilie thanks the Peter und Traudl Engelhorn Foundation for a postdoctoral fellowship. This work was supported in part by grants of the Swiss National Science Foundation, the Synapsis Foundation-Alzheimer Research Switzerland, and the Heidi Seiler-Stiftung to Amedeo Caflisch.

ABBREVIATIONS

1SN	1-step nucleation
SN	2-step nucleation
Aβ	amyloid-β peptide
ABSINTH	self-assembly of biomolecules studied by an implicit, novel, and tunable Hamiltonian
AD	Alzheimer's disease
CHC	central hydrophobic cluster
cryo-EM	cryo-electron microscopy
C-ter	C-terminus
DPS	discrete path sampling
EEF1	effective energy function 1
GB	generalized Born
GBSW	generalized Born with a simple switching
IAPP	islet amyloid polypeptide
IDP	intrinsically disordered protein
LD	Langevin dynamics
MD	molecular dynamics
MhREX	multiplexed Hamiltonian replica exchange
ML	machine learning
MM-GBSA	molecular mechanics−generalized Born surface area
MSM	Markov state model
MT	microtubule
NAC	non-amyloid component
N-ter	N-terminus
PACE	proteins with atomic details in coarse-grained environment
PCA	principal component analysis
PD	Parkinson's disease
PIGS	progress index guided sampling
REMD	replica exchange molecular dynamics
R_g	radius of gyration
SASA	solvent accesible surface area
SAXS	small-angle X-ray scattering
SMD	steered molecular dynamics
SPC	simple point charge water model
ssNMR	solution state nuclear magnetic resonance
TI	thermodynamic integration
TICA	time-lagged independent component analysis
TIP3P	transferable intermolecular potential with 3 points
TSE	transmissible spongiform encephalopathy

REFERENCES

(1) Knowles, T. P. J.; Vendruscolo, M.; Dobson, C. M. The Amyloid State and its Association with Protein Misfolding Diseases. *Nat. Rev. Mol. Cell Biol.* **2014**, *15*, 384−396.
(2) Sipe, J. D.; Cohen, A. S. Review: History of the Amyloid Fibril. *J. Struct. Biol.* **2000**, *130*, 88−98.
(3) Dobson, C. M. Protein Misfolding, Evolution and Disease. *Trends Biochem. Sci.* **1999**, *24*, 329−332.
(4) Greenwald, J.; Kwiatkowski, W.; Riek, R. Peptide Amyloids in the Origin of Life. *J. Mol. Biol.* **2018**, *430*, 3735−3750.
(5) Riek, R.; Eisenberg, D. S. The Activities of Amyloids from a Structural Perspective. *Nature* **2016**, *539*, 227−235.
(6) Sipe, J. D.; Benson, M. D.; Buxbaum, J. N.; Ikeda, S.-i.; Merlini, G.; Saraiva, M. J. M.; Westermark, P. Nomenclature 2014: Amyloid Fibril Proteins and Clinical Classification of the Amyloidosis. *Amyloid* **2014**, *21*, 221−224.
(7) Koo, E. H.; Lansbury, P. T.; Kelly, J. W. Amyloid Diseases: Abnormal Protein Aggregation in Neurodegeneration. *Proc. Natl. Acad. Sci. U. S. A.* **1999**, *96*, 9989−9990.
(8) Chiti, F.; Dobson, C. M. Protein Misfolding, Amyloid Formation, and Human Disease: A Summary of Progress Over the Last Decade. *Annu. Rev. Biochem.* **2017**, *86*, 27−68.
(9) Chiti, F.; Dobson, C. M. Protein Misfolding, Functional Amyloid, and Human Disease. *Annu. Rev. Biochem.* **2006**, *75*, 333−366.
(10) Dueholm, M. S.; Nielsen, P. H.; Chapman, M.; Otzen, D. *Amyloid Fibrils and Prefibrillar Aggregates*; Wiley-VCH Verlag GmbH and Co. KGaA, 2013; pp 411−438.
(11) Cherny, I.; Gazit, E. Amyloids: Not Only Pathological Agents but Also OrderedNanomaterials. *Angew. Chem., Int. Ed.* **2008**, *47*, 4062−4069.
(12) Sleutel, M.; Van den Broeck, I.; Van Gerven, N.; Feuillie, C.; Jonckheere, W.; Valotteau, C.; Dufrene, Y. F.; Remaut, H. Nucleation and growth of a bacterial functional amyloid at single-fiber resolution. *Nat. Chem. Biol.* **2017**, *13*, 902−908.
(13) Fowler, D. M.; Koulov, A. V.; Balch, W. E.; Kelly, J. W. Functional Amyloid - from Bacteria to Humans. *Trends Biochem. Sci.* **2007**, *32*, 217−224.
(14) McGlinchey, R. P.; Shewmaker, F.; McPhie, P.; Monterroso, B.; Thurber, K.; Wickner, R. B. The Repeat Domain of the Melanosome Fibril Protein Pmel17 forms the Amyloid Core Promoting Melanin Synthesis. *Proc. Natl. Acad. Sci. U. S. A.* **2009**, *106*, 13731−13736.
(15) Maji, S. K.; Perrin, M. H.; Sawaya, M. R.; Jessberger, S.; Vadodaria, K.; Riss- man, R. A.; Singru, P. S.; Nilsson, K. P. R.; Simon, R.; Schubert, D.; Eisenberg, D.; Rivier, J.; Sawchenko, P.; Vale, W.; Riek, R. Functional Amyloids as Natural Storage of Peptide Hormones in Pituitary Secretory Granules. *Science* **2009**, *325*, 1−6.
(16) Si, K.; Kandel, E. R. The Role of Functional Prion-Like Proteins in the Persistence of Memory. *Cold Spring Harbor Perspect. Biol.* **2016**, *8*, a021774
(17) Li, D.; Jones, E. M.; Sawaya, M. R.; Furukawa, H.; Luo, F.; Ivanova, M.; Sievers, S. A.; Wang, W.; Yaghi, O. M.; Liu, C.; Eisenberg, D. S. Structure-Based Design of Functional Amyloid Materials. *J. Am. Chem. Soc.* **2014**, *136*, 18044−18051.

DOI: 10.1021/acs.chemrev.8b00731
Chem. Rev. XXXX, XXX, XXX−XXX

(18) Al-Garawi, Z. S.; Morris, K. L.; Marshall, K. E.; Eichler, J.; Serpell, L. C. The Diversity and Utility of Amyloid Fibrils formed by short Amyloidogenic Peptides. *Interface Focus* **2017**, *7*, 20170027
(19) Li, J.; McQuade, T.; Siemer, A. B.; Napetschnig, J.; Moriwaki, K.; Hsiao, Y.-S.; Damko, E.; Moquin, D.; Walz, T.; McDermott, A.; Chan, F. K.-M.; Wu, H. The RIP1/RIP3 Necrosome Forms a Functional Amyloid Signaling Complex Required for Programmed Necrosis. *Cell* **2012**, *150*, 339−350.
(20) Lomakin, A.; Teplow, D. B.; Kirschner, D. A.; Benedek, G. B. Kinetic Theory of Fibrillogenesis of Amyloid β-protein. *Proc. Natl. Acad. Sci. U. S. A.* **1997**, *94*, 7942−7947.
(21) Hellstrand, E.; Boland, B.; Walsh, D. M.; Linse, S. Amyloid β-Protein Aggregation Produces Highly Reproducible Kinetic Data and Occurs by a Two-Phase Process. *ACS Chem. Neurosci.* **2010**, *1*, 13−18.
(22) Ferrone, F. A.; Hofrichter, J.; Eaton, W. A. Kinetics of Sickle Hemoglobin Polymerization: II. A Double Nucleation Mechanism. *J. Mol. Biol.* **1985**, *183*, 611−631.
(23) Rochet, J.-C.; Lansbury, P. T. Amyloid Fibrillogenesis: Themes and Variations. *Curr. Opin. Struct. Biol.* **2000**, *10*, 60−68.
(24) Buell, A. K.; Galvagnion, C.; Gaspar, R.; Sparr, E.; Vendruscolo, M.; Knowles, T. P. J.; Linse, S.; Dobson, C. M. Solution Conditions Determine the Relative Importance of Nucleation and Growth Processes in α-Synuclein Aggregation. *Proc. Natl. Acad. Sci. U. S. A.* **2014**, *111*, 7671−7676.
(25) Gaspar, R.; Meisl, G.; Buell, A. K.; Young, L.; Kaminski, C. F.; Knowles, T. P. J.; Sparr, E.; Linse, S. Secondary Nucleation of Monomers on Fibril Surface Sominates α-Synuclein Aggregation and Provides Autocatalytic Amyloid Amplification. *Q. Rev. Biophys.* **2017**, *50*, e6.
(26) Arosio, P.; Beeg, M.; Nicoud, L.; Morbidelli, M. Time Evolution of Amyloid Fibril Length Distribution Described by a Population Balance Model. *Chem. Eng. Sci.* **2012**, *78*, 21−32.
(27) Xue, W.-F.; Radford, S. E. An Imaging and Systems Modeling Approach to Fibril Breakage Enables Prediction of Amyloid Behavior. *Biophys. J.* **2013**, *105*, 2811−9.
(28) Ignatova, Z.; Gierasch, L. M. Inhibition of Protein Aggregation in Vitro and in Vivo by a Natural Osmoprotectant. *Proc. Natl. Acad. Sci. U. S. A.* **2006**, *103*, 13357−13361.
(29) Giehm, L.; Luis Pinto Oliveira, C.; Christiansen, G.; Pedersen, J.; Otzen, D. SDS-Induced Fibrillation of α-Synuclein: An Alternative Fibrillation Pathway. *J. Mol. Biol.* **2010**, *401*, 115−33.
(30) Lindberg, D. J.; Wesen, E.; Bjoerkeroth, J.; Rocha, S.; Esbjoerner, E. K. Lipid Membranes Catalyse the Fibril Formation of the Amyloid-β (1−42) Peptide through Lipid-Fibril Interactions that Reinforce Secondary Pathways. *Biochim. Biophys. Acta, Biomembr.* **2017**, *1859*, 1921−1929.
(31) Galvagnion, C.; Brown, J. W. P.; Ouberai, M. M.; Flagmeier, P.; Vendruscolo, M.; Buell, A. K.; Sparr, E.; Dobson, C. M. Chemical Properties of Lipids Strongly Affect the Kinetics of the Membrane-induced Aggregation of α-Synuclein. *Proc. Natl. Acad. Sci. U. S. A.* **2016**, *113*, 7065−7070.
(32) Fusco, G.; Chen, S.; Williamson, P.; Cascella, R.; Perni, M.; Jarvis, J.; Cecchi, C.; Vendruscolo, M.; Chiti, F.; Cremades, N.; Ying, L.; M. Dobson, C.; De Simone, A. Structural Basis of Membrane Disruption and Cellular Toxicity by α-Synuclein Oligomers. *Science* **2017**, *358*, 1440−1443.
(33) Chaudhary, H.; Stefanovic, A. N.; Subramaniam, V.; Claessens, M. M. Membrane Interactions and Fibrillization of α-Synuclein Play an Essential Role in Membrane Disruption. *FEBS Lett.* **2014**, *588*, 4457−4463.
(34) Chaudhary, H.; Subramaniam, V.; Claessens, M. M. A. E. Direct Visualization of Model Membrane Remodeling by α-Synuclein Fibrillization. *ChemPhysChem* **2017**, *18*, 1620−1626.
(35) Sun, Y.; Hung, W.-C.; Lee, M.-T.; Huang, H. W. Membrane-mediated Amyloid Formation of PrP 106−126: A Kinetic Study. *Biochim. Biophys. Acta, Biomembr.* **2015**, *1848*, 2422−2429.
(36) Engel, M. F. M.; Khemtémourian, L.; Kleijer, C. C.; Meeldijk, H. J. D.; Jacobs, J.; Verkleij, A. J.; de Kruijff, B.; Killian, J. A.; Höppener, J. W. M. Membrane Damage by Human Islet Amyloid Polypeptide through Fibril Growth at the Membrane. *Proc. Natl. Acad. Sci. U. S. A.* **2008**, *105*, 6033−6038.
(37) Williams, T. L.; Serpell, L. C. Membrane and Surface Interactions of Alzheimer's Aβ Peptide-Insights into the Mechanism of Cytotoxicity. *FEBS J.* **2011**, *278*, 3905−3917.
(38) Murphy, R. M. Kinetics of Amyloid Formation and Membrane Interaction with Amyloidogenic Proteins. *Biochim. Biophys. Acta, Biomembr.* **2007**, *1768*, 1923−1934.
(39) Jayasinghe, S. A.; Langen, R. Membrane Interaction of Islet Amyloid Polypeptide. *Biochim. Biophys. Acta, Biomembr.* **2007**, *1768*, 2002−2009.
(40) Arosio, P.; Knowles, T. P. J.; Linse, S. On the Lag Phase in Amyloid Fibril Formation. *Phys. Chem. Chem. Phys.* **2015**, *17*, 7606−7618.
(41) Shvadchak, V. V.; Claessens, M. M. A. E.; Subramaniam, V. Fibril Breaking Accelerates α-Synuclein Fibrillization. *J. Phys. Chem. B* **2015**, *119*, 1912−1918.
(42) Hoyer, W.; Cherny, D.; Subramaniam, V.; Jovin, T. M. Rapid Self-assembly of α-Synuclein Observed by In Situ Atomic Force Microscopy. *J. Mol. Biol.* **2004**, *340*, 127−139.
(43) Elber, R. Long-timescale Simulation Methods. *Curr. Opin. Struct. Biol.* **2005**, *15*, 151−56.
(44) Scheraga, H. A.; Khalili, M.; Liwo, A. Protein-Folding Dynamics: Overview of Molecular Simulation Techniques. *Annu. Rev. Phys. Chem.* **2007**, *58*, 57−83.
(45) Tozzini, V. Multiscale Modeling of Proteins. *Acc. Chem. Res.* **2010**, *43*, 220−230.
(46) Kmiecik, S.; Gront, D.; Kolinski, M.; Wieteska, L.; Dawid, A. E.; Kolinski, A. Coarse-Grained Protein Models and Their Applications. *Chem. Rev.* **2016**, *116*, 7898−7936.
(47) Somavarapu, A. K.; Kepp, K. P. The Dependence of Amyloid-β Dynamics on Protein Force Fields and Water Models. *ChemPhysChem* **2015**, *16*, 3278−3289.
(48) Brucale, M.; Schuler, B.; Samori, B. Single-Molecule Studies of Intrinsically Disordered Proteins. *Chem. Rev.* **2014**, *114*, 3281−3317.
(49) Robustelli, P.; Piana, S.; Shaw, D. E. Developing a Molecular Dynamics Force Field for Both Folded and Disordered Protein States. *Proc. Natl. Acad. Sci. U. S. A.* **2018**, *115*, E4758−E4766.
(50) Harper, J. D.; Lansbury, P. T. Models of Amyloid Seeding in Alzheimer's Disease and Scrapie: Mechanistic Truths and Physiological Consequences of the Time-Dependent Solubility of Amyloid Proteins. *Annu. Rev. Biochem.* **1997**, *66*, 385−407.
(51) Nilsson, M. R. Techniques to Study Amyloid Fibril Formation in Vitro. *Methods* **2004**, *34*, 151−160.
(52) Eanes, E. D.; Glenner, G. G. X-ray Diffraction Studies on Amyloid Filaments. *J. Histochem. Cytochem.* **1968**, *16*, 673−677.
(53) Rambaran, R. N.; Serpell, L. C. Amyloid Fibrils Abnormal Protein Assembly. *Prion* **2008**, *2*, 112−117.
(54) Vilar, M.; Chou, H.-T.; Lührs, T.; Maji, S. K.; Riek-Loher, D.; Verel, R.; Manning, G.; Stahlberg, H.; Riek, R. The Fold of α-Synuclein Fibrils. *Proc. Natl. Acad. Sci. U. S. A.* **2008**, *105*, 8637−8642.
(55) Xu, S. Cross-β-Sheet Structure in Amyloid Fiber Formation. *J. Phys. Chem. B* **2009**, *113*, 12447−12455.
(56) Sunde, M.; Serpell, L. C.; Bartlam, M.; Fraser, P. E.; Pepys, M. B.; Blake, C. C. Common Core Structure of Amyloid Fibrils by Synchrotron X-ray Diffraction. *J. Mol. Biol.* **1997**, *273*, 729−739.
(57) Fitzpatrick, A. W. P.; et al. Atomic Structure and Hierarchical Assembly of a Cross-β Amyloid Fibril. *Proc. Natl. Acad. Sci. U. S. A.* **2013**, *110*, 5468−5473.
(58) Eisenberg, D. S.; Sawaya, M. R. Structural Studies of Amyloid Proteins at the Molecular Level. *Annu. Rev. Biochem.* **2017**, *86*, 69−95.
(59) Kirschner, D. A.; Abraham, C.; Selkoe, D. J. X-ray diffraction from intraneuronal paired helical filaments and extraneuronal amyloid fibers in Alzheimer disease indicates cross-beta conformation. *Proc. Natl. Acad. Sci. U.S.A.* **1986**, *83*, 503−507.
(60) Loizos, S.; Chrysa, T. S.; Christos, G. S. Amyloidosis: Review and Imaging Findings. *Seminars in Ultrasound, CT and MRI* **2014**, *35*, 225−239.

DOI: 10.1021/acs.chemrev.8b00731
Chem. Rev. XXXX, XXX, XXX−XXX

(61) Bleem, A.; Daggett, V. Structural and Functional Diversity among Amyloid Proteins: Agents of Disease, Building Blocks of Biology, and Implications for Molecular Engineering. *Biotechnol. Bioeng.* **2017**, *114*, 7−20.
(62) Baldwin, A. J.; Knowles, T. P. J.; Tartaglia, G. G.; Fitzpatrick, A. W.; Devlin, G. L.; Shammas, S. L.; Waudby, C. A.; Mossuto, M. F.; Meehan, S.; Gras, S. L.; Christodoulou, J.; Anthony-Cahill, S. J.; Barker, P. D.; Vendruscolo, M.; Dobson, C. M. Metastability of Native Proteins and the Phenomenon of Amyloid Formation. *J. Am. Chem. Soc.* **2011**, *133*, 14160−14163.
(63) Gazit, E. The 'Correctly Folded' State of Proteins: Is It a Metastable State? *Angew. Chem., Int. Ed.* **2002**, *41*, 257−259.
(64) Shewmaker, F.; McGlinchey, R. P.; Thurber, K. R.; McPhie, P.; Dyda, F.; Tycko, R.; Wickner, R. B. The Functional Curli Amyloid Is Not Based on In-register Parallel β-Sheet Structure. *J. Biol. Chem.* **2009**, *284*, 25065−25076.
(65) Buell, A. K.; Dhulesia, A.; White, D. A.; Knowles, T. P. J.; Dobson, C. M.; Welland, M. E. Detailed Analysis of the Energy Barriers for Amyloid Fibril Growth. *Angew. Chem., Int. Ed.* **2012**, *51*, 5247−5251.
(66) Jarrett, J. T.; Lansbury, P. T. Seeding 'One-dimensional Crystallization' of Amyloid: A Pathogenic Mechanism in Alzheimer's Disease and Scrapie? *Cell* **1993**, *73*, 1055−1058.
(67) Come, J. H.; Lansbury, P. T. Predisposition of Prion Protein Homozygotes to Creutzfeldt-Jakob Disease can be Explained by a Nucleation-dependent Polymerization Mechanism. *J. Am. Chem. Soc.* **1994**, *116*, 4109−4110.
(68) Hofrichter, J.; Ross, P. D.; Eaton, W. A. Kinetics and Mechanism of Deoxyhemoglobin S Gelation: A New Approach to Understanding Sickle Cell Disease. *Proc. Natl. Acad. Sci. U. S. A.* **1974**, *71*, 4864−4868.
(69) Eaton, W. A.; Hofrichter, J. *Sickle Cell Hemoglobin Polymerization*; Advances in Protein Chemistry; Academic Press, 1990; Vol. *40*; pp 63−279.
(70) Auer, S.; Ricchiuto, P.; Kashchiev, D. Two-Step Nucleation of Amyloid Fibrils: Omnipresent or Not? *J. Mol. Biol.* **2012**, *422*, 723−730.
(71) Sengupta, U.; Nilson, A.; Kayed, R. The Role of Amyloid-β Oligomers in Toxicity, Propagation, and Immunotherapy. *EBioMedicine* **2016**, *6*, 42−49.
(72) Walsh, D. M.; Lomakin, A.; Benedek, G. B.; Condron, M. M.; Teplow, D. B. Amyloid β-Protein Fibrillogenesis: Detection of a Protofibrillar Intermediate. *J. Biol. Chem.* **1997**, *272*, 22364−22372.
(73) Harper, J. D.; Lieber, C. M.; Lansbury, P. T. Atomic Force Microscopic Imaging of Seeded Fibril Formation and Fibril Branching by the Alzheimer's Disease Amyloid-β Protein. *Chem. Biol.* **1997**, *4*, 951−959.
(74) Cline, E.; Assuncao Bicca, M.; Viola, K.; L Klein, W. The Amyloid-β Oligomer Hypothesis: Beginning of the Third Decade. *J. Alzheimer's Dis.* **2018**, *64*, S567−S616.
(75) Rangachari, V.; Moore, B. D.; Reed, D. K.; Sonoda, L. K.; Bridges, A. W.; Conboy, E.; Hartigan, D.; Rosenberry, T. L. Amyloid-β(1−42) Rapidly Forms ProtoFibrils and Oligomers by Distinct Pathways in Low Concentrations of Sodium Dodecylsulfate. *Biochemistry* **2007**, *46*, 12451−12462.
(76) Baskakov, I. V.; Legname, G.; Baldwin, M. A.; Prusiner, S. B.; Cohen, F. E. Pathway Complexity of Prion Protein Assembly into Amyloid. *J. Biol. Chem.* **2002**, *277*, 21140−21148.
(77) Orgel, L. E. Prion Replication and Secondary Nucleation. *Chem. Biol.* **1996**, *3*, 413−414.
(78) Padrick, S. B.; Miranker, A. D. Islet Amyloid: Phase Partitioning and Secondary Nucleation Are Central to the Mechanism of Fibrillogenesis. *Biochemistry* **2002**, *41*, 4694−4703.
(79) Kumar, A.; Paslay, L. C.; Lyons, D.; Morgan, S. E.; Correia, J. J.; Rangachari, V. Specific Soluble Oligomers of Amyloid-β Peptide Undergo Replication and Form Non-Fibrillar Aggregates in Interfacial Environments. *J. Biol. Chem.* **2012**, *287*, 21253−21264.
(80) Linse, S. Monomer-dependent Secondary Nucleation in Amyloid Formation. *Biophys. Rev.* **2017**, *9*, 329−338.
(81) Stefanovic, A. N. D.; Lindhoud, S.; Semerdzhiev, S. A.; Claessens, M. M. A. E.; Subramaniam, V. Oligomers of Parkinson's Disease-Related α-Synuclein Mutants Have Similar Structures but Distinctive Membrane Permeabilization Properties. *Biochemistry* **2015**, *54*, 3142−3150.
(82) Kandel, N.; Zheng, T.; Huo, Q.; Tatulian, S. A. Membrane Binding and Pore Formation by a Cytotoxic Fragment of Amyloid β Peptide. *J. Phys. Chem. B* **2017**, *121*, 10293−10305.
(83) Peelaerts, W.; Bousset, L.; Van der Perren, A.; Moskalyuk, A.; Pulizzi, R.; Giugliano, M.; Haute, C.; Melki, R.; Baekelandt, V. α-Synuclein Strains Cause Distinct Synucleinopathies after Local and Systemic Administration. *Nature* **2015**, *522*, 340−344.
(84) Peelaerts, W.; Baekelandt, V. α-Synuclein Strains and the Variable Pathologies of Synucleinopathies. *J. Neurochem.* **2016**, *139*, 256−274.
(85) Caughey, B.; Lansbury, P. T. Protofibrils, Pores, Fibrils, and Neurodegeneration: Separating the Responsible Protein Aggregates from the Innocent Bystanders. *Annu. Rev. Neurosci.* **2003**, *26*, 267−298.
(86) Conway, K. A.; Lee, S.-J.; Rochet, J.-C.; Ding, T. T.; Williamson, R. E.; Lansbury, P. T. Acceleration of Oligomerization, Not Fibrillization, is a Shared Property of Both α-Synuclein Mutations Linked to Early-onset Parkinson's Disease: Implications for Pathogenesis and Therapy. *Proc. Natl. Acad. Sci. U. S. A.* **2000**, *97*, 571−576.
(87) Powers, E. T.; Powers, D. L. Mechanisms of Protein Fibril Formation: Nucleated Polymerization with Competing Off-Pathway Aggregation. *Biophys. J.* **2008**, *94*, 379−391.
(88) Ferkinghoff-Borg, J.; Fonslet, J.; Andersen, C. B.; Krishna, S.; Pigolotti, S.; Yagi, H.; Goto, Y.; Otzen, D.; Jensen, M. H. Stop-and-go Kinetics in Amyloid Fibrillation. *Phys. Rev. E* **2010**, *82*, No. 010901.
(89) Woerdehoff, M. M.; Bannach, O.; Shaykhalishahi, H.; Kulawik, A.; Schiefer, S.; Will- bold, D.; Hoyer, W.; Birkmann, E. Single Fibril Growth Kinetics of α-Synuclein. *J. Mol. Biol.* **2015**, *427*, 1428−1435.
(90) Ban, T.; Hoshino, M.; Takahashi, S.; Hamada, D.; Hasegawa, K.; Naiki, H.; Goto, Y. Direct Observation of Aβ Amyloid Fibril Growth and Inhibition. *J. Mol. Biol.* **2004**, *344*, 757−767.
(91) Pinotsi, D.; Buell, A. K.; Galvagnion, C.; Dobson, C. M.; Kaminski Schierle, G. S.; Kaminski, C. F. Direct Observation of Heterogeneous Amyloid Fibril Growth Kinetics via Two-Color Super-Resolution Microscopy. *Nano Lett.* **2014**, *14*, 339−345.
(92) Toernquist, M.; Michaels, T. C. T.; Sanagavarapu, K.; Yang, X.; Meisl, G.; Cohen, S. I. A.; Knowles, T. P. J.; Linse, S. Secondary Nucleation in Amyloid Formation. *Chem. Commun.* **2018**, *54*, 8667−8684.
(93) Chatani, E.; Yamamoto, N. Recent Progress on Understanding the Mechanisms of Amyloid Nucleation. *Biophys. Rev.* **2018**, *10*, 527−534.
(94) Cohen, S. I. A.; Linse, S.; Luheshi, L. M.; Hellstrand, E.; White, D. A.; Rajah, L.; Otzen, D. E.; Vendruscolo, M.; Dobson, C. M.; Knowles, T. P. J. Proliferation of Amyloid-β42 Aggregates Occurs through a Secondary Nucleation Mechanism. *Proc. Natl. Acad. Sci. U. S. A.* **2013**, *110*, 9758−9763.
(95) Eden, K.; Morris, R.; Gillam, J.; MacPhee, C.; Allen, R. Competition between Primary Nucleation and Autocatalysis in Amyloid Fibril Self-Assembly. *Biophys. J.* **2015**, *108*, 632−643.
(96) Michaels, T. C.; Saric, A.; Habchi, J.; Chia, S.; Meisl, G.; Vendruscolo, M.; Dobson, C. M.; Knowles, T. P. Chemical Kinetics for Bridging Molecular Mechanisms and Macroscopic Measurements of Amyloid Fibril Formation. *Annu. Rev. Phys. Chem.* **2018**, *69*, 273−298.
(97) Knowles, T. P. J.; Mezzenga, R. Amyloid Fibrils as Building Blocks for Natural andArtificial Functional Materials. *Adv. Mater.* **2016**, *28*, 6546−6561.
(98) Nicoud, L.; Lazzari, S.; Balderas Barragan, D.; Morbidelli, M. Fragmentation of Amyloid Fibrils Occurs in Preferential Positions Depending on the Environmental Conditions. *J. Phys. Chem. B* **2015**, *119*, 4644−4652.
(99) Carulla, N.; Caddy, G. L.; Hall, D. R.; Zurdo, J.; Gairi, M.; Feliz, M.; Giralt, E.; Robinson, C.; M Dobson, C. Molecular Recycling within Amyloid Fibrils. *Nature* **2005**, *436*, 554−8.
(100) Sgourakis, N. G.; Yan, Y.; McCallum, S. A.; Wang, C.; Garcia, A. E. The Alzheimer's Peptides Aβ40 and 42 Adopt Distinct

DOI: 10.1021/acs.chemrev.8b00731
Chem. Rev. XXXX, XXX, XXX−XXX

Conformations in Water: A Combined MD/NMR Study. *J. Mol. Biol.* **2007**, *368*, 1448−1457.
(101) Sgourakis, N. G.; Merced-Serrano, M.; Boutsidis, C.; Drineas, P.; Du, Z.; Wang, C.; Garcia, A. E. Atomic-Level Characterization of the Ensemble of the Aβ(1−42) Monomer in Water Using Unbiased Molecular Dynamics Simulations and Spectral Algorithms. *J. Mol. Biol.* **2011**, *405*, 570−583.
(102) Rosenman, D. J.; Connors, C. R.; Chen, W.; Wang, C.; Garcia, A. E. Aβ Monomers Transiently Sample Oligomer and Fibril-Like Configurations: Ensemble Characterization Using a Combined MD/NMR Approach. *J. Mol. Biol.* **2013**, *425*, 3338−3359.
(103) Rosenman, D. J.; Wang, C.; Garcia, A. E. Characterization of Aβ Monomers through the Convergence of Ensemble Properties among Simulations with Multiple Force Fields. *J. Phys. Chem. B* **2016**, *120*, 259−277.
(104) Velez-Vega, C.; Escobedo, F. A. Characterizing the Structural Behavior of Selected Aβ-42 Monomers with Different Solubilities. *J. Phys. Chem. B* **2011**, *115*, 4900−4910.
(105) Olubiyi, O. O.; Strodel, B. Structures of the Amyloid β-Peptides. Aβ1−40 and Aβ1−42 as Influenced by pH and a d-Peptide. *J. Phys. Chem. B* **2012**, *116*, 3280−3291.
(106) Vitalis, A.; Caflisch, A. Micelle-Like Architecture of the Monomer Ensemble of Alzheimer's Amyloid-β Peptide in Aqueous Solution and Its Implications for Aβ Aggregation. *J. Mol. Biol.* **2010**, *403*, 148−165.
(107) Mudedla, S. K.; Murugan, N. A.; Agren, H. Free Energy Landscape for Alpha-Helix to Beta-Sheet Interconversion in Small Amyloid Forming Peptide under Nanoconfinement. *J. Phys. Chem. B* **2018**, *122*, 9654−9664.
(108) Highly Disordered Amyloid-β Monomer Probed by Single-Molecule FRET and MD Simulation. *Biophys. J.* **2018**, *114*, 870
(109) Ilie, I. M.; Nayar, D.; den Otter, W. K.; van der Vegt, N. F. A.; Briels, W. J. Intrinsic Conformational Preferences and Interactions in α-Synuclein Fibrils. Insights from Molecular Dynamics simulations. *J. Chem. Theory Comput.* **2018**, *14*, 3298−3310.
(110) Allison, J. R.; Varnai, P.; Dobson, C. M.; Vendruscolo, M. Determination of the Free Energy Landscape of α-Synuclein Using Spin Label Nuclear Magnetic Resonance Measurements. *J. Am. Chem. Soc.* **2009**, *131*, 18314−18326.
(111) Agir, J. S.; Sandipan, M.; Anders, I. Distinct Phases of Free α-Synuclein-A Monte Carlo Study. *Proteins: Struct., Funct., Genet.* **2012**, *80*, 2169−2177.
(112) Yu, H.; Han, W.; Ma, W.; Schulten, K. Transient β-hairpin Formation in α-Synuclein Monomer Revealed by Coarse-grained Molecular Dynamics Simulation. *J. Chem. Phys.* **2015**, *143*, 243142.
(113) Nath, A.; Sammalkorpi, M.; DeWitt, D. C.; Trexler, A. J.; Elbaum-Garfinkle, S.; O'Hern, C. S.; Rhoades, E. The Conformational Ensembles of α-Synuclein and Tau: Combining Single-Molecule FRET and Simulations. *Biophys. J.* **2012**, *103*, 1940−1949.
(114) Zerze, G. H.; Miller, C. M.; Granata, D.; Mittal, J. Free Energy Surface of an Intrinsically Disordered Protein: Comparison between Temperature Replica Exchange Molecular Dynamics and Bias-Exchange MetaDynamics. *J. Chem. Theory Comput.* **2015**, *11*, 2776−2782.
(115) Reddy, A. S.; Wang, L.; Singh, S.; Ling, Y. L.; Buchanan, L.; Zanni, M. T.; Skinner, J. L.; de Pablo, J. J. Stable and Metastable States of Human Amylin in Solution. *Biophys. J.* **2010**, *99*, 2208−2216.
(116) Chiu, C.-c.; Singh, S.; de Pablo, J. J. Effect of Proline Mutations on the Monomer Conformations of Amylin. *Biophys. J.* **2013**, *105*, 1227−1235.
(117) Singh, S.; Chiu, C.-c.; Reddy, A. S.; de Pablo, J. J. α-Helix to β-Hairpin Transition of Human Amylin Monomer. *J. Chem. Phys.* **2013**, *138*, 155101.
(118) Larini, L.; Gessel, M. M.; Lapointe, N. E.; Do, T. D.; Bowers, M. T.; Feinstein, S. C.; Shea, J.-E. Initiation of Assembly of Tau(273−284) and its ΔK280 Mutant: an Experimental and Computational Study. *Phys. Chem. Chem. Phys.* **2013**, *15*, 8916−28.
(119) Luo, Y.; Ma, B.; Nussinov, R.; Wei, G. Structural Insight into Tau Protein's Paradox of Intrinsically Disordered Behavior, Self-Acetylation Activity, and Aggregation. *J. Phys. Chem. Lett.* **2014**, *5*, 3026−3031.
(120) De Simone, A.; Zagari, A.; Derreumaux, P. Structural and Hydration Properties of the Partially Unfolded States of the Prion Protein. *Biophys. J.* **2007**, *93*, 1284−1292.
(121) Chebaro, Y.; Derreumaux, P. The Conversion of Helix H2 to β-Sheet Is Accelerated in the Monomer and Dimer of the Prion Protein upon T183A Mutation. *J. Phys. Chem. B* **2009**, *113*, 6942−6948.
(122) Camilloni, C.; Schaal, D.; Schweimer, K.; Schwarzinger, S.; Simone, A. D. Energy Landscape of the Prion Protein Helix 1 Probed by MetaDynamics and NMR. *Biophys. J.* **2012**, *102*, 158−167.
(123) Huang, D.; Caflisch, A. Evolutionary Conserved Tyr169 Stabilizes the β2−α2 Loop of the Prion Protein. *J. Am. Chem. Soc.* **2015**, *137*, 2948−2957.
(124) Caldarulo, E.; Barducci, A.; Wüthrich, K.; Parrinello, M. Prion Protein β2−α2 Loop Conformational Landscape. *Proc. Natl. Acad. Sci. U. S. A.* **2017**, *114*, 9617−9622.
(125) Tian, P.; Lindorff-Larsen, K.; Boomsma, W.; Jensen, M. H.; Otzen, D. E. A Monte Carlo Study of the Early Steps of Functional Amyloid Formation. *PLoS One* **2016**, *11*, 1−18.
(126) DeBenedictis, E.; Ma, D.; Keten, S. Structural Predictions for Curli Amyloid Fibril Subunits CsgA and CsgB. *RSC Adv.* **2017**, *7*, 48102−48112.
(127) Kuperstein, I.; et al. Neurotoxicity of Alzheimer's Disease Aβ Peptides is Induced by Small Changes in the Aβ42 to Aβ40 ratio. *EMBO J.* **2010**, *29*, 3408−3420.
(128) El-Agnaf, O. M.; Mahil, D. S.; Patel, B. P.; Austen, B. M. Oligomerization and Toxicity of β-Amyloid-42 Implicated in Alzheimer's Disease. *Biochem. Biophys. Res. Commun.* **2000**, *273*, 1003−1007.
(129) Selkoe, D. J.; Hardy, J. The Amyloid Hypothesis of Alzheimer's Disease at 25 Years. *EMBO Mol. Med.* **2016**, *8*, 595−608.
(130) Ball, K.; Phillips, A.; Wemmer, D.; Head-Gordon, T. Differences in β-strand Populations of Monomeric Aβ40 and Aβ42. *Biophys. J.* **2013**, *104*, 2714−2724.
(131) Vitalis, A.; Pappu, R. V. ABSINTH: A New Continuum Solvation Model for Simulations of Polypeptides in Aqueous Solutions. *J. Comput. Chem.* **2009**, *30*, 673−699.
(132) Colvin, M. T.; Silvers, R.; Ni, Q. Z.; Can, T. V.; Sergeyev, I.; Rosay, M.; Dono- van, K. J.; Michael, B.; Wall, J.; Linse, S.; Griffin, R. G. Atomic Resolution Structure of Monomorphic Aβ42 Amyloid Fibrils. *J. Am. Chem. Soc.* **2016**, *138*, 9663−9674.
(133) Roeder, K.; Wales, D. J. Energy Landscapes for the Aggregation of Aβ17−42. *J. Am. Chem. Soc.* **2018**, *140*, 4018−4027.
(134) Onufriev, A.; Bashford, D.; Case, D. A. Modification of the Generalized Born Model Suitable for Macromolecules. *J. Phys. Chem. B* **2000**, *104*, 3712−3720.
(135) Shea, J.-E.; Urbanc, B. Insights into Aβ; Aggregation: A Molecular Dynamics Perspective. *Curr. Top. Med. Chem.* **2013**, *P12*, 2596−2610.
(136) Tran, L.; Ha-Duong, T. Exploring the Alzheimer Amyloid-β Peptide Conformational Ensemble: A Review of Molecular Dynamics Approaches. *Peptides* **2015**, *69*, 86−91.
(137) Nasica-Labouze, J.; et al. Amyloid β Protein and Alzheimer's Disease: When Computer Simulations Complement Experimental Studies. *Chem. Rev.* **2015**, *115*, 3518−3563.
(138) Chiricotto, M.; Tran, T. T.; Nguyen, P. H.; Melchionna, S.; Sterpone, F.; Derreumaux, P. Coarse-grained and All-atom Simulations towards the Early and Late Steps of Amyloid Fibril Formation. *Isr. J. Chem.* **2017**, *57*, 564−573.
(139) Lorenzen, N.; Lemminger, L.; Pedersen, J. N.; Nielsen, S. B.; Otzen, D. E. The N-terminus of α-Synuclein is Essential for Both Monomeric and Oligomeric Interactions with Membranes. *FEBS Lett.* **2014**, *588*, 497−502.
(140) Uversky, V. N. A Protein-Chameleon: Conformational Plasticity of α-Synuclein, a Disordered Protein Involved in Neuro-degenerative Disorders. *J. Biomol. Struct. Dyn.* **2003**, *21*, 211−234.

DOI: 10.1021/acs.chemrev.8b00731
Chem. Rev. XXXX, XXX, XXX−XXX

(141) Tuttle, M. D.; et al. Solid-state NMR Structure of a Pathogenic Fibril of Full-length Human α-Synuclein. *Nat. Struct. Mol. Biol.* **2016**, *23*, 409−415.
(142) Han, W.; Wan, C.-K.; Jiang, F.; Wu, Y.-D. PACE Force Field for Protein Simulations. 1. Full Parameterization of Version 1 and Verification. *J. Chem. Theory Comput.* **2010**, *6*, 3373−3389.
(143) Marrink, S. J.; Risselada, H. J.; Yefimov, S.; Tieleman, D. P.; de Vries, A. H. The MARTINI Force Field: Coarse Grained Model for Biomolecular Simulations. *J. Phys. Chem. B* **2007**, *111*, 7812−7824.
(144) Rohl, C. A.; Strauss, C. E.; Misura, K. M.; Baker, D. *Numerical Computer Methods, Part D*; Academic Press, 2004; Vol. 383, pp 66−93.
(145) Kayed, R.; Bernhagen, J.; Greenfield, N.; Sweimeh, K.; Brunner, H.; Voelter, W.; Kapurniotu, A. Conformational Transitions of Islet Amyloid Polypeptide (IAPP) in Amyloid Formation in Vitro. *J. Mol. Biol.* **1999**, *287*, 781−796.
(146) Roberts, A. N.; Leighton, B.; Todd, J. A.; Cockburn, D.; Schofield, P. N.; Sutton, R.; Holt, S.; Boyd, Y.; Day, A. J.; Foot, E. A. Molecular and Functional Characterization of Amylin, a Peptide Associated with Type 2 Diabetes Mellitus. *Proc. Natl. Acad. Sci. U. S. A.* **1989**, *86*, 9662−9666.
(147) Morriss-Andrews, A.; Shea, J.-E. Simulations of Protein Aggregation: Insights from Atomistic and Coarse-Grained Models. *J. Phys. Chem. Lett.* **2014**, *5*, 1899−1908.
(148) Akter, R.; Cao, P.; Noor, H.; Ridgway, Z.; Tu, L.-H.; Wang, H.; Wong, A.; Zhang, X.; Abedini, A.; Marie Schmidt, A.; Raleigh, P.; Islet Amyloid Polypeptide, D. Structure, Function, and Pathophysiology. *J. Diabetes Res.* **2016**, *2016*, 1−18.
(149) Moore, S. J.; Sonar, K.; Bharadwaj, P.; Deplazes, E.; Mancera, R. L. Characterisation of the Structure and Oligomerisation of Islet Amyloid Polypeptides (IAPP): A Review of Molecular Dynamics Simulation Studies. *Molecules* **2018**, *23*, 2142
(150) Hoffmann, K. Q.; McGovern, M.; Chiu, C.-c.; de Pablo, J. J. Secondary Structure of Rat and Human Amylin across Force Fields. *PLoS One* **2015**, *10*, 1−24.
(151) Kayed, R.; Bernhagen, J.; Greenfield, N.; Sweimeh, K.; Brunner, H.; Voelter, W.; Kapurniotu, A. Conformational Transitions of Islet Amyloid Polypeptide (IAPP) in Amyloid Formation in Vitro. *J. Mol. Biol.* **1999**, *287*, 781−796.
(152) Ciasca, G.; Campi, G.; Battisti, A.; Rea, G.; Rodio, M.; Papi, M.; Pernot, P.; Tenen- baum, A.; Bianconi, A. Continuous Thermal Collapse of the Intrinsically Disordered Protein Tau Is Driven by Its Entropic Flexible Domain. *Langmuir* **2012**, *28*, 13405−13410.
(153) von Bergen, M.; Friedhoff, P.; Biernat, J.; Heberle, J.; Mandelkow, E.-M.; Man- delkow, E. Assembly of τ Protein into Alzheimer Paired Helical Filaments Depends on a Local Sequence Motif (306VQIVYK311) Forming β Structure. *Proc. Natl. Acad. Sci. U. S. A.* **2000**, *97*, 5129−5134.
(154) Battisti, A.; Ciasca, G.; Grottesi, A.; Bianconi, A.; Tenenbaum, A. Temporary Secondary Structures in Tau, an Intrinsically Disordered Protein. *Mol. Simul.* **2012**, *38*, 525−533.
(155) Battisti, A.; Ciasca, G.; Grottesi, A.; Tenenbaum, A. Thermal Compaction of the Intrinsically Disordered Protein Tau: Entropic, Structural, and Hydrophobic Factors. *Phys. Chem. Chem. Phys.* **2017**, *19*, 8435−8446.
(156) Zhong, Q.; Congdon, E. E.; Nagaraja, H. N.; Kuret, J. Tau Isoform Composition Influences Rate and Extent of Filament Formation. *J. Biol. Chem.* **2012**, *287*, 20711−20719.
(157) Si, K. Prions: What Are They Good For? *Annu. Rev. Cell Dev. Biol.* **2015**, *31*, 149−169.
(158) Aguzzi, A.; Calella, A. M. Prions: Protein Aggregation and Infectious Diseases. *Physiol. Rev.* **2009**, *89*, 1105−1152.
(159) Riesner, D. Biochemistry and Structure of PrPC and PrPSc. *Br. Med. Bull.* **2003**, *66*, 21−33.
(160) Thody, S. A.; Mathew, M.; Udgaonkar, J. B. Mechanism of Aggregation and Membrane Interactions of Mammalian Prion Protein. *Biochim. Biophys. Acta, Biomembr.* **2018**, *1860*, 1927−1935.
(161) Gallo, P.; Rapsinski, G.; Wilson, R.; Oppong, G.; Sriram, U.; Goulian, M.; Buttaro, B.; Caricchio, R.; Gallucci, S.; Tuekel, C. Amyloid-DNA Composites of Bacterial Biofilms Stimulate Autoimmunity. *Immunity* **2015**, *42*, 1171−1184.
(162) Shewmaker, F.; McGlinchey, R. P.; Thurber, K. R.; McPhie, P.; Dyda, F.; Tycko, R.; Wickner, R. B. The Functional Curli Amyloid Is Not Based on In-register Parallel β-Sheet Structure. *J. Biol. Chem.* **2009**, *284*, 25065−25076.
(163) Evans, M. L.; Chapman, M. R. Curli Biogenesis: Order Out of Disorder. *Biochim. Biophys. Acta, Mol. Cell Res.* **2014**, *1843*, 1551−1558.
(164) Wang, X.; Zhou, Y.; Ren, J.-J.; Hammer, N. D.; Chapman, M. R. Gatekeeper Residues in the Major Curlin Subunit Modulate Bacterial Amyloid fiber Biogenesis. *Proc. Natl. Acad. Sci. U. S. A.* **2010**, *107*, 163−168.
(165) Kim, D. E.; Chivian, D.; Baker, D. Protein Structure Prediction and Analysis Using the Robetta Server. *Nucleic Acids Res.* **2004**, *32*, W526−W531.
(166) Wang, B.; Bu, D.; Zhu, J.; Sun, S.; Wang, C.; Zhang, H.; Zheng, W.-M.; Xu, D.; Ning, K.; Li, S. C. FALCON@home: A High-throughput Protein Structure Prediction Server Based on Remote Homologue Recognition. *Bioinformatics* **2016**, *32*, 462−464.
(167) Xu, D.; Zhang, Y. Ab Initio Protein Structure Assembly Using Continuous Structure Fragments and Optimized Knowledge-based Force Field. *Proteins: Struct., Funct., Genet.* **2012**, *80*, 1715−1735.
(168) Peng, J.; Xu, J. Raptorx: Exploiting Structure Information for Protein Alignment by Statistical Inference. *Proteins: Struct., Funct., Genet.* **2011**, *79*, 161−171.
(169) Knowles, T. P. J.; Waudby, C. A.; Devlin, G. L.; Cohen, S. I. A.; Aguzzi, A.; Vendruscolo, M.; Terentjev, E. M.; Welland, M. E.; Dobson, C. M. An Analytical Solution to the Kinetics of Breakable Filament Assembly. *Science* **2009**, *326*, 1533−1537.
(170) Buell, A.; Dobson, C. M.; Knowles, T. P. J. The Physical Chemistry of the Amyloid Phenomenon: Thermodynamics and Kinetics of Filamentous Protein Aggregation. *Essays Biochem.* **2014**, *56*, 11−39.
(171) Cohen, S. I.; Vendruscolo, M.; Dobson, C. M.; Knowles, T. P. From Macroscopic Measurements to Microscopic Mechanisms of Protein Aggregation. *J. Mol. Biol.* **2012**, *421*, 160−171.
(172) Vacha, R.; Frenkel, D. Relation Between Molecular Shape and the Morphology of Self-Assembling Aggregates: A Simulation Study. *Biophys. J.* **2011**, *101*, 1432−1439.
(173) Bieler, N. S.; Knowles, T. P. J.; Frenkel, D.; Vacha, R. Connecting Macroscopic Observables and Microscopic Assembly Events in Amyloid Formation Using Coarse Grained Simulations. *PLoS Comput. Biol.* **2012**, *8*, 1−10.
(174) Saric, A.; Chebaro, Y. C.; Knowles, T. P. J.; Frenkel, D. Crucial Role of Nonspecific Interactions in Amyloid Nucleation. *Proc. Natl. Acad. Sci. U. S. A.* **2014**, *111*, 17869−17874.
(175) Michaels, T. C. T.; Liu, L. X.; Curk, S.; Bolhuis, P. G.; Saric, A.; Knowles, T. P. J. Reaction Rate Theory for Supramolecular Kinetics: Application to Protein Aggregation. *Mol. Phys.* **2018**, *0*, 1−11.
(176) Ilie, I. M.; den Otter, W. K.; Briels, W. J. A Coarse Grained Protein Model with Internal Degrees of Freedom. Application to α-Synuclein Aggregation. *J. Chem. Phys.* **2016**, *144*, No. 085103.
(177) Ilie, I. M.; Briels, W. J.; den Otter, W. K. An Elementary Singularity-free Rotational Brownian Dynamics Algorithm for Anisotropic Particles. *J. Chem. Phys.* **2015**, *142*, 114103.
(178) Barz, B.; Urbanc, B. Minimal Model of Self-Assembly: Emergence of Diversity and Complexity. *J. Phys. Chem. B* **2014**, *118*, 3761−3770.
(179) Pellarin, R.; Caflisch, A. Interpreting the Aggregation Kinetics of Amyloid Peptides. *J. Mol. Biol.* **2006**, *360*, 882−892.
(180) Pellarin, R.; Guarnera, E.; Caflisch, A. Pathways and Intermediates of Amyloid Fibril Formation. *J. Mol. Biol.* **2007**, *374*, 917−924.
(181) Pellarin, R.; Schuetz, P.; Guarnera, E.; Caflisch, A. Amyloid Fibril Polymorphism is under Kinetic Control. *J. Am. Chem. Soc.* **2010**, *132*, 14960−14970.
(182) Bellesia, G.; Shea, J.-E. Self-assembly of β-Sheet Forming Peptides into Chiral Fibrillar Aggregates. *J. Chem. Phys.* **2007**, *126*, 245104.

DOI: 10.1021/acs.chemrev.8b00731
Chem. Rev. XXXX, XXX, XXX−XXX

(183) Bellesia, G.; Shea, J.-E. Diversity of Kinetic Pathways in Amyloid Fibril Formation. *J. Chem. Phys.* **2009**, *131*, 111102.
(184) Wu, C.; Shea, J.-E. Coarse-grained Models for Protein Aggregation. *Curr. Opin. Struct. Biol.* **2011**, *21*, 209−220.
(185) Li, M. S.; Klimov, D. K.; Straub, J. E.; Thirumalai, D. Probing the Mechanisms of Fibril Formation using Lattice Models. *J. Chem. Phys.* **2008**, *129*, 175101.
(186) Abeln, S.; Vendruscolo, M.; Dobson, C. M.; Frenkel, D. A Simple Lattice Model That Captures Protein Folding, Aggregation and Amyloid Formation. *PLoS One* **2014**, *9*, 1−8.
(187) Zhuravlev, P. I.; Reddy, G.; Straub, J. E.; Thirumalai, D. Propensity to Form Amyloid Fibrils Is Encoded as Excitations in the Free Energy Landscape of Monomeric Proteins. *J. Mol. Biol.* **2014**, *426*, 2653−2666.
(188) Baftizadeh, F.; Biarnes, X.; Pietrucci, F.; Affinito, F.; Laio, A. Multidimensional View of Amyloid Fibril Nucleation in Atomistic Detail. *J. Am. Chem. Soc.* **2012**, *134*, 3886−3894.
(189) Baftizadeh, F.; Pietrucci, F.; Biarnés, X.; Laio, A. Nucleation Process of a Fibril Precursor in the C-Terminal Segment of Amyloid-β. *Phys. Rev. Lett.* **2013**, *110*, 168103.
(190) Chebaro, Y.; Mousseau, N.; Derreumaux, P. Structures and Thermodynamics of Alzheimer's Amyloid-β Aβ(16−35) Monomer and Dimer by Replica Exchange Molecular Dynamics Simulations: Implication for Full-Length Aβ Fibrillation. *J. Phys. Chem. B* **2009**, *113*, 7668−7675.
(191) Man, V. H.; Nguyen, P. H.; Derreumaux, P. Conformational Ensembles of the Wild- Type and S8C Aβ1−42 Dimers. *J. Phys. Chem. B* **2017**, *121*, 2434−2442.
(192) Cote, S.; Laghaei, R.; Derreumaux, P.; Mousseau, N. Distinct Dimerization for Various Alloforms of the Amyloid-Beta Protein: Aβ1−40, Aβ1−42, and Aβ1−40(D23N). *J. Phys. Chem. B* **2012**, *116*, 4043−4055.
(193) Man, V. H.; Nguyen, P. H.; Derreumaux, P. High-Resolution Structures of the Amyloid-β 1−42 Dimers from the Comparison of Four Atomistic Force Fields. *J. Phys. Chem. B* **2017**, *121*, 5977−5987.
(194) Tarus, B.; Tran, T. T.; Nasica-Labouze, J.; Sterpone, F.; Nguyen, P. H.; Derreumaux, P. Structures of the Alzheimer's Wild-Type Aβ1−40 Dimer from Atomistic Simulations. *J. Phys. Chem. B* **2015**, *119*, 10478−10487.
(195) Nguyen, P. H.; Sterpone, F.; Campanera, J. M.; Nasica-Labouze, J.; Derreumaux, P. Impact of the A2V Mutation on the Heterozygous and Homozygous Aβ1−40 Dimer Structures from Atomistic Simulations. *ACS Chem. Neurosci.* **2016**, *7*, 823−832.
(196) Nguyen, P. H.; Sterpone, F.; Pouplana, R.; Derreumaux, P.; Campanera, J. M. Dimerization Mechanism of Alzheimer Aβ40 Peptides: The High Content of Intrapeptide- Stabilized Conformations in A2V and A2T Heterozygous Dimers Retards Amyloid Fibril Formation. *J. Phys. Chem. B* **2016**, *120*, 12111−12126.
(197) Cao, Y.; Jiang, X.; Han, W. Self-Assembly Pathways of β-Sheet-Rich Amyloid-β(1−40) Dimers: Markov State Model Analysis on Millisecond Hybrid-Resolution Simulations. *J. Chem. Theory Comput.* **2017**, *13*, 5731−5744.
(198) Sharma, B.; Ranganathan, S. V.; Belfort, G. Weaker N-Terminal Interactions for the Protective over the Causative Aβ Peptide Dimer Mutants. *ACS Chem. Neurosci.* **2018**, *9*, 1247−1253.
(199) Das, P.; Chacko, A. R.; Belfort, G. Alzheimer's Protective Cross-Interaction between Wild-Type and A2T Variants Alters Aβ42 Dimer Structure. *ACS Chem. Neurosci.* **2017**, *8*, 606−618.
(200) Barz, B.; Liao, Q.; Strodel, B. Pathways of Amyloid-β Aggregation Depend on Oligomer Shape. *J. Am. Chem. Soc.* **2018**, *140*, 319−327.
(201) Zoete, V.; Meuwly, M.; Karplus, M. A Comparison of the Dynamic Behavior of Monomeric and Dimeric Insulin Shows Structural Rearrangements in the Active Monomer. *J. Mol. Biol.* **2004**, *342*, 913−929.
(202) Zoete, V.; Meuwly, M.; Karplus, M. Study of the Insulin Dimerization: Binding Free Energy Calculations and Per-residue Free Energy decomposition. *Proteins: Struct., Funct., Genet.* **2005**, *61*, 79−93.
(203) Raghunathan, S.; El Hage, K.; Desmond, J. L.; Zhang, L.; Meuwly, M. The Role of Water in the Stability of Wild-type and Mutant Insulin Dimers. *J. Phys. Chem. B* **2018**, *122*, 7038−7048.
(204) Dupuis, N. F.; Wu, C.; Shea, J.-E.; Bowers, M. T. The Amyloid Formation Mechanism in Human IAPP: Dimers Have β-Strand Monomer-Monomer Interfaces. *J. Am. Chem. Soc.* **2011**, *133*, 7240−7243.
(205) Qi, R.; Luo, Y.; Ma, B.; Nussinov, R.; Wei, G. Conformational Distribution and α-Helix to β-Sheet Transition of Human Amylin Fragment Dimer. *Biomacromolecules* **2014**, *15*, 122−131.
(206) Ilitchev, A. I.; Giammona, M. J.; Do, T. D.; Wong, A. G.; Buratto, S. K.; Shea, J.-E.; Raleigh, D. P.; Bowers, M. T. Human Islet Amyloid Polypeptide N-Terminus Fragment Self-Assembly: Effect of Conserved Disulfide Bond on Aggregation Propensity. *J. Am. Soc. Mass Spectrom.* **2016**, *27*, 1010−1018.
(207) Guo, A. Z.; Fluitt, A. M.; de Pablo, J. J. Early-stage Human Islet Amyloid Polypeptide Aggregation: Mechanisms Behind Dimer Formation. *J. Chem. Phys.* **2018**, *149*, No. 025101.
(208) Ganguly, P.; Do, T. D.; Larini, L.; LaPointe, N. E.; Sercel, A. J.; Shade, M. F.; Feinstein, S. C.; Bowers, M. T.; Shea, J.-E. Tau Assembly: The Dominant Role of PHF6 (VQIVYK) in Microtubule Binding Region Repeat R3. *J. Phys. Chem. B* **2015**, *119*, 4582−4593.
(209) Chamachi, N. G.; Chakrabarty, S. Replica Exchange Molecular Dynamics Study of Dimerization in Prion Protein: Multiple Modes of Interaction and Stabilization. *J. Phys. Chem. B* **2016**, *120*, 7332−7345.
(210) Tian, P.; Boomsma, W.; Wang, Y.; Otzen, D. E.; Jensen, M. H.; Lindorff-Larsen, K. Structure of a Functional Amyloid Protein Subunit Computed Using Sequence Variation. *J. Am. Chem. Soc.* **2015**, *137*, 22−25.
(211) Qiao, Q.; Qi, R.; Wei, G.; Huang, X. Dynamics of the Conformational Transitions during the Dimerization of an Intrinsically Disordered Peptide: a Case Study on the Human Islet Amyloid Polypeptide Fragment. *Phys. Chem. Chem. Phys.* **2016**, *18*, 29892−29904.
(212) Ridgway, Z.; Zhang, X.; Wong, A. G.; Abedini, A.; Schmidt, A. M.; Raleigh, D. P. Analysis of the Role of the Conserved Disulfide in Amyloid Formation by Human Islet Amyloid Polypeptide in Homogeneous and Heterogeneous Environments. *Biochemistry* **2018**, *57*, 3065−3074.
(213) Gsponer, J.; Haberthür, U.; Caflisch, A. The Role of Side-chain Interactions in the Early Steps of Aggregation: Molecular Dynamics Simulations of an Amyloid-forming Peptide from the Yeast Prion Sup35. *Proc. Natl. Acad. Sci. U. S. A.* **2003**, *100*, 5154−5159.
(214) Urbanc, B.; Cruz, L.; Yun, S.; Buldyrev, S. V.; Bitan, G.; Teplow, D. B.; Stanley, H. E. In Silico Study of Amyloid β-Protein Folding and Oligomerization. *Proc. Natl. Acad. Sci. U. S. A.* **2004**, *101*, 17345−17350.
(215) Sun, Y.; Ge, X.; Xing, Y.; Wang, B.; Ding, F. β-Barrel Oligomers as Common Intermediates of Peptides Self-Assembling into Cross-β Aggregates. *Sci. Rep.* **2018**, *8*, 10353.
(216) Sun, Y.; Kakinen, A.; Xing, Y.; Pilkington, E. H.; Davis, T. P.; Ke, P. C.; Ding, F. Nucleation of β-Rich Oligomers and β-Barrels in the Early Aggregation of Human Islet Amyloid Polypeptide. *Biochim. Biophys. Acta, Mol. Basis Dis.* **2019**, *1865*, 434−444.
(217) Collu, F.; Spiga, E.; Chakroun, N.; Rezaei, H.; Fraternali, F. Probing the Early Stages of Prion Protein (PrP) Aggregation with Atomistic Molecular Dynamics Simulations. *Chem. Commun.* **2018**, *54*, 8007−8010.
(218) Carballo-Pacheco, M.; Ismail, A. E.; Strodel, B. Oligomer Formation of Toxic and Functional Amyloid Peptides Studied with Atomistic Simulations. *J. Phys. Chem. B* **2015**, *119*, 9696−9705.
(219) Tjernberg, L. O.; Naeslund, J.; Lindqvist, F.; Johansson, J.; Karlstroem, A. R.; Thy- berg, J.; Terenius, L.; Nordstedt, C. Arrest of Amyloid Fibril Formation by a Pentapeptide Ligand. *J. Biol. Chem.* **1996**, *271*, 8545−8548.
(220) Bieschke, J.; Siegel, S. J.; Fu, Y.; Kelly, J. W. Alzheimer's Aβ Peptides Containing an Isostructural Backbone Mutation Afford Distinct Aggregate Morphologies but Analogous Cytotoxicity.

DOI: 10.1021/acs.chemrev.8b00731
Chem. Rev. XXXX, XXX, XXX−XXX

Evidence for a Common Low-Abundance Toxic Structure(s)? *Biochemistry* **2008**, *47*, 50−59.
(221) Nagel-Steger, L.; Owen, M. C.; Strodel, B. An Account of Amyloid Oligomers: Facts and Figures Obtained from Experiments and Simulations. *ChemBioChem* **2016**, *17*, 657−676.
(222) Huang, J.; MacKerell, A. D. Force Field Development and Simulations of Intrinsically Disordered Proteins. *Curr. Opin. Struct. Biol.* **2018**, *48*, 40−48.
(223) Sterpone, F.; Melchionna, S.; Tuffery, P.; Pasquali, S.; Mousseau, N.; Cragnolini, T.; Chebaro, Y.; St-Pierre, J.-F.; Kalimeri, M.; Barducci, A.; Laurin, Y.; Tek, A.; Baaden, M.; Nguyen, P. H.; Derreumaux, P. The OPEP Protein Model: From Single Molecules, Amyloid Formation, Crowding and Hydrodynamics to DNA/RNA systems. *Chem. Soc. Rev.* **2014**, *43*, 4871−4893.
(224) Carballo-Pacheco, M.; Ismail, A. E.; Strodel, B. On the Applicability of Force Fields To Study the Aggregation of Amyloidogenic Peptides Using Molecular Dynamics Simulations. *J. Chem. Theory Comput.* **2018**, *14*, 6063−6075.
(225) Esler, W. P.; Stimson, E. R.; Jennings, J. M.; Vinters, H. V.; Ghilardi, J. R.; Lee, J. P.; Mantyh, P. W.; Maggio, J. E. Alzheimer's Disease Amyloid Propagation by a Template-Dependent Dock-Lock Mechanism. *Biochemistry* **2000**, *39*, 6288−6295.
(226) Nguyen, P. H.; Li, M. S.; Stock, G.; Straub, J. E.; Thirumalai, D. Monomer Adds to Preformed Structured Oligomers of Aβ-Peptides by a Two-stage Dock-Lock Mechanism. *Proc. Natl. Acad. Sci. U. S. A.* **2007**, *104*, 111−116.
(227) O'Brien, E. P.; Okamoto, Y.; Straub, J. E.; Brooks, B. R.; Thirumalai, D. Thermodynamic Perspective on the Dock-Lock Growth Mechanism of Amyloid Fibrils. *J. Phys. Chem. B* **2009**, *113*, 14421−14430.
(228) Han, W.; Schulten, K. Fibril Elongation by Aβ17−42: Kinetic Network Analysis of Hybrid-Resolution Molecular Dynamics Simulations. *J. Am. Chem. Soc.* **2014**, *136*, 12450−12460.
(229) Reddy, G.; Straub, J. E.; Thirumalai, D. Dynamics of Locking of Peptides onto Growing Amyloid Fibrils. *Proc. Natl. Acad. Sci. U. S. A.* **2009**, *106*, 11948−11953.
(230) Straub, J. E.; Thirumalai, D. Toward a Molecular Theory of Early and Late Events in Monomer to Amyloid Fibril Formation. *Annu. Rev. Phys. Chem.* **2011**, *62*, 437−463.
(231) Lee, J. P.; Stimson, E. R.; Ghilardi, J. R.; Mantyh, P. W.; Lu, Y.-A.; Felix, A. M.; Llanos, W.; Behbin, A.; Cummings, M. a. 1H NMR of A.beta. Amyloid Peptide Congeners in Water Solution. Conformational Changes Correlate with Plaque Competence. *Biochemistry* **1995**, *34*, 5191−5200.
(232) Petkova, A. T.; Ishii, Y.; Balbach, J. J.; Antzutkin, O. N.; Leapman, R. D.; Delaglio, F.; Tycko, R. A Structural Model for Alzheimer's β-Amyloid Fibrils Based on Experimental Constraints from Solid State NMR. *Proc. Natl. Acad. Sci. U. S. A.* **2002**, *99*, 16742−16747.
(233) Takeda, T.; Klimov, D. K. Probing Energetics of Aβ Fibril Elongation by Molecular Dynamics Simulations. *Biophys. J.* **2009**, *96*, 4428−4437.
(234) Takeda, T.; Klimov, D. K. Replica Exchange Simulations of the Thermodynamics of Aβ Fibril Growth. *Biophys. J.* **2009**, *96*, 442−452.
(235) Lührs, T.; Ritter, C.; Adrian, M.; Riek-Loher, D.; Bohrmann, B.; Döbeli, H.; Schubert, D.; Riek, R. 3D Structure of Alzheimer's Amyloid-β(1−42) Fibrils. *Proc. Natl. Acad. Sci. U. S. A.* **2005**, *102*, 17342−17347.
(236) Han, M.; Hansmann, U. H. E. Replica Exchange Molecular Dynamics of the Thermodynamics of Fibril Growth of Alzheimer's Aβ42 Peptide. *J. Chem. Phys.* **2011**, *135*, No. 065101.
(237) Gurry, T.; Stultz, C. M. Mechanism of Amyloid-β Fibril Elongation. *Biochemistry* **2014**, *53*, 6981−6991.
(238) Torrie, G. M.; Valleau, J. P. Monte Carlo Free Energy Estimates using Non-Boltzmann Sampling: Application to the Sub-critical Lennard-Jones fluid. *Chem. Phys. Lett.* **1974**, *28*, 578−581.
(239) Torrie, G.; Valleau, J. Nonphysical Sampling Distributions in Monte Carlo Free Energy Estimation: Umbrella sampling. *J. Comput. Phys.* **1977**, *23*, 187−199.
(240) Kästner, J. Umbrella Sampling. *Wiley Interdiscip. Rev. Comput. Mol. Sci.* **2011**, *1*, 932−942.
(241) Schwierz, N.; Frost, C. V.; Geissler, P. L.; Zacharias, M. Dynamics of Seeded Aβ40-Fibril Growth from Atomistic Molecular Dynamics Simulations: Kinetic Trapping and Reduced Water Mobility in the Locking Step. *J. Am. Chem. Soc.* **2016**, *138*, 527−539.
(242) Wales, D. J. Discrete Path Sampling. *Mol. Phys.* **2002**, *100*, 3285−3305.
(243) Bacci, M.; Vymetal, J.; Mihajlovic, M.; Caflisch, A.; Vitalis, A. Amyloid β Fibril Elongation by Monomers Involves Disorder at the Tip. *J. Chem. Theory Comput.* **2017**, *13*, 5117−5130.
(244) Nelson, R.; Sawaya, M. R.; Balbirnie, M.; Madsen, A. O.; Riekel, C.; Grothe, R.; Eisenberg, D. Structure of the Cross-β Spine of Amyloid-like Fibrils. *Nature* **2005**, *435*, 773.
(245) Sawaya, M. R.; Sambashivan, S.; Nelson, R. J.; Ivanova, M. I.; Sievers, S. A.; Apostol, M. I.; Thompson, M. J.; Balbirnie, M.; Wiltzius, J. J. W.; McFarlane, H. T.; Madsen, A. O.; Riekel, C.; Eisenberg, D. S. Atomic Structures of Amyloid Cross-β Spines Reveal Varied Steric Zippers. *Nature* **2007**, *447*, 453−457.
(246) Sasmal, S.; Schwierz, N.; Head-Gordon, T. Mechanism of Nucleation and Growth of Aβ40 Fibrils from All-Atom and Coarse-Grained Simulations. *J. Phys. Chem. B* **2016**, *120*, 12088−12097.
(247) Lu, J.-X.; Qiang, W.; Yau, W.-M.; D Schwieters, C.; C Meredith, S.; Tycko, R. Molecular Structure of β-Amyloid Fibrils in Alzheimer's Disease Brain Tissue. *Cell* **2013**, *154*, 1257−68.
(248) Ilie, I. M.; den Otter, W. K.; Briels, W. J. The Attachment of α-synuclein to a Fiber: A Coarse Grain Approach. *J. Chem. Phys.* **2017**, *146*, 115102.
(249) Buchete, N.-V.; Tycko, R.; Hummer, G. Molecular Dynamics Simulations of Alzheimer's β-Amyloid Protofilaments. *J. Mol. Biol.* **2005**, *353*, 804−821.
(250) Baumketner, A.; Griffin Krone, M.; Shea, J. Role of the Familial Dutch Mutation E22Q in the Folding and Aggregation of the 15−28 Fragment of the Alzheimer amyloid-β Protein. *Proc. Natl. Acad. Sci. U. S. A.* **2008**, *105*, 6027−32.
(251) Schor, M.; Vreede, J.; Bolhuis, P. Elucidating the Locking Mechanism of Peptides onto Growing Amyloid Fibrils through Transition Path Sampling. *Biophys. J.* **2012**, *103*, 1296−1304.
(252) Ivanova, M. I.; Sievers, S. A.; Sawaya, M. R.; Wall, J. S.; Eisenberg, D. Molecular Basis for Insulin Fibril Assembly. *Proc. Natl. Acad. Sci. U. S. A.* **2009**, *106*, 18990−18995.
(253) Lemkul, J. A.; Bevan, D. R. Assessing the Stability of Alzheimer's Amyloid Protofibrils Using Molecular Dynamics. *J. Phys. Chem. B* **2010**, *114*, 1652−1660.
(254) Rodriguez, R. A.; Chen, L. Y.; Plascencia-Villa, G.; Perry, G. Thermodynamics of Amyloid-β Fibril Elongation: Atomistic Details of the Transition State. *ACS Chem. Neurosci.* **2018**, *9*, 783−789.
(255) Sgourakis, N. G.; Yau, W.-M.; Qiang, W. Modeling an In-Register, Parallel "Iowa" Aβ Fibril Structure Using Solid-State NMR Data from Labeled Samples with Rosetta. *Structure* **2015**, *23*, 216−227.
(256) Davidson, D. S.; Brown, A. M.; Lemkul, J. A. Insights into Stabilizing Forces in Amyloid Fibrils of Differing Sizes from Polarizable Molecular Dynamics Simulations. *J. Mol. Biol.* **2018**, *430*, 3819−3834.
(257) Fitzpatrick, A. W.; Falcon, B.; He, S.; Murzin, A. G.; Murshudov, G.; Garringer, H. J.; Crowther, R. A.; Ghetti, B.; Goedert, M.; Scheres, S. H. Cryo-EM Structures of Tau Filaments from Alzheimer's Disease Brain. *Nature* **2017**, *547*, 185−190.
(258) Nielsen, J. T.; Bjerring, M.; Jeppesen, M. D.; Pedersen, R. O.; Pedersen, J. M.; Hein, K. L.; Vosegaard, T.; Skrydstrup, T.; Otzen, D. E.; Nielsen, N. C. Unique Identification of Supramolecular Structures in Amyloid Fibrils by Solid-State NMR Spectroscopy. *Angew. Chem., Int. Ed.* **2009**, *48*, 2118−2121.
(259) Ilie, I. M.; Caflisch, A. Disorder at the Tips of a Disease-Relevant Aβ42 Amyloid Fibril: A Molecular Dynamics Study. *J. Phys. Chem. B* **2018**, *122*, 11072−11082.
(260) Tofoleanu, F.; Yuan, Y.; Pickard, F.; Tywoniuk, B.; Brooks, B. R.; Buchete, N.- V. Structural Modulation of Human Amylin Protofilaments by Naturally-Occurring Mutations. *J. Phys. Chem. B* **2018**, *122*, 5657−5665.
(261) Luca, S.; Yau, W.-M.; Leapman, R.; Tycko, R. Peptide Conformation and Supramolecular Organization in Amylin Fibrils:

DOI: 10.1021/acs.chemrev.8b00731
Chem. Rev. XXXX, XXX, XXX−XXX

Constraints from Solid-State NMR. *Biochemistry* **2007**, *46*, 13505−13522.
(262) Schor, M.; Mey, A. S. J. S.; Noe, F.; MacPhee, C. E. Shedding Light on the Dock-Lock Mechanism in Amyloid Fibril Growth Using Markov State Models. *J. Phys. Chem. Lett.* **2015**, *6*, 1076−1081.
(263) Buchete, N.-V.; Hummer, G. Structure and Dynamics of Parallel β-Sheets, Hydrophobic Core, and Loops in Alzheimer's Aβ Fibrils. *Biophys. J.* **2007**, *92*, 3032−9.
(264) Okumura, H.; Itoh, S. G. Structural and Fluctuational Difference Between Two Ends of Aβ Amyloid Fibril: MD Simulations Predict Only One End has Open Conformations. *Sci. Rep.* **2016**, *106*, 38422.
(265) Zhang, R.; Hu, X.; Khant, H.; Ludtke, S. J.; Chiu, W.; Schmid, M. F.; Frieden, C.; Lee, J.-M. Interprotofilament Interactions Between Alzheimer's Aβ1−42 Peptides in Amyloid Fibrils Revealed by CryoEM. *Proc. Natl. Acad. Sci. U. S. A.* **2009**, *106*, 4653−4658.
(266) Schmidt, M.; Sachse, C.; Richter, W.; Xu, C.; Fändrich, M.; Grigorieff, N. Comparison of Alzheimer Aβ(1−40) and Aβ(1−42) Amyloid Fibrils Reveals Similar Protofilament Structures. *Proc. Natl. Acad. Sci. U. S. A.* **2009**, *106*, 19813−19818.
(267) Hwang, W.; Zhang, S.; Kamm, R. D.; Karplus, M. Kinetic Control of Dimer Structure Formation in Amyloid Fibrillogenesis. *Proc. Natl. Acad. Sci. U. S. A.* **2004**, *101*, 12916−12921.
(268) Saric, A.; Buell, A. K.; Meisl, G.; Michaels, T. C. T.; Dobson, C. M.; Linse, S.; Knowles, T.; Frenkel, D. Physical Determinants of the Self-replication of Protein Fibrils. *Nat. Phys.* **2016**, *12*, 874−880.
(269) Schwierz, N.; Frost, C. V.; Geissler, P. L.; Zacharias, M. From Aβ Filament to Fibril: Molecular Mechanism of Surface-Activated Secondary Nucleation from All-Atom MD Simulations. *J. Phys. Chem. B* **2017**, *121*, 671−682.
(270) Bellaiche, M. M. J.; Best, R. B. Molecular Determinants of Aβ42 Adsorption to Amyloid Fibril Surfaces. *J. Phys. Chem. Lett.* **2018**, *9*, 6437−6443.
(271) Xiao, Y.; Ma, B.; McElheny, D.; Parthasarathy, S.; Long, F.; Hoshi, M.; Nussinov, R.; Ishii, Y. Aβ(1−42) Fibril Structure Illuminates Self-Recognition and Replication of Amyloid in Alzheimer's Disease. *Nat. Struct. Mol. Biol.* **2015**, *22*, 499−505.
(272) Cohen, S. I. A.; Cukalevski, R.; Michaels, T.; Saric, A.; Tornquist, M.; Vendruscolo, M.; Dobson, C. M.; Buell, A.; Knowles, T.; Linse, S. Distinct Thermodynamic Signature of Oligomer Generation in the Aggregation of the Amyloid-β Peptide. *Nat. Chem.* **2018**, *10*, 523
(273) Karthika, S.; Radhakrishnan, T. K.; Kalaichelvi, P. A Review of Classical and Non-classical Nucleation Theories. *Cryst. Growth Des.* **2016**, *16*, 6663−6681.
(274) Muthukumar, M. Nucleation in Polymer Crystallization. *Advances in Chemical Physics* ; Wiley-Blackwell, 2004; Chapter 1, pp 1−63.
(275) Ndlovu, H.; Ashcroft, A.; Radford, S.; Harris, S. Effect of Sequence Variation on the Mechanical Response of Amyloid Fibrils Probed by Steered Molecular Dynamics Simulation. *Biophys. J.* **2012**, *102*, 587−596.
(276) Dror, R. O.; Dirks, R. M.; Grossman, J.; Xu, H.; Shaw, D. E. Biomolecular Simulation: A Computational Microscope for Molecular Biology. *Annu. Rev. Biophys.* **2012**, *41*, 429−452.
(277) Bottaro, S.; Lindorff-Larsen, K. Biophysical Experiments and Biomolecular Simulations: A Perfect Match? *Science* **2018**, *361*, 355−360.
(278) Amaro, R. E.; Mulholland, A. J. Multiscale Methods in Drug Design Bridge Chemical and Biological Complexity in the Search for Cures. *Nat. Rev. Chem.* **2018**, *2*, 0148
(279) Karplus, M.; McCammon, J. A. Molecular Dynamics Simulations of Biomolecules. *Nat. Struct. Biol.* **2002**, *9*, 646−652.
(280) van Gunsteren, W. F.; Dolenc, J.; Mark, A. E. Molecular Simulation as an Aid to Experimentalists. *Curr. Opin. Struct. Biol.* **2008**, *18*, 149−153.
(281) van Gunsteren, W. F.; Daura, X.; Hansen, N.; Mark, A. E.; Oostenbrink, C.; Riniker, S.; Smith, L. J. Validation of Molecular Simulation: An Overview of Issues. *Angew. Chem., Int. Ed.* **2018**, *57*, 884−902.
(282) Glaettli, A.; van Gunsteren, W. F. Are NMR-Derived Model Structures for β-Peptides Representative for the Ensemble of Structures Adopted in Solution? *Angew. Chem., Int. Ed.* **2004**, *43*, 6312−6316.
(283) Bowman, G. R. Accurately Modeling Nanosecond Protein Dynamics Requires at Least Microseconds of Simulation. *J. Comput. Chem.* **2016**, *37*, 558−566.
(284) Sawle, L.; Ghosh, K. Convergence of Molecular Dynamics Simulation of Protein Native States: Feasibility vs Self-Consistency Dilemma. *J. Chem. Theory Comput.* **2016**, *12*, 861−869.
(285) Saric, A.; Michaels, T. C. T.; Zaccone, A.; Knowles, T. P. J.; Frenkel, D. Kinetics of Spontaneous Filament Nucleation via Oligomers: Insights from Theory and Simulation. *J. Chem. Phys.* **2016**, *145*, 211926.
(286) Pande, V. S.; Beauchamp, K.; Bowman, G. R. Everything You Wanted to Know about Markov State Models but Were Afraid to Ask. *Methods* **2010**, *52*, 99−105.
(287) Husic, B. E.; Pande, V. S. Markov State Models: From an Art to a Science. *J. Am. Chem. Soc.* **2018**, *140*, 2386−2396.
(288) Bacci, M.; Caflisch, A.; Vitalis, A. On the Removal of Initial State Bias from Simulation Data. *J. Chem. Phys.* **2019**, *150*, 104105
(289) Bolhuis, P. G.; Chandler, D.; Dellago, C.; Geissler, P. L. Transition Path Sampling: Throwing Ropes Over Rough Mountain Passes, in the Dark. *Annu. Rev. Phys. Chem.* **2002**, *53*, 291−318.
(290) Ban, T.; Yamaguchi, K.; Goto, Y. Direct Observation of Amyloid Fibril Growth, Propagation, and Adaptation. *Acc. Chem. Res.* **2006**, *39*, 663−670.
(291) Zaccone, A.; Terentjev, I.; Herling, T. W.; Knowles, T. P. J.; Aleksandrova, A.; Terentjev, E. M. Kinetics of Fragmentation and Dissociation of Two-strand Protein Filaments: Coarse-Grained Simulations and Experiments. *J. Chem. Phys.* **2016**, *145*, 105101.
(292) Lee, C.-T.; Terentjev, E. M. Mechanisms and Rates of Nucleation of Amyloid Fibrils. *J. Chem. Phys.* **2017**, *147*, 105103.
(293) Sidhu, A.; Segers-Nolten, I.; Raussens, V.; Claessens, M. M. A. E.; Subramaniam, V. Distinct Mechanisms Determine α-Synuclein Fibril Morphology during Growth and Maturation. *ACS Chem. Neurosci.* **2017**, *8*, 538−547.
(294) Congdon, E. E.; Kim, S.; Bonchak, J.; Songrug, T.; Matzavinos, A.; Kuret, J. Nucleation-Dependent Tau Filament Formation: The Importance of Dimerization and an Estimation of Elementary Rate Constants. *J. Biol. Chem.* **2008**, *283*, 13806−13816.
(295) Collins, S. R.; Douglass, A.; Vale, R. D.; Weissman, J. S. Mechanism of Prion Propagation: Amyloid Growth Occurs by Monomer Addition. *PLoS Biol.* **2004**, *2*, e321.
(296) Smith, J. F.; Knowles, T. P. J.; Dobson, C. M.; MacPhee, C. E.; Welland, M. E. Characterization of the Nanoscale Properties of Individual Amyloid Fibrils. *Proc. Natl. Acad. Sci. U. S. A.* **2006**, *103*, 15806−15811.
(297) Roberts, R. G. Good Amyloid, Bad Amyloid-What's the Difference? *PLoS Biol.* **2016**, *14*, 1−3.
(298) Herrmann, U. S.; et al. Structure-Based Drug Design Identifies Polythiophenes as Antiprion Compounds. *Sci. Transl. Med.* **2015**, *7*, 299ra123−299ra123.
(299) Glabe, C. G. Common Mechanisms of Amyloid Oligomer Pathogenesis in Degenerative Disease. *Neurobiol. Aging* **2006**, *27*, 570−575.
(300) Di Scala, C.; Yahi, N.; Boutemeur, S.; Flores, A.; Rodriguez, L.; Chahinian, H.; Fantini, J. Common Molecular Mechanism of Amyloid Pore Formation by Alzheimer's Beta-amyloid Peptide and Alpha-synuclein. *Sci. Rep.* **2016**, *6*, 28781.
(301) Lashuel, H. A.; Petre, B. M.; Wall, J.; Simon, M.; Nowak, R. J.; Walz, T.; Lansbury, P. T. α-Synuclein, Especially the Parkinson's Disease-associated Mutants, Forms Pore-like Annular and Tubular Protofibrils. *J. Mol. Biol.* **2002**, *322*, 1089−1102.
(302) Press-Sandler, O.; Miller, Y. Molecular Mechanisms of Membrane-Associated Amyloid Aggregation: Computational Perspective and Challenges. *Biochim. Biophys. Acta, Biomembr.* **2018**, *1860*, 1889−1905.

DOI: 10.1021/acs.chemrev.8b00731
Chem. Rev. XXXX, XXX, XXX−XXX

(303) Sokolov, Y.; Kozak, J. A.; Kayed, R.; Chanturiya, A.; Glabe, C.; Hall, J. E. Soluble Amyloid Oligomers Increase Bilayer Conductance by Altering Dielectric Structure. *J. Gen. Physiol.* **2006**, *128*, 637−647.
(304) Butterfield, S.; Lashuel, H. Amyloidogenic Protein-Membrane Interactions: Mechanistic Insight from Model Systems. *Angew. Chem., Int. Ed.* **2010**, *49*, 5628−5654.
(305) Simons, T. J. B. Calcium and Neuronal function. *Neurosurgical Rev.* **1988**, *11*, 119−129.
(306) Pinton, P.; Giorgi, C.; Siviero, R.; Zecchini, E.; Rizzuto, R. Calcium and Apoptosis: ER-mitochondria Ca2+ Transfer in the Control of Apoptosis. *Oncogene* **2008**, *27*, 6407−6418.
(307) Kayed, R.; Lasagna-Reeves, C. Molecular Mechanisms of Amyloid Oligomers Toxicity. *J. Alzheimer's Dis.* **2012**, *33*, S67−S78.
(308) Demuro, A.; Smith, M.; Parker, I. Single-channel Ca2+ Imaging Implicates Aβ1−42 Amyloid Pores in Alzheimer's Disease Pathology. *J. Cell Biol.* **2011**, *195*, 515−524.
(309) Kiely, A. P.; Asi, Y. T.; Kara, E.; Limousin, P.; Ling, H.; Lewis, P.; Proukakis, C.; Quinn, N.; Lees, A. J.; Hardy, J.; Revesz, T.; Houlden, H.; Holton, J. L. α-Synucleinopathy Associated with G51D SNCA Mutation: A Link between Parkinson's Disease and Multiple System Atrophy? *Acta Neuropathol.* **2013**, *125*, 753−769.
(310) Volles, M. J.; Lansbury, P. T. Vesicle Permeabilization by Protofibrillar α-Synuclein is Sensitive to Parkinson's Disease-Linked Mutations and Occurs by a Pore-Like Mechanism. *Biochemistry* **2002**, *41*, 4595−4602.
(311) Lashuel, H. A.; Hartley, D.; Petre, B. M.; Walz, T.; Jr Lansbury, P. T. Amyloid Pores from Pathogenic Mutations. *Nature* **2002**, *418*, 291.
(312) Sciacca, M. F. M.; Pappalardo, M.; Attanasio, F.; Milardi, D.; La Rosa, C.; Grasso, D. M. Are Fibril Growth and Membrane Damage Linked Processes? An Experimental and Computational Study of IAPP12−18 and IAPP21−27 Peptides. *New J. Chem.* **2010**, *34*, 200−207.
(313) Mirzabekov, T. A.; Lin, M.-c.; Kagan, B. L. Pore Formation by the Cytotoxic Islet Amyloid Peptide Amylin. *J. Biol. Chem.* **1996**, *271*, 1988−1992.
(314) Anguiano, M.; Nowak, R. J.; Lansbury, P. T. Protofibrillar Islet Amyloid Polypeptide Permeabilizes Synthetic Vesicles by a Pore-Like Mechanism that May Be Relevant to Type II Diabetes. *Biochemistry* **2002**, *41*, 11338−11343.
(315) Brender, J. R.; Lee, E. L.; Cavitt, M. A.; Gafni, A.; Steel, D. G.; Ramamoorthy, A. Amyloid Fiber Formation and Membrane Disruption are Separate Processes Localized in Two Distinct Regions of IAPP, the Type-2-Diabetes-Related Peptide. *J. Am. Chem. Soc.* **2008**, *130*, 6424−6429.
(316) Robinson, L. S.; Ashman, E. M.; Hultgren, S. J.; Chapman, M. R. Secretion of Curli Fibre Subunits is Mediated by the Outer Membrane-Localized CsgG Protein. *Mol. Microbiol.* **2006**, *59*, 870−881.
(317) Morriss-Andrews, A.; Brown, F. L. H.; Shea, J.-E. A Coarse-Grained Model for Peptide Aggregation on a Membrane Surface. *J. Phys. Chem. B* **2014**, *118*, 8420−8432.
(318) Strodel, B.; Lee, J. W. L.; Whittleston, C. S.; Wales, D. J. Transmembrane Structures for Alzheimer's Aβ1−42 Oligomers. *J. Am. Chem. Soc.* **2010**, *132*, 13300−13312.
(319) Sciacca, M. F.; Tempra, C.; Scollo, F.; Milardi, D.; Rosa, C. L. Amyloid Growth and Membrane Damage: Current Themes and Emerging Perspectives from Theory and Experiments on Aβ and hIAPP. *Biochim. Biophys. Acta, Biomembr.* **2018**, *1860*, 1625−1638.
(320) Phillips, R.; Kondev, J.; Theriot, J. *Physical Biology of the Cell*; Garland Science, Taylor & Francis Group: New York, 2008.
(321) van Anders, G.; Ahmed, N. K.; Smith, R.; Engel, M.; Glotzer, S. C. Entropically Patchy Particles: Engineering Valence through Shape Entropy. *ACS Nano* **2014**, *8*, 931−940.
(322) Santos, A.; Millan, J. A.; Glotzer, S. C. Facetted Patchy Particles through Entropy-Driven Patterning of Mixed Ligand SAMS. *Nanoscale* **2012**, *4*, 2640−2650.
(323) Bucciantini, M.; Rigacci, S.; Stefani, M. Amyloid Aggregation: Role of Biological Membranes and the Aggregate-Membrane System. *J. Phys. Chem. Lett.* **2014**, *5*, 517−527.
(324) Friedman, R.; Pellarin, R.; Caflisch, A. Amyloid Aggregation on Lipid Bilayers and Its Impact on Membrane Permeability. *J. Mol. Biol.* **2009**, *387*, 407−415.
(325) Cattani, J.; Subramaniam, V.; Drescher, M. Room-Temperature in-Cell EPR Spectroscopy: Alpha-synuclein Disease Variants Remain Intrinsically Disordered in the Cell. *Phys. Chem. Chem. Phys.* **2017**, *19*, 18147−18151.
(326) Theillet, F.-X.; Binolfi, A.; Bekei, B.; Martorana, A.; Rose, H.; Stuiver, M.; Verzini, S.; Lorenz, D.; van Rossum, M.; Goldfarb, D.; Selenko, P. Structural Disorder of Monomeric α-Synuclein Persists in Mammalian Cells. *Nature* **2016**, *530*, 45−50.
(327) Pauwels, K.; Lebrun, P.; Tompa, P. To be Disordered or not to be Disordered: Is that Still a Question for Proteins in the Cell? *Cell. Mol. Life Sci.* **2017**, *74*, 3185−3204.
(328) Fakhree, M. A. A.; Nolten, I. S.; Blum, C.; Claessens, M. M. A. E. Different Conformational Subensembles of the Intrinsically Disordered Protein α-Synuclein in Cells. *J. Phys. Chem. Lett.* **2018**, *9*, 1249−1253.
(329) Radak, B. K.; Chipot, C.; Suh, D.; Jo, S.; Jiang, W.; Phillips, J. C.; Schulten, K.; Roux, B. Constant-pH Molecular Dynamics Simulations for Large Biomolecular Systems. *J. Chem. Theory Comput.* **2017**, *13*, 5933−5944.
(330) Harada, R.; Sugita, Y.; Feig, M. Protein Crowding Affects Hydration Structure and Dynamics. *J. Am. Chem. Soc.* **2012**, *134*, 4842−4849.
(331) Perakslis, E.; Riordan, H.; Friedhoff, L.; Nabulsi, A.; Pich, E. M. A Call for a Global and Bigger Data Approach to Alzheimer Disease. *Nat. Rev. Drug Discovery* **2018**, DOI: 10.1038/nrd.2018.86
(332) Cummings, J. L.; Morstorf, T.; Zhong, K. Alzheimer's Disease Drug-Development Pipeline: Few Candidates, Frequent Failures. *Alzheimer's Res. Ther.* **2014**, *6*, 37.
(333) Doig, A. J.; del Castillo-Frias, M. P.; Berthoumieu, O.; Tarus, B.; Nasica-Labouze, J.; Sterpone, F.; Nguyen, P. H.; Hooper, N. M.; Faller, P.; Derreumaux, P. Why Is Research on Amyloid-β Failing to Give New Drugs for Alzheimer's Disease? *ACS Chem. Neurosci.* **2017**, *8*, 1435−1437.
(334) Savelieff, M. G.; Nam, G.; Kang, J.; Lee, H. J.; Lee, M.; Lim, M. H. Development of Multifunctional Molecules as Potential Therapeutic Candidates for Alzheimer's Disease, Parkinson's Disease, and Amyotrophic Lateral Sclerosis in the Last Decade. *Chem. Rev.* **2019**, *119*, 1221
(335) Miller, B. R.; Nguyen, H.; Hu, C. J.-H.; Lin, C.; Nguyen, Q. T. New and Emerging Drugs and Targets for Type 2 Diabetes: Reviewing the Evidence. *Am. Health Drug Benefits* **2014**, *7*, 452−463.
(336) Eisele, Y. S.; Monteiro, C.; Fearns, C.; Encalada, S. E.; Wiseman, R. L.; Powers, E. T.; Kelly, J. W. Targeting Protein Aggregation for the Treatment of Degenerative Diseases. *Nat. Rev. Drug Discovery* **2015**, *14*, 759−780.
(337) Stangou, A. J.; Banner, N. R.; Hendry, B. M.; Rela, M.; Portmann, B.; Wendon, J.; Monaghan, M.; MacCarthy, P.; Buxton-Thomas, M.; Mathias, C. J.; Liepnieks, J. J.; O'Grady, J.; Heaton, N. D.; Benson, M. D. Hereditary Fibrinogen A α-Chain Amyloidosis: Phenotypic Characterization of a Systemic Disease and the Role of Liver Transplantation. *Blood* **2010**, *115*, 2998−3007.
(338) Gertz, M. A. Immunoglobulin Light Chain Amyloidosis Diagnosis and Treatment Algorithm 2018. *Blood Cancer J.* **2018**, *8*, 1169−1180.
(339) Rappley, I.; Monteiro, C.; Novais, M.; Baranczak, A.; Solis, G.; Wiseman, R. L.; Helmke, S.; Maurer, M. S.; Coelho, T.; Powers, E. T.; Kelly, J. W. Quantification of Transthyretin Kinetic Stability in Human Plasma Using Subunit Exchange. *Biochemistry* **2014**, *53*, 1993−2006.
(340) Sekijima, Y.; Dendle, M.; Kelly, J. Orally Administered Diflunisal Stabilizes Transthyretin Against Dissociation Required for Amyloidogenesis. *Amyloid* **2006**, *13*, 236−49.
(341) Jackson, M. P.; Hewitt, E. W. Why are Functional Amyloids Non-Toxic in Humans? *Biomolecules* **2017**, *7*, E71.
(342) Caron, N. S.; Dorsey, E. R.; Hayden, M. R. Therapeutic Approaches to Huntington Disease: From the Bench to the Clinic. *Nat. Rev. Drug Discovery* **2018**, *17*, 728.

DOI: 10.1021/acs.chemrev.8b00731
Chem. Rev. XXXX, XXX, XXX−XXX

(343) Kaur, K.; Gill, J. S.; Bansal, P. K.; Deshmukh, R. Neuro-Inflammation-A Major Cause for Striatal Dopaminergic Degeneration in Parkinson's Disease. *J. Neurol. Sci.* **2017**, *381*, 308−314.
(344) Pearson, H. A.; Peers, C. Physiological Roles for Amyloid β Peptides. *J. Physiol.* **2006**, *575*, 5−10.
(345) Plant, L. D.; Boyle, J. P.; Smith, I. F.; Peers, C.; Pearson, H. A. The Production of Amyloid β Peptide Is a Critical Requirement for the Viability of Central Neurons. *J. Neurosci.* **2003**, *23*, 5531−5535.
(346) Brothers, H. M.; Gosztyla, M. L.; Robinson, S. R. The Physiological Roles of Amyloid-β Peptide Hint at New Ways to Treat Alzheimer's Disease. *Front. Aging Neurosci.* **2018**, *10*, 118.
(347) Bendor, J.; Logan, T.; Edwards, R. The Function of α-Synuclein. *Neuron* **2013**, *79*, 1044−1066.
(348) Lashuel, H.; Overk, C. R.; Oueslati, A.; Masliah, E. The Many Faces of α-Synuclein: From Structure and Toxicity to Therapeutic Target. *Nat. Rev. Neurosci.* **2013**, *14*, 38−48.
(349) Westermark, P.; Andersson, A.; Westermark, G. T. Islet Amyloid Polypeptide, Islet Amyloid, and Diabetes Mellitus. *Physiol. Rev.* **2011**, *91*, 795−826.
(350) Pallas-Bazarra, N.; Jurado-Arjona, J.; Navarrete, M.; Esteban, J. A.; Hernández, F.; Ávila, J.; Llorens-Martín, M. Novel Function of Tau in Regulating the Effects of External Stimuli on Adult Hippocampal Neurogenesis. *EMBO J.* **2016**, *35*, 1417−1436.
(351) Wulf, M.-A.; Senatore, A.; Aguzzi, A. The Biological Function of the Cellular Prion Protein: An Update. *BMC Biol.* **2017**, *15*, 34.
(352) Küffer, A.; et al. The Prion Protein is an Agonistic Ligand of the G Protein-coupled Receptor Adgrg6. *Nature* **2016**, *536*, 464−468.
(353) Otzen, D. E. Functional Amyloid: Turning Swords into Plowshares. *Prion* **2010**, *4*, 256−64.
(354) van Gerven, N.; van der Verren, S. E. V.; Reiter, D. M.; Remaut, H. The Role of Functional Amyloids in Bacterial Virulence. *J. Mol. Biol.* **2018**, *430*, 3657−3684.
(355) Hervas, R.; et al. Molecular Basis of Orb2 Amyloidogenesis and Blockade of Memory Consolidation. *PLoS Biol.* **2016**, *14*, 1−32.
(356) Urrea, L.; Segura-Feliu, M.; Masuda-Suzukake, M.; Hervera, A.; Pedraz, L.; García Az- nar, J. M.; Vila, M.; Samitier, J.; Torrents, E.; Ferrer, I.; Gavín, R.; Hagesawa, M.; del Río, J. A. Involvement of Cellular Prion Protein in α-Synuclein Transport in Neurons. *Mol. Neurobiol.* **2018**, *55*, 1847−1860.
(357) Bove-Fenderson, E.; Urano, R.; Straub, J. E.; Harris, D. A. Cellular Prion Protein Targets Amyloid-β Fibril Ends via its C-Terminal Domain to Prevent Elongation. *J. Biol. Chem.* **2017**, *292*, 16858−16871.
(358) Pflanzner, T.; Petsch, B.; Andre-Dohmen, B.; Muller-Schiffmann, A.; Tschickardt, S.; Weggen, S.; Stitz, L.; Korth, C.; Pietrzik, C. U. Cellular Prion Protein Participates in Amyloid-β Transcytosis Across the Blood-Brain Barrier. *J. Cereb. Blood Flow Metab.* **2012**, *32*, 628−32.
(359) Clinton, L. K.; Blurton-Jones, M.; Myczek, K.; Trojanowski, J. Q.; LaFerla, F. M. Synergistic Interactions between Aβ, Tau, and α-Synuclein: Acceleration of Neuropathology and Cognitive Decline. *J. Neurosci.* **2010**, *30*, 7281−7289.
(360) Mandal, P. K.; Pettegrew, J. W.; Masliah, E.; Hamilton, R. L.; Mandal, R. Interaction between Aβ Peptide and α-Synuclein: Molecular Mechanisms in Overlapping Pathology of Alzheimer's and Parkinson's in Dementia with Lewy Body Disease. *Neurochem. Res.* **2006**, *31*, 1153−1162.
(361) Tsigelny, I. F.; Crews, L.; Desplats, P.; Shaked, G. M.; Sharikov, Y.; Mizuno, H.; Spencer, B.; Rockenstein, E.; Trejo, M.; Platoshyn, O.; Yuan, J. X.-J.; Masliah, E. Mechanisms of Hybrid Oligomer Formation in the Pathogenesis of Combined Alzheimer's and Parkinson's Diseases. *PLoS One* **2008**, *3*, 1−15.
(362) Oikawa, T.; Nonaka, T.; Terada, M.; Tamaoka, A.; Hisanaga, S.-i.; Hasegawa, M. α-Synuclein Fibrils Exhibit Gain-of-Toxic-Function, Promoting Tau Aggregation and Inhibiting Microtubule Assembly. *J. Biol. Chem.* **2016**, *291*, 15046−15056.
(363) Chen, S.; et al. Exposure to the Functional Bacterial Amyloid Protein Curli Enhances Alpha-Synuclein Aggregation in Aged Fischer 344 Rats and Caenorhabditis Elegans. *Sci. Rep.* **2016**, *6*, 1−10.
(364) Baram, M.; Atsmon Raz, Y.; Ma, B.; Nussinov, R.; Miller, Y. Amylin-Aβ Oligomers at Atomic Resolution Using Molecular Dynamics Simulations: A Link Between Type 2 Diabetes and Alzheimer's Disease. *Phys. Chem. Chem. Phys.* **2016**, *18*, 2330−8.
(365) Rojas, A. V.; Maisuradze, G. G.; Scheraga, H. A. Dependence of the Formation of Tau and Aβ Peptide Mixed Aggregates on the Secondary Structure of the N-Terminal Region of Aβ. *J. Phys. Chem. B* **2018**, *122*, 7049−7056.
(366) Orlova, E. V.; Saibil, H. R. Structural Analysis of Macromolecular Assemblies by Electron Microscopy. *Chem. Rev.* **2011**, *111*, 7710−7748.
(367) Bai, X.-C.; McMullan, G.; Scheres, S. H. W. How Cryo-EM is Revolutionizing Structural Biology. *Trends Biochem. Sci.* **2015**, *40*, 49−57.
(368) Renaud, J.-P.; Chari, A.; Ciferri, C.; Liu, W.-t.; Remigy, H.-W.; Stark, H.; Wies- mann, C. Cryo-EM in Drug Discovery: Achievements, Limitations and Prospects. *Nat. Rev. Drug Discovery* **2018**, *17*, 471−492.
(369) Gremer, L.; Schölzel, D.; Schenk, C.; Reinartz, E.; Labahn, J.; Ravelli, R. B. G.; Tusche, M.; Lopez-Iglesias, C.; Hoyer, W.; Heise, H.; Willbold, D.; Schröder, G. F. Fibril Structure of Amyloid-β(1−42) by Cryoelectron Microscopy. *Science* **2017**, *358*, 116−119.
(370) Falcon, B.; Zhang, W.; Murzin, A. G.; Murshudov, G.; Garringer, H.; Vidal, R.; Anthony Crowther, R.; Ghetti, B.; Scheres, S.; Goedert, M. Structures of Filaments from Pick's Disease Reveal a Novel Tau Protein Fold. *Nature* **2018**, *561*, 137−140.
(371) Guerrero-Ferreira, R.; Taylor, N. M.; Mona, D.; Ringler, P.; Lauer, M. E.; Riek, R.; Britschgi, M.; Stahlberg, H. Cryo-EM Structure of Alpha-Synuclein Fibrils. *eLife* **2018**, *7*, No. e36402.
(372) Li, B.; Ge, P.; Murray, K. A.; Sheth, P.; Zhang, M.; Nair, G.; Sawaya, M. R.; Shin, W. S.; Boyer, D. R.; Ye, S.; Eisenberg, D. S.; Zhou, Z. H.; Jiang, L. Cryo- EM of Full-Length α-Synuclein Reveals Fibril Polymorphs with a Common Structural Kernel. *Nat. Commun.* **2018**, DOI: 10.1038/s41467-018-05971-2
(373) Iadanza, M.; Jackson, M.; Ranson, N.; W Hewitt, E.; Radford, S. A New Era for Understanding Amyloid Structures and Disease. *Nat. Rev. Mol. Cell Biol.* **2018**, *19*, 755
(374) Fitzpatrick, A. W. P.; Lorenz, U. J.; Vanacore, G. M.; Zewail, A. H. 4D Cryo-Electron Microscopy of Proteins. *J. Am. Chem. Soc.* **2013**, *135*, 19123−19126.
(375) Jonic, S. Cryo-electron Microscopy Analysis of Structurally Heterogeneous Macromolecular Complexes. *Comput. Struct. Biotechnol. J.* **2016**, *14*, 385−390.
(376) Kaledhonkar, S.; Fu, Z.; White, H.; Frank, J. Time-Resolved Cryo-Electron Microscopy Using a Microfluidic Chip. In *Protein Complex Assembly: Methods and Protocols*; Marsh, J. A., Ed.; Springer New York: New York, NY, 2018; pp 59−71.
(377) Lee, A.; Tsekouras, K.; Calderon, C.; Bustamante, C.; Presse, S. Unraveling the Thousand Word Picture: An Introduction to Super-Resolution Data Analysis. *Chem. Rev.* **2017**, *117*, 7276−7330.
(378) Lavecchia, A. Machine-Learning Approaches in Drug Discovery: Methods and Applications. *Drug Discovery Today* **2015**, *20*, 318−331.
(379) Nakagawa Lima, A.; Allison Philot, E.; Trossini, G.; Scott, A. L.; Goncalves Mal- tarollo, V.; Honorio, K. Use of Machine Learning Approaches for Novel Drug Discovery. *Expert Opin. Drug Discovery* **2016**, *11*, 225−39.
(380) Keskin, O.; Tuncbag, N.; Gursoy, A. Predicting Protein-Protein Interactions from the Molecular to the Proteome Level. *Chem. Rev.* **2016**, *116*, 4884−4909.
(381) Zhou, H.-X.; Pang, X. Electrostatic Interactions in Protein Structure, Folding, Binding, and Condensation. *Chem. Rev.* **2018**, *118*, 1691−1741.
(382) He, B.; Wang, K.; Liu, Y.; Xue, B. Q.; Uversky, V. N.; Dunker, A. K. Predicting Intrinsic Disorder in Proteins: An Overview. *Cell Res.* **2009**, *19*, 929−949.
(383) Chiti, F.; Stefani, M.; Taddei, N.; Ramponi, G.; Dobson, C. M. Rationalization of the Effects of Mutations on Peptide and Protein Aggregation Rates. *Nature* **2003**, *424*, 805−808.

DOI: 10.1021/acs.chemrev.8b00731
Chem. Rev. XXXX, XXX, XXX−XXX

(384) Caflisch, A. Computational Models for the Prediction of Polypeptide Aggregation Propensity. *Curr. Opin. Chem. Biol.* **2006**, *10*, 437−444.
(385) Huggins, D. J.; Biggin, P. C.; Damgen, M. A.; Essex, J. W.; Harris, S. A.; Henchman, R. H.; Khalid, S.; Kuzmanic, A.; Laughton, C. A.; Michel, J.; Mulholland, A. J.; Rosta, E.; Sansom, M. S. P.; van der Kamp, M. W. Biomolecular Simulations: From Dynamics and Mechanisms to Computational Assays of Biological Activity. *Wiley Interdiscip. Rev. Comput. Mol. Sci.* **2018**, *0*, e1393.
(386) Wilson, C. J.; Bommarius, A. S.; Champion, J. A.; Chernoff, Y. O.; Lynn, D. G.; Paravastu, A. K.; Liang, C.; Hsieh, M.-C.; Heemstra, J. M. Biomolecular Assemblies: Moving from Observation to Predictive Design. *Chem. Rev.* **2018**, *118*, 11519
(387) Alber, F.; Foerster, F.; Korkin, D.; Topf, M.; Sali, A. Integrating Diverse Data for Structure Determination of Macromolecular Assemblies. *Annu. Rev. Biochem.* **2008**, *77*, 443−477.
(388) Ward, A. B.; Sali, A.; Wilson, I. A. Integrative Structural Biology. *Science* **2013**, *339*, 913−915.
(389) Camilloni, C.; Vendruscolo, M. Statistical Mechanics of the Denatured State of a Protein Using Replica-Averaged Metadynamics. *J. Am. Chem. Soc.* **2014**, *136*, 8982−8991.
(390) Follis, A. V.; Hammoudeh, D. I.; Wang, H.; Prochownik, E. V.; Metallo, S. J. Structural Rationale for the Coupled Binding and Unfolding of the c-Myc Oncoprotein by Small Molecules. *Chem. Biol.* **2008**, *15*, 1149−1155.
(391) Heller, G. T.; Aprile, F. A.; Vendruscolo, M. Methods of Probing the Interactions Between Small Molecules and Disordered Proteins. *Cell. Mol. Life Sci.* **2017**, *74*, 3225−3243.
(392) Rodrigues, J. P. G. L. M.; Bonvin, A. M. J. J. Integrative Computational Modeling of Protein Interactions. *FEBS J.* **2014**, *281*, 1988−2003.
(393) Russel, D.; Lasker, K.; Webb, B.; Velazquez-Muriel, J.; Tjioe, E.; Schneidman-Duhovny, D.; Peterson, B.; Sali, A. Putting the Pieces Together: Integrative Modeling Platform Software for Structure Determination of Macromolecular Assemblies. *PLoS Biol.* **2012**, *10*, 1−5.
(394) Vallat, B.; Webb, B.; Westbrook, J. D.; Sali, A.; Berman, H. M. Development of a Prototype System for Archiving Integrative/Hybrid Structure Models of Biological Macromolecules. *Structure* **2018**, *26*, 894−904.e2.
(395) Webb, B.; Viswanath, S.; Bonomi, M.; Pellarin, R.; Greenberg, C. H.; Saltzberg, D.; Sali, A. Integrative Structure Modeling with the Integrative Modeling Platform. *Protein Sci.* **2018**, *27*, 245−258.
(396) Xu, X.; Yan, C.; Wohlhueter, R.; Ivanov, I. Integrative Modeling of Macromolecular Assemblies from Low to Near-Atomic Resolution. *Comput. Struct. Biotechnol. J.* **2015**, *13*, 492−503.
(397) Singla, J.; McClary, K. M.; White, K. L.; Alber, F.; Sali, A.; Stevens, R. C. Opportunities and Challenges in Building a Spatiotemporal Multi-Scale Model of the Human Pancreatic β Cell. *Cell* **2018**, *173*, 11−19.
(398) Gopal, S. M.; Mukherjee, S.; Cheng, Y.-M.; Feig, M. PRIMO/PRIMONA: A Coarse-Grained Model for Proteins and Nucleic Acids that Preserves Near-Atomistic Accuracy. *Proteins: Struct., Funct., Genet.* **2010**, *78*, 1266−1281.
(399) Kar, P.; Feig, M. Hybrid All-Atom/Coarse-Grained Simulations of Proteins by Direct Coupling of CHARMM and PRIMO Force Fields. *J. Chem. Theory Comput.* **2017**, *13*, 5753−5765.
(400) Rojas, A. V.; Liwo, A.; Scheraga, H. A. Molecular Dynamics with the United-Residue Force Field: Ab Initio Folding Simulations of Multichain Proteins. *J. Phys. Chem. B* **2007**, *111*, 293−309.
(401) Rojas, A.; Liwo, A.; Browne, D.; Scheraga, H. A. Mechanism of Fiber Assembly: Treatment of Aβ Peptide Aggregation with a Coarse-Grained United-Residue Force Field. *J. Mol. Biol.* **2010**, *404*, 537
(402) Mondal, B.; Reddy, G. Cosolvent Effects on the Growth of Protein Aggregates Formed by a Single Domain Globular Protein and an Intrinsically Disordered Protein. *J. Phys. Chem. B* **2019**, *123*, 1950
(403) Zhmurov, A.; Dima, R. I.; Kholodov, Y.; Barsegov, V. Sop-GPU: Accelerating Biomolecular Simulations in the Centisecond Timescale Using Graphics Processors. *Proteins: Struct., Funct., Genet.* **2010**, *78*, 2984−2999.
(404) Jarosz-Griffiths, H. H.; Noble, E.; Rushworth, J. V.; Hooper, N. M. Amyloid-β Receptors: The Good, the Bad, and the Prion Protein. *J. Biol. Chem.* **2016**, *291*, 3174−3183.

DOI: 10.1021/acs.chemrev.8b00731
Chem. Rev. XXXX, XXX, XXX−XXX